National Library of Canada
Acquisitions and Bibliographic Services Branch
395 Wellington Street
Ottawa, Ontario
K1A 0N4

Bibliothèque nationale du Canada
Direction des acquisitions et des services bibliographiques
395, rue Wellington
Ottawa (Ontario)
K1A 0N4

Your file Votre référence

Our file Notre référence

NOTICE

The quality of this microform is heavily dependent upon the quality of the original thesis submitted for microfilming. Every effort has been made to ensure the highest quality of reproduction possible.

If pages are missing, contact the university which granted the degree.

Some pages may have indistinct print especially if the original pages were typed with a poor typewriter ribbon or if the university sent us an inferior photocopy.

Reproduction in full or in part of this microform is governed by the Canadian Copyright Act, R.S.C. 1970, c. C-30, and subsequent amendments.

AVIS

La qualité de cette microforme dépend grandement de la qualité de la thèse soumise au microfilmage. Nous avons tout fait pour assurer une qualité supérieure de reproduction.

S'il manque des pages, veuillez communiquer avec l'université qui a conféré le grade.

La qualité d'impression de certaines pages peut laisser à désirer, surtout si les pages originales ont été dactylographiées à l'aide d'un ruban usé ou si l'université nous a fait parvenir une photocopie de qualité inférieure.

La reproduction, même partielle, de cette microforme est soumise à la Loi canadienne sur le droit d'auteur, SRC 1970, c. C-30, et ses amendements subséquents.

Canada

University of Alberta

Triaxial Testing on Very Loose Sands for Flow Liquefaction Analyses

BY

ALIREZA AYOUBIAN ESHTEHARD

A thesis submitted to the Faculty of Graduate Studies and Research in partial fulfillment of the requirements for the degree of Master of Science

in

GEOTECHNICAL ENGINEERING

DEPARTMENT OF CIVIL ENGINEERING

Edmonton, Alberta

Spring 1996

National Library of Canada

Acquisitions and Bibliographic Services Branch

395 Wellington Street
Ottawa, Ontario
K1A 0N4

Bibliothèque nationale du Canada

Direction des acquisitions et des services bibliographiques

395, rue Wellington
Ottawa (Ontario)
K1A 0N4

Your file Votre référence

Our file Notre référence

The author has granted an irrevocable non-exclusive licence allowing the National Library of Canada to reproduce, loan, distribute or sell copies of his/her thesis by any means and in any form or format, making this thesis available to interested persons.

L'auteur a accordé une licence irrévocable et non exclusive permettant à la Bibliothèque nationale du Canada de reproduire, prêter, distribuer ou vendre des copies de sa thèse de quelque manière et sous quelque forme que ce soit pour mettre des exemplaires de cette thèse à la disposition des personnes intéressées.

The author retains ownership of the copyright in his/her thesis. Neither the thesis nor substantial extracts from it may be printed or otherwise reproduced without his/her permission.

L'auteur conserve la propriété du droit d'auteur qui protège sa thèse. Ni la thèse ni des extraits substantiels de celle-ci ne doivent être imprimés ou autrement reproduits sans son autorisation.

ISBN 0-612-10692-6

Canada

University of Alberta

Library Release Form

Name of Author:	**Alireza Ayoubian Eshtehard**
Title of Thesis:	**Triaxial Testing on Very Loose Sands for Flow Liquefaction Analyses**
Degree:	**Master of Science**
Year this Degree Granted:	**1996**

Permission is hereby granted to the University of Alberta Library to reproduce single copies of this thesis and to lend or sell such copies for private, scholarly, or scientific research purposes only.

The author reserves all other publication and other rights in association with the copyright in the thesis, and except as hereinbefore provided, neither the thesis nor any substantial portion thereof may be printed or otherwise reproduced in any material form whatever without the author's prior written permission.

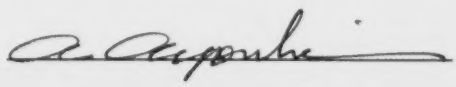

Alireza Ayoubian Eshtehard

3A, 9014-112 Street
Edmonton, Alberta
T6G 2C5

Date: January 5, 1996

University of Alberta

Faculty of Graduate Studies and Research

The undersigned certify that they have read, and recommend to the Faculty of Graduate Studies and Research for acceptance, a thesis entitled **Triaxial Testing on Very Loose Sands for Flow Liquefaction Analyses** submitted by **Alireza Ayoubian Eshtehard** in partial fulfillment of the requirements for the degree of **Master of Science** in **Geotechnical Engineering**.

Dr. P. K. Robertson (Supervisor)

Dr. D. C. Sego

Dr. D. Chan

Dr. J. Szymanski

Date: December 15, 1995

Dedication

To my parents, and my lovely grandmother, Kobra Parsa

ABSTRACT

Shear wave velocity (V_S) measurements were carried out on reconstituted samples of Montana sand, to evaluate its in-situ state. The velocity measurements were used to develop a relationship between void ratio (e), mean effective normal stress (p′), and V_S. After consolidation, the specimens were sheared to determine the Ultimate Steady State (USS) parameters. By using the e-p′-V_S relationship and measuring V_S in the field, the in-situ state of the sand can be estimated when the ground water level, in-situ K_o, and bulk density of soil are known. The obtained V_S and USS parameters were combined with the state parameter concept to define the contractive/dilative boundary in V_S-σ'_v plot. As a result, a flow liquefaction evaluation procedure was introduced.

An experimental program was carried out to study the effect of "anisotropic consolidation", "direction of loading", and "initial state" on the behaviour of two sands. Very loose reconstituted (moist-tamped), and undisturbed samples of Syncrude sand and Fraser River sand were tested. The response of these sands were found to be significantly affected by initial static shear, and the direction of loading. Anisotropically consolidated samples were more brittle in undrained loading than isotropically consolidated specimens. The reconstituted samples loaded in compression exhibited much more brittle response than those sheared in extension loading. The results clearly showed that the response of sandy soils can be misunderstood from conventional triaxial compression tests on isotropically consolidated specimens. The responses of undisturbed samples were different from those of reconstituted specimens due to their different initial states. A method was developed to test the frozen, undisturbed samples under their in-situ states. It was also shown that there appears to be a single "ultimate steady state line" for a given sand. The results from this study and other available data were used to develop Response Charts to link the in-situ state of the sands to their Response Parameters. From these charts the profiles of Response Parameters versus depth can be obtained.

Acknowledgment

The research described in this thesis was carried out in the graduate soil mechanics laboratory of the Geotechnical group, Department of Civil Engineering, University of Alberta, and was supervised by Professor P. K. Robertson.

The author would like to express his sincere gratitude to Dr. P. K. Robertson for his constant support, continuous guidance, and encouragement throughout this research. The opportunity to work with him has been a valuable and successful experience.

I would like to thank Professor N. R. Morgenstern, and Professor D. C. Sego for their advice and suggestions.

Special thanks to the technical staff, Gerry Cyre and Steve Gamble for their assistance during the experimental work. They provided support in the development, and modification of the apparatus, and testing of the frozen specimens.

I wish to thank Dr. Morgenstern, Dr. Robertson, Dr. Sego, Dr. Chan, Dr. Eisenstein, Dr. Cruden, and Dr. Barron for enriching my knowledge of Geotechnical engineering through their excellent courses.

I would like to thank my fellow graduate students Roger Skirrow, AnnajiRao Chillarige, and Amin Touhidi for their suggestions and discussions during the testing program. I also like to thank Catherine Fear and Barb Hofmann for their cooperation in data analysis and laboratory work. I wish to express thanks to all my friends in the Geotechnical Engineering graduate program.

The financial support provided by NSERC (Natural Science and Engineering Research Council of Canada) and CANLEX (Canadian Liquefaction Experiment) is gratefully acknowledged.

I am deeply indebted to my parents, my grandmother and my brother for their everlasting moral support and encouragement. All the love and help that they have given me over the years can not be measured in mere words.

Table of Contents

Page

1. Introduction **1**

Thesis Outline 4

2. Literature Review **6**

2.1 Liquefaction Phenomena 6

2.1.1 Critical State Soil Mechanics Concepts 6

2.1.1.1 Ultimate Steady State Concept 7

2.1.1.2 Ultimate Steady State Line (USSL) 8

2.1.1.3 Ultimate Steady State Parameters 10

2.1.1.4 Collapse Surface 12

2.1.2 Liquefaction Terminology 13

2.1.3 Monotonic Loading Behaviour 16

2.1.4 Brittleness Index 17

2.2 Shear Wave Velocity Measurement 19

2.2.1 Bender Element Technology 22

2.2.2 The e-p′-V_S Relationship 23

2.2.3 Using e-p′-V_S Relationship to Evaluate Flow Liquefaction 25

Figures 29

3. Experimental Work **38**

3.1 Material Tested 38

3.1.1 Montana Tailings Sand 38

3.1.2 Syncrude Tailings Sand 38

3.1.3 Fraser River Sand....39
3.2 Testing Apparatus....40
3.3 Sample Preparation Method....43
3.3.1 Reconstituted Samples....43
3.3.2 Frozen Undisturbed Samples....44
3.4 Back Pressure Saturation....45
3.5 Consolidation....46
3.5.1 Isotropically Consolidation (IC) Tests....46
3.5.2 Anisotropically Consolidated (AC) Tests....47
3.5.2.1 Reconstituted Samples....47
3.5.2.2 Frozen Undisturbed Samples....48
3.6 Shear Wave Velocity Measurements....48
3.6.1 Bender Element System....50
3.7 Void Ratio Calculation....51
3.7.1 Reconstituted Samples....51
3.7.2 Frozen Undisturbed Samples....54
3.8 Monotonic Loading....55
3.8.1 Isotropically Consolidated (IC) Tests....55
3.8.2 Anisotropically Consolidated (AC) Tests....56
3.9 Resolution of Measurements....56
Figures....57

4. Test Results....64
4.1 Isotropically Consolidated (IC) Tests....64
4.1.1 V_S measurements and e-p′-V_S Relationship....64
4.1.2 Shear Loading Results and Ultimate Steady State Parameters....66
4.2 Anisotropically Consolidated (AC) Tests....69
4.2.1 Reconstituted Samples....69

4.2.1.1 Syncrude Sand (SS) Test Results.....69
4.2.1.2 Fraser River Sand (FS) Test Results.....71
4.2.2 Undisturbed Frozen Samples.....72
4.2.2.1 Syncrude Sand (SSF) Test Results.....74
4.2.2.2 Fraser River Sand (FSF) Test Results.....75
Tables.....76
Figures.....79

5. Discussion and Analysis.....100
5.1 Isotropically Consolidated (IC) Tests.....100
5.1.1 Evaluation of In-situ States.....100
5.1.1.1 Effect of K_o.....101
5.1.1.2 Evaluation of Flow Liquefaction.....102
5.2 Anisotropically Consolidated (AC) Tests.....103
5.2.1 Effect of "Static Shear (q_o)".....104
5.2.2 Effect of "Direction of Loading".....105
5.2.3 Effect of "Initial State".....106
5.2.4 Comparison of Laboratory and In-situ V_S.....108
5.2.5 Evaluation of Ultimate Steady State Lines.....109
5.2.6 Response Charts.....110
Tables.....115
Figures.....117

6. Summary and Conclusions.....138
6.1 Recommendation for Future Research.....144

References.....146

Appendix A- Triaxial Testing Procedure.....158

List of Tables

Page

Table 4.1 Shear wave velocity measurements (V_S) during consolidation for the triaxial tests on Montana Sand.....76

Table 4.2 Mean effective normal stress (p′) and void ratio (e) at USS for triaxial tests on Montana sand.....76

Table 4.3 Summary of ultimate steady state parameters and shear wave velocity parameters for Montana tailings sand as well as, Syncrude, Ottawa, Fraser River, Alaska, and Hong Kong sand.....77

Table 4.4 Summary of consolidation stresses and void ratios for AC tests on reconstituted samples of Syncrude sand (SS) and Fraser River sand (FS).....78

Table 4.5 Summary of consolidation stresses and void ratios for AC tests on undisturbed samples of Syncrude sand (SSF) and Fraser River sand (FSF).....78

Table 5.1 Laboratory and in-situ shear wave velocities.....115

Table 5.2 Response Parameters for all the AC tests on Fraser River sand and Syncrude sand.....116

List of Figures

Page

Figure 2.1 State Boundary Surface for Remolded Clay (after Sasitharan, 1994)....29

Figure 2.2 Schematic of State Boundary Surface for Very Loose Sand (after Chillarige, 1995)....30

Figure 2.3 Ultimate Steady State Line along with the Projections on e-p′, q-e, and q-p′ Planes (after Chillarige, 1995)....31

Figure 2.4 Factors Influencing the Undrained Monotonic Response (after Fear *et al.*, 1995)....32

Figure 2.5 Relationship between State Parameter (Ψ) and Soil Behaviour....33

Figure 2.6 Definitions of USS parameters
a) e-log p′ space
b) normalized stress path....34

Figure 2.7 Collapse Surface in e-p′-q Space (Sladen *et al.*, 1985)....35

Figure 2.8 Schematic of Undrained Monotonic Behaviour of Sand in Triaxial Compression (after Robertson, 1994)....36

Figure 2.9 Suggested Flow Chart for Evaluation of Soil Liquefaction (after Robertson, 1994)....37

Figure 3.1 Grain Size Distribution for Montana Sand....57

Figure 3.2 Grain Size Distribution for Syncrude Sand....58

Figure 3.3 Grain Size Distribution for Fraser River Sand....59

Figure 3.4 Schematic Diagram of the Test Set up for Isotropically Consolidated Tests (after Cunning, 1994)....60

Figure 3.5 Schematic Diagram of the Test Set up for Anisotropically

Consolidated Tests.....61

Figure 3.6 Flush Mounted Bender Element System in Triaxial Load Head and Base Pedestal (after Cunning, 1994)..... 62

Figure 3.7 Typical Shear Wave Signal and Trigger Wave Obtained from the Tests on Montana Sand.....63

Figure 4.1 Normalized Shear Wave Velocity (V_{S1}) vs Void Ratio (e) for Montana Sand.....79

Figure 4.2 Shear Wave Velocity Contours and Consolidation States for Selected Samples of Montana Sand.....80

Figure 4.3 Void Ratio (e) vs p'_{uss} and Ultimate Steady State Parameters for Montana Sand.....81

Figure 4.4 q_{uss} vs p'_{uss} and Ultimate Steady State Parameters for Montana Sand.....82

Figure 4.5 Consolidation Curves and Ultimate Steady States for Triaxial Tests on Montana Sand.....83

Figure 4.6 Normalized Stress Paths for Triaxial Tests on Montana Sand..... 84

Figure 4.7 Deviator Stress (q) vs Axial Strain for Triaxial Tests on Montana Sand.....85

Figure 4.8 Pore Pressure during Undrained Shear vs Axial Strain for Triaxial Tests on Montana Sand..... 86

Figure 4.9 Volume Change (decrease +ve) vs Axial Strain for the Drained Test on Montana Sand..... 87

Figure 4.10 Consolidation Curves and Ultimate Steady States for AC Tests on Syncrude Sand..... 88

Figure 4.11 Stress Paths for AC Tests on Syncrude Sand..... 89

Figure 4.12 Syncrude Sand AC Test Results
a) Deviator Stress (q) vs Axial Strain
b) Change in Pore Pressure vs Axial Strain..... 90

Figure 4.13 Consolidation Curves and Ultimate Steady States for AC Tests on Fraser River Sand..... 91

Figure 4.14 Stress Paths for AC Tests on Fraser River Sand..... 92

Figure 4.15 Fraser River Sand AC Test Results
a) Deviator Stress (q) vs Strain
b) Change in Pore Pressure vs Strain..... 93

Figure 4.16 In-situ and Ultimate Steady State for AC Test on Undisturbed Sample of Syncrude Sand..... 94

Figure 4.17 Stress Path for AC Test on Undisturbed Sample of Syncrude Sand (SSF)..... 95

Figure 4.18 Syncrude Sand AC Test Results
(Undisturbed Sample)
a) Deviator Stress (q) vs Axial Strain
b) Pore Pressure vs Axial Strain..... 96

Figure 4.19 In-situ and Ultimate Steady State for AC Test on Undisturbed Sample of Fraser River Sand..... 97

Figure 4.20 Stress Path for AC Test on Undisturbed Sample of Fraser River Sand (FSF)..... 98

Figure 4.21 Fraser River Sand AC Test Results
(Undisturbed Sample)
a) Deviator Stress (q) vs Axial Strain
b) Pore Pressure vs Axial Strain..... 99

Figure 5.1 Profiles of State Parameter (Ψ) in terms of Shear Wave Velocity and Vertical Effective Stress for K_o= 0.5 for Montana Sand..... 117

Figure 5.2 Shear Wave Velocity at Ultimate State (Ψ) vs Vertical Effective Stress for Varying K_o Values for Montana Sand..... 118

Figure 5.3 Contractive/dilative Boundaries for Several sands (K_o= 0.5)..... 119

Figure 5.4 Effect of "Static Shear (q_o)" on Syncrude Sand
a) Stress Paths

b) Stress vs Strain..... 120

Figure 5.5 Effect of "Static Shear (q_o)" on Fraser River Sand
a) Stress Paths
b) Stress vs Strain..... 121

Figure 5.6 Effect of "Direction of Loading" on Syncrude Sand
a) Stress Paths
b) Stress vs Strain..... 122

Figure 5.7 Effect of "Direction of Loading" on Fraser River Sand
a) Stress Paths
b) Stress vs Strain..... 123

Figure 5.8 Effect of "Initial State" on Syncrude Sand
a) Stress Paths
b) Stress Paths for Dense Samples..... 124

Figure 5.9 Effect of "Initial State" on Fraser River Sand
a) Stress Paths
b) Stress Paths for Dense Samples..... 125

Figure 5.10 Ultimate States of All AC Tests on Syncrude Sand and Their Locations Relative to the Reference USSL..... 126

Figure 5.11 Ultimate States of All AC Tests on Fraser River Sand and Their Locations Relative to the Reference USSL..... 127

Figure 5.12 Response Parameters for Triaxial Compression and Extension Tests (after Fear *et al.*, 1995)..... 128

Figure 5.13 Brittleness Index vs RSR for All AC Tests on Fraser River Sand..... 129

Figure 5.14 S_{min}/p'_o vs RSR for All AC Tests on Fraser River Sand..... 130

Figure 5.15 ε_{amin} vs RSR for All AC Tests on Fraser River Sand..... 131

Figure 5.16 Brittleness Index vs RSR for All AC Tests on Syncrude Sand. 132

Figure 5.17 S_{min}/p'_o vs RSR for All AC Tests on Syncrude Sand..... 133

Figure 5.18 ε_{amin} vs RSR for All AC Tests on Syncrude Sand..... 134

Figure 5.19 Brittleness Index vs RSR for All AC Tests on Fraser River Sand and Syncrude Sand.....135

Figure 5.20 S_{min}/p'_o vs RSR for All AC Tests on Fraser River Sand and Syncrude Sand.....136

Figure 5.21 ε_{amin} vs RSR for All AC Tests on Fraser River Sand and Syncrude Sand.....137

List of Symbols

A	intercept of V_{SI}-e line at e=0
AC	Anisotropically Consolidated
ASTM	American Society for Testing and Materials
B	slope of V_{SI}-e line
C	grain characteristics
CANLEX	Canadian Liquefaction Experiment
C_c	coefficient of curvature
CO_2	carbon dioxide
CPT	Cone Penetration Test
C_u	coefficient of uniformity
D	diameter of sample
D_{50}	mean grain size
D_{20}	the soil diameter at which 20% of the soil weight is finer
DAP	Double Acting Piston
e	void ratio
e_c	void ratio at the end of consolidation
e_i	initial void ratio
e_f	final void ratio
e_{max}	maximum void ratio
e_{min}	minimum void ratio
ELC	External Load Cell
e_{uss}	void ratio at ultimate steady state
f_{out}	frequency of shear wave (out put wave)
FS	Fraser River Sand
FSF	Frozen Fraser Sand
G_o	small strain shear modulus
G_s	specific gravity of soil
H	height of sample
HCT	Hollow Cylinder Torsion
Hz	Hertz
I_B	brittleness index
IC	Isotropically Consolidated
ILC	Internal Load Cell
K_o	coefficient of earth pressure at rest
L	distance between the two sets of bender elements
LSS	Limited Strain Softening
LVDT	Linear Voltage Displacement Transducer
M	slope of the steady state line in p′-q plane
M_s	dry mass of soil
MS	Montana Sand

MT	Moist Tamping
m1	constant
m2	constant
ma	constant
mp	constant
n	stress exponent
na	stress exponent
nb	stress exponent
NCL	Normal Consolidation Line
P_a	atmospheric pressure
p'	mean effective normal stress
p'_o	mean effective normal stress at the start of shearing
p'_{uss}	mean effective normal stress at ultimate steady state
q	deviatoric stress
q_o	initial static deviatoric stress (at the start of shearing)
QSS	Quasi Steady State
QSSL	Quasi-Steady State Line
q_{uss}	deviatoric stress at ultimate steady state
RSR	Reference Stress Ratio
S	membrane compliance induced volume change per unit area of membrane per log-cycle change in effective confining stress
SASW	Spectral Analysis of Surface Waves
SBS	State Boundary Surface
SCPT	Seismic Cone Penetration Test
SF	Supporting Frame
SH	Strain Hardening
S_{min}	minimum shear strength at USS or QSS
S_o	static shear
S_p	shear strength at peak
SPT	Standard Penetration Test
SS	Syncrude Sand
SSF	Frozen Syncrude Sand
ss	strain softening
S_r	degree of saturation
S_s	soil structure
T	temperature
TCA	Triaxial Compression Anisotropic
TCI	Triaxial Compression Isotropic
TEA	Triaxial Extension Anisotropic
Δt	travel time of the shear wave throughout the sample
USS	Ultimate Steady State
USSL	Ultimate Steady State Line
UT	undisturbed
V	initial frozen specimen volume

ΔV_c	volume change during consolidation
VCD	Volume Change Device
$\Delta V_{cons.}$	volume change during consolidation
$V_{exp.}$	volume of expelled water during freezing
$V_{initial}$	initial volume of sample
$\Delta V_{mem.}$	volume change due to membrane penetration
V_P	compression wave velocity
V_S	shear wave velocity
V_s	volume of dry mass (= W_s/G_s)
$\Delta V_{sat.}$	volume change during saturation and cell assembly
V_{Sl}	normalized shear wave velocity
ΔV_{thaw}	volume change during thawing and set up
W	initial frozen specimen weight
WP	Water Pluviation
W_s	final weight of dry soil
α_σ	inclination of σ_1 to the soil's vertical deposition direction
Γ	intercept of the USSL in e-lnp′ space at p′=1 kPa
ε_a	axial strain
ε_{amin}	axial strain at minimum strength
ε_v	volumetric strain
λ	wavelength
λ_{ln}	slope of the ultimate steady state line in e-lnp′ space
ρ	mass density of material
ρ_w	density of water
σ'_a	effective stress in the direction of wave propagation
σ'_p	effective stress in the direction of particle motion
σ'_c	effective stress in the direction perpendicular to a and p
σ'_h	effective principal stress in the horizontal direction
σ'_v	effective principal stress in the vertical direction
σ'_1	major principal effective stress
σ'_3	minor principal effective stress
τ_o	octahedral shear stress
ϕ'	mobilized friction angle
ϕ_{cv}	constant volume (steady state) friction angle
Ψ	state parameter

CHAPTER 1

INTRODUCTION

Liquefaction has been the topic of extensive geotechnical engineering research over the past 25 years. To evaluate the response of structures constructed with or on sandy soils, it is important to understand the soil behaviour at its in-situ state, and under appropriate loading conditions. The earthquakes in Niigata, Japan, and Alaska, USA in 1964 are certainly the events that focused world attention on the phenomenon of soil liquefaction. Since 1964, much work has been carried out to explain and understand liquefaction of cohesionless material. Terzaghi and Peck (1948) referred to the phenomenon of sudden or static liquefaction of very loose sands by minor triggering mechanisms as "spontaneous liquefaction", associated with flow slides. Several cases of liquefaction induced flow failures have been presented by Terzaghi (1956), Morgenstern (1967), Seed (1968), Schwarz (1982) and Chaney and Fang (1991). The recent, major earthquake in Kobe, Japan in 1995 has illustrated the significance and extent of damage caused by soil liquefaction. Liquefaction is also a design challenge for large sand structures, such as mine tailings impoundments, and earth dams.

Studies have concentrated on defining liquefaction as the condition where effective stresses approach zero due to undrained cyclic loading (Seed *et al.*, 1983). During monotonic undrained loading a loose sand can reach peak

resistance and then rapidly strain soften to a condition with constant resistance termed as steady state by Castro (1969).

Roscoe *et al.* (1958) and, Been and Jefferies (1985) showed that the large strain behaviour of a soil can be expressed in terms of its initial in-situ state relative to the ultimate steady state line at the same stress level. Therefore; the in-situ state of a sand defined by the void ratio and mean effective stress can be used to identify the large strain behaviour of sands.

The evaluation of in-situ state can be undertaken by either obtaining high quality undisturbed samples or by performing in-situ tests. Undisturbed samples of cohesionless soils can be difficult and expensive to obtain. Ground freezing is one method to attain high quality samples (Sego *et al.*, 1994; Yoshimi *et al.*, 1989).

The primary in-situ tests used to estimate geotechnical parameters for cohesionless soils are the Standard Penetration Test (SPT), and the Cone Penetration Test (CPT). Numerous empirical correlations exist to estimate the in-situ state of sands from penetration test results. Many of these correlations, are based on relative density, and are strongly influenced by soil compressibility (Robertson and Campanella, 1983).

One of the objectives of this research is to evaluate a procedure to estimate the in-situ state of sands using shear wave velocity measurements in laboratories and fields. Triaxial tests were carried out on reconstituted samples of Montana sand to develop a relationship between void ratio (e), mean normal effective stress (p′), and shear wave velocity (V_S). This relationship coupled with in-situ measurements of V_S, soil bulk density, K_o, and information regarding ground water conditions can be used to predict the in-situ state of a sand. The estimated in-situ state of a sand can then be compared to its ultimate steady state to predict the large strain response of the sand.

In addition to the in-situ state of sands, there are other factors governing the response of sandy soils. These factors include initial static shear stress (q_o),

direction of loading, and soil structure. Since much of our existing knowledge concerning liquefaction has come from laboratory studies, it is important that laboratory tests be conducted under the correct in-situ state of the sand and the appropriate direction of loading.

Soil behaviour has been found to be inherently anisotropic. There is evidence suggesting that the response of isotropically consolidated samples is different from that of anisotropically consolidated specimens (Vaid *et al.*, 1995a). However, most of the published data comes from isotropic tests on sands. Vaid *et al.* (1995a) also showed that there are different responses in compression and extension directions of loading.

An objective of this study is to conduct a laboratory testing program on reconstituted, and undisturbed samples of Syncrude and Fraser River sand to investigate the effect of anisotropic consolidation, and directions of loading. Since all the available data on anisotropic behaviour of sands were obtained from laboratory tests on dense or medium loose samples, the reconstituted specimens in this research were tested under "very loose" states. Undisturbed specimens were also tested under their in-situ states to compare their behaviours with those of reconstituted samples, and evaluate the effect of soil structure, as well. Ultimately, the effect of "initial state" was investigated when the results of testing the reconstituted and undisturbed samples were shown together. Shear wave velocities were measured at the end of consolidation of undisturbed samples to compare them with the in-situ V_S measurements.

Thesis Outline

Chapter two of this thesis presents information on Liquefaction phenomena, its terminology, and different types of liquefaction failures. The chapter also provides background information for the description of sand behaviour within the frame work of Critical State Soil Mechanics. Ultimate steady state concepts including USSL, USS parameter, and collapse surface concepts are reviewed. The application of shear wave velocity measurement, and the evolution of bender element technology are discussed. The development of the equation that defines the contractive/dilative boundary for a sand at large strains is included in this chapter. This equation is expressed in terms of soil constants which were obtained in this study.

The third chapter provides information regarding the material tested, and the experimental work carried out in this research. Different types of triaxial tests undertaken in this study are introduced. The chapter also describes the triaxial testing setup, and shear wave velocity measuring system. Sample preparation method, and void ratio calculation procedures for both reconstituted and undisturbed samples are thoroughly discussed.

Chapter four presents the test results obtained from this research. The shear wave velocity parameters, USS parameters, and the resulted e-p′-V_S relationship for Montana sand are introduced in this chapter. The results form anisotropically consolidated tests (compression and extension) on reconstituted, and undisturbed samples of Syncrude sand, and Fraser River sand are presented. The stress paths, and stress-strain plots from the shearing results are also shown.

The discussion and analyses of the results are presented in chapter five. The contractive/dilative boundary in V_S-σ'_v plot, and the flow liquefaction evaluation procedure for Montana sand are introduced. The influence of K_o is

studied, as well. The effect of static shear, direction of loading, and initial state on Syncrude sand and Fraser River sand are investigated in this chapter. The results of triaxial tests on undisturbed frozen specimens are compared with those of reconstituted samples. The results from this study, and other available data were combined to develop the Response Charts. The charts are used to link the in-situ state of a sand to Response Parameters, namely brittleness index (I_B), minimum undrained shear strength (S_{min}), and axial strain at minimum shear strength (ε_{amin}).

The summary and conclusions are presented in chapter six. The recommendations for future studies are also included in this chapter.

Appendix A describes the triaxial testing procedure for reconstituted samples in more details.

CHAPTER 2

LITERATURE REVIEW

2.1 Liquefaction Phenomena

Liquefaction of sands is a major problem in the areas of earthquake loading, and for the design of mine tailings and earth dams. The liquefaction phenomena involves excessive deformation of saturated soils under either **monotonic** or **cyclic** loading conditions. The collapse of a saturated sand structure is so rapid that the generated excess pore pressure does not have a chance to dissipate.

2.1.1 Critical State Soil Mechanics Concepts

In the frame work of Critical State Soil Mechanics, a state of a soil can be represented by a point in the three dimensional space of void ratio (e), mean effective normal stress (p′), and deviatoric stress (q). In this space, state boundaries separate states that an element of soil can or can not achieve. The state of a cohesionless soil can be loose or dense of the ultimate steady state. When loaded in shear, a loose soil contracts to reach its ultimate steady state and a dense soil dilates to ultimate steady state. Therefore, loose deposits of sands

may go through large deformations when sheared in undrained loading, and are generally more critical from design and stability point of view.

The concept of critical state soil mechanics was first introduced for clays by Roscoe *et al.* (1958). They described that void ratio (e), mean effective normal stress ($p'=(\sigma'_1+2\sigma'_3)/3$), and deviator stress ($q=\sigma'_1-\sigma'_3$) are uniquely related at critical state. Based on this concept, the states in which samples can or can not exist are separated by a surface that is called the State Boundary Surface (SBS) or the Roscoe surface (Figure 2.1). Normally consolidated clays have a stress state on this surface and over consolidated clays have a state inside this surface. Research has shown that there is a line in this space that all samples will reach when sheared to large strains (Roscoe *et al.*, 1958).

Castro (1969) applied the concept of critical state soil mechanics to cohesionless material. The application of critical state soil mechanics to sands was less successful, mainly because there appears to be no unique normal consolidation line for these materials and evaluations of the critical state line for sands was problematic. Castro showed that loose samples of sand under undrained monotonic loading will reach a peak strength and then will strain soften to their ultimate steady state with a constant resistance. Castro also showed that steady state is only a function of void ratio. Figure 2.2 shows a schematic of the state boundary surface for very loose, contractive sands. Also in this figure undrained stress paths are shown.

2.1.1.1 Ultimate Steady State Concept

The **steady state** of a sand is defined by Poulos (1981) as follows:

"*The steady state of deformation for any mass of particles is that state in which the mass is continuously deforming at constant volume, constant normal effective stress, constant shear stress, and constant velocity. The steady state of*

deformation is achieved only after all particle orientation has reached a statistically steady state condition and after all particle breakage, if any, is completed , so that the shear stress needed to continue deformation and the velocity of deformation remain constant."

Steady state has traditionally been measured using undrained triaxial tests on loose sand samples. **Critical state** has been defined as the state at which a soil continues to deform at constant stress and constant void ratio (Roscoe *et al.*, 1958). Been *et al.* (1991) showed that the critical and steady state are equal for sands and independent of stress path, sample preparation method and initial density. The critical or steady state is thus an ultimate state to which the sample will go after large strains under monotonic loading.

Castro *et al.* (1982) have reported no significant difference between results from stress-controlled and strain-controlled tests. Also data presented by Schimming *et al.* (1966), and Hungr and Morgenstern (1984) support the supposition that the behavior of sands is independent of strain rate. Therefore, "critical state" and "steady state" are the same for sands.

The critical or steady state of a soil will be referred to as Ultimate Steady State (USS) in this thesis.

2.1.1.2 Ultimate Steady State Line (USSL)

Based on critical state concepts for sands, there is a line in e-p′-q space that all sands will reach after being loaded in shear to their ultimate state at large strains. This line is referred to as Ultimate Steady State Line (USSL). The location of this line in e-p′-q space and its projections on different planes are shown in Figure 2.3.

Critical State Soil Mechanics concepts imply that a soil is either dilative or contractive to failure depending on the state of the soil relative to the ultimate

steady state line. The state of a sand is the description of the physical conditions under which it exists. Void ratio (or density) and stresses are the main state variables for soils. In addition to void ratio and effective stresses, several other factors may also influence the response of a sand, including direction of loading, (for example compression or extension), soil structure (i.e. fabric, aging, cementation), grain characteristics, and initial deviatoric stress (q_o). These factors are shown in Figure 2.4.

Been and Jefferies (1985) introduced the concept of state parameter to describe the state of a sand. The difference between the initial in-situ void ratio and the void ratio at ultimate steady state at the same mean normal effective stress is termed the **State Parameter (Ψ)**. Figure 2.5 shows that a sand with a state above the USSL (positive state parameter) will contract at large strains to its ultimate steady state, however a sand with a state below the USSL (negative state parameter) will dilate at large strains to reach the USS. Therefore, the ultimate steady state line represents a boundary between contractive and dilative behaviour at large strains. Roscoe and Poorooshasb (1963) reported that sand samples with the same state parameter will have similar response. Sladen *et al.* (1985) also showed that this hypothesis is valid for sands loose of steady state. The state of a sand can also be expressed in terms of p'_o/p'_{uss} (Figure 2.5) where p'_o is the mean effective normal stress at the start of shearing, and p'_{uss} is the value of p' at the same void ratio at ultimate steady state (Sladen *et al.*, 1985; and Fear *et al.*, 1995). Robertson and Fear (1995) refer to the ratio p'_o/p'_{uss} as the **Reference Stress Ratio (RSR)**. The state parameter (Ψ) and RSR are related by the slope of the ultimate steady state line (λ_{ln}) as follows:

$$\frac{p'_o}{p'_{uss}} = \exp\left(\frac{\Psi}{\lambda_{ln}}\right) = \text{Reference Stress Ratio (RSR)} \qquad [2.1]$$

The ultimate steady state line for sands is generally approximated by a straight line in an e-logp′ plot over a limited stress range. This is a reasonable approximation for sub-angular or subrounded quartz sands in the mean normal effective stress range of 10-700 kPa. However, the curvature of this line has been reported by Been *et al.* (1991). For mean stresses generally greater than 1000 kPa, the slope of the USSL is steeper. This is due to breakage of grains which results in a different load response. The slope of the USSL and the break point is dependent on the sand grain characteristics. The shape of the ultimate steady state line at stresses less than 10 kPa is difficult to determine experimentally. Test results by Tatsuoka *et al.* (1986) suggest that the USSL becomes flatter at low stress levels.

Been and Jefferies (1985) have shown that a unique USSL exists for a given sand which is independent of stress path, sample preparation or drainage conditions. Poulos *et al.* (1988) showed no effect of stress-controlled versus strain-controlled testing on the USSL for Syncrude tailings sand. Kuerbis *et al.* (1988) and Vaid *et al.* (1990) showed testing in extension resulted in a different steady state from compression testing. However, in their work they refer to steady state and phase transformation interchangeably.

2.1.1.3 Ultimate Steady State Parameters

In order to introduce ultimate steady state parameters, the three dimensional space of void ratio (e), mean effective normal stress (p′) and deviator stress (q) is shown on two planes in Figures 2.6 (a and b). The following definitions are used to describe triaxial testing results:

$$p' = \frac{1}{3} \times (\sigma'_v + 2\sigma'_h) \qquad [2.2]$$

$$q = \sigma'_v - \sigma'_h \qquad [2.3]$$

where;

σ'_v= effective principal stress in the vertical direction

σ'_h= effective principal stress in the horizontal direction

p′= mean normal effective stress

q= deviatoric stress

Figure 2.6a shows a plot of void ratio (e) against log p′ with an ultimate steady state line (USSL). A plot of normalized stress path (p'/p'_{uss} against q/p'_{uss}) is shown in Figure 2.6b. In this plot, USSL is seen as a point. Also in this figure, the constant volume friction angle (ϕcv) line or USSL is seen as the line that passes through the origin and steady state point with a slope of "M". The mobilized friction angle (ϕ') at USS is related to the slope of this line by the following relationships (Atkinson and Bransby, 1978):

$$M_C = \frac{6 \times \sin\phi'}{3 - \sin\phi'} \qquad \text{for compression tests} \qquad [2.4]$$

$$M_E = \frac{6 \times \sin\phi'}{3 + \sin\phi'} \qquad \text{for extension tests} \qquad [2.5]$$

where, M_C and M_E are the slopes of constant volume friction angle lines in compression and extension tests, respectively.

The mobilized friction angle at ultimate steady state is found to be a unique property for a given sand, and independent of initial void ratio, confining stress, anisotropic consolidation ratio (K_o), and the direction of loading (compression or extension) (Vaid and Chern, 1983; Vaid *et al.*, 1990a; Vaid and Thomas, 1995).

USS parameters are described as follows using these two plots:

Γ= the intercept of the USSL at p′=1 kPa in void ratio (e) against log p′ plot

λ_{log}= the slope of the USSL in void ratio (e) against log p′ plot

$M=q_{uss}/p'_{uss}$ (the slope of the USSL in p′-q plane)

2.1.1.4 Collapse Surface

Sladen *et al.* (1985) introduced the concept of "collapse surface". Their analyses of undrained triaxial tests suggest that there is a **"collapse surface"** in the three dimensional void ratio-shear stress-normal stress space. They showed that the peak points of the normalized stress paths for different states fall close to a straight line and that this line passes through the ultimate steady state point. In non-normalized stress paths, the position of these lines change with void ratio, while the slope remains essentially the same. Sladen *et al.* (1985) called this line the "collapse line" and since there are an infinite number of these lines in the space of p′-q-e, they form a surface which passes through the steady state line. This surface was termed a collapse surface (Figure 2.7). The collapse surface is not a state boundary surface as the post peak stress paths can pass slightly above it.

Sladen *et al.* (1985) reported that the slope of the collapse surface may be dependent on stress history. Data from Castro *et al.* (1982) on anisotropically consolidated samples suggests that the slope of collapse surface for anisotropically consolidated samples may be slightly higher than that of isotropically consolidated tests. Sladen *et al.* (1985) also showed that anisotropically consolidated samples fail almost immediately after being loaded in undrained conditions, and only a small amount of excess pore pressure is required to trigger their collapse. These samples have previously been loaded

under static condition (fully drained) and can have a state quite close to the collapse surface.

2.1.2 Liquefaction Terminology

There is some confusion in the literature about the definition and terminology of soil liquefaction. The definition of liquefaction given by Castro *et al.* (1982) was slightly modified by Sladen *et al.* (1985) as follows:

"Liquefaction is a phenomenon wherein a mass of soil loses a large percentage of its shear resistance, when subjected to monotonic, cyclic, or shock loading, and flows in a manner resembling a liquid until the shear stresses acting on the mass are as low as the reduced shear resistance."

It should be noted that up to the point of failure, loading can be either drained or undrained.

Cassagrande (1975) defined liquefaction as the flow of loose saturated sand. Seed (1979) described liquefaction as the condition of zero effective confining stress ($\Delta\sigma'_3=0$) under undrained cyclic loading. Ishihara (1993) defined liquefaction as the point when 5% double amplitude axial strain was reached during undrained cyclic loading.

Robertson (1994) summarized the behavior of sand in undrained loading. There are three major categories that can be used to define the response of cohesionless soils in undrained loading (Figure 2.8):

1) Strain softening response (ss)

2) Strain hardening response (SH)

3) Limited strain softening response (LSS)

In void ratio-mean effective normal stress (e-p′) space, a soil with an initial void ratio higher than the ultimate steady state (loose of steady state) will strain soften (ss) at large strains in undrained shear. Sladen and Oswell (1988)

termed this type of sand "very loose sand". Very loose sands are rarely used intentionally in civil engineering practice but they may exist as natural deposits or hydraulically placed fills in some construction activities. Very loose sands can experience flow liquefaction.

A soil with an initial void ratio lower than the ultimate steady state (dense of steady state) will strain harden (SH) in undrained shear to reach steady state at large strains. For a soil with an initial state higher than but close to the ultimate steady state, the response can be limited strain softening (LSS) to a quasi-steady state (QSS) (Ishihara, 1993), but eventually, at large strains, the response is strain hardening to its ultimate state. The effective stress path for a LSS behaviour shows an elbow which corresponds to the phase transformation from contractive to dilative responses. At this point, excess pore pressures stops increasing and start to decrease in response to the tendency for dilation.

If a soil slope or structure, such as an earth dam or tailings dam, is composed entirely of a strain softening soil, and if the in-situ gravitational shear stresses are larger than the ultimate steady state or minimum strength (i.e. relatively steep slope consisting of very loose sand), a catastrophic collapse and flow slide can take place if the soil is triggered to strain soften. Examples of flow liquefaction failures are Fort Peck dam (Casagrande, 1965), Aberfan flowslide (Bishop, 1973), Zealand flowslide (Koppejan *et al.*, 1948) and the Stava tailings dam. The trigger mechanism for a catastrophic flow slide can be either dynamic, such as earthquake loading, or monotonic loading. Sasitharan *et al.* (1994) have shown that undrained collapse can be triggered by certain types of drained monotonic loading such as a slow rise in ground water level.

A soil structure composed entirely of strain hardening material will not generally undergo undrained failure, unless the soil becomes looser due to pore water redistribution. If a soil structure is composed of strain softening and strain hardening soil and strain softening soil is triggered to collapse, a flow failure and slide may occur. This will occur only if, after stress redistribution

due to the softening of the strain softening soil, the strain hardening soil is unable to support the additional gravitational shear stresses. A flow slide will occur only if a kinimatically admissible mechanism can develop.

Robertson (1994) proposed a flow chart for the evaluation of liquefaction of sands. This flow chart is shown in Figure 2.9. In order to describe the type of liquefaction it is important to evaluate the material characteristics in terms of strain softening or strain hardening. For **flow liquefaction,** the in-situ shear stresses should be higher than the ultimate or minimum strength. Whether a slope or soil structure will fail and slide will depend on the amount of strain softening material relative to strain hardening soil within the structure, the brittleness of the strain softening soil, and the geometry of the structure. The resulting deformations of a soil structure with both strain softening and strain hardening soils will depend on factors such as distribution of soils, geometry, amount and type of loading, brittleness of strain softening soil, and drainage conditions.

For strain hardening materials, flow liquefaction will generally not occur, but during undrained cyclic loading, **cyclic liquefaction** is possible. When in-situ shear stresses are lower than the cyclic shear stress, shear stress reversal will take place, and if extensive shear cyclic loadings occurs, eventually a condition of zero effective stress can be developed. When a soil element reaches the condition of zero effective stress, the soil has very little stiffness and large deformations can take place during cyclic loading. However, when cyclic loading stops, the deformations essentially stop, except for those due to local pore pressure redistribution within the mass. The amount and extent of deformations during cyclic loading will depend on the density of the soil, the size and duration of cyclic loading, and the extent to which shear stress reversal occurs. Examples of cyclic liquefaction were observed during and after the major earthquakes in Niigata in 1964 and Kobe in 1995 in the form of sand

boils, lateral spreads, slumping of small embankments and ground surface cracks.

If in-situ gravitational shear stresses are higher than the cyclic shear stress, shear stress reversal may not take place, and it may not be possible to reach the condition of zero effective stress, and deformations will be smaller, i.e. **cyclic mobility** will occur. Deformations during cyclic loading will stabilize, unless the soil is very loose and flow liquefaction is triggered. The resulting movements are due to external causes, and occur only during cyclic loading.

If cyclic liquefaction occurs and drainage paths are restricted due to overlying less permeable layers, the sand near the surface can become looser due to pore water redistribution, resulting in possible subsequent flow liquefaction, given the right geometry.

Earthquake induced flow liquefaction movements tend to occur after cyclic loading due to the progressive nature of the load redistribution. However, if the soil is sufficiently loose and the static shear stresses are large enough, the earthquake loading may trigger essentially spontaneous liquefaction within the first few cycles of loading.

2.1.3 Monotonic Loading Behaviour

In monotonic loading, a **loose sand** when loaded to failure from its initial state, exhibits a continuous increase in pore pressure for undrained shear or a continuous decrease in void ratio for drained shear. During an **undrained test**, the void ratio remains constant and no volume change takes place. In a **drained test**, pore pressure does not change and volume changes take place. Shear stresses approach a constant value at a much higher stress levels relative to an undrained test with the corresponding constant volume (Been *et al.*, 1991).

A **dense sand**, under monotonic loading, shows a decrease in pore pressure when loaded in **undrained** shear or an increase in volume in **drained** loading. In an undrained test on a dense sand, pore pressure increases initially (initial contraction), but eventually decreases to a constant value (dilation) (Been *et al.*, 1991; Ishihara *et al.*, 1991).

Fabric can be an important factor influencing laboratory test results on sands. Vaid *et al.* (1995b) showed that moist tamped specimens have the most contractive (strain softening) responses. Air pluviated specimens are also strain softening, but to a smaller degree than moist tamped samples. In contrast, water pluviated specimens at the same void ratio and confining stress may exhibit a dilative response in triaxial compression.

Vaid *et al.* (1990) also suggested that significant differences in sand behavior occur in extension and compression loading due to inherent anisotropy in water pluviated samples. Alarcon-Guzman *et al.* (1988) argue that the initial anisotropy affects the response of a sand. Vaid *et al.* (1995a) showed that for isotropically consolidated water pluviated samples, the sand under undrained loading is strain hardening in triaxial compression, but strain softening in triaxial extension. They have also shown that static shear at constant confining stress promotes a more contractive response.

2.1.4 Brittleness Index

Bishop (1971) expressed the reduction in undrained shear strength in terms of a brittleness index, I_B. The definition of brittleness Index can be modified for compression and extension tests as follows (Fear *et al*, 1995);

a) triaxial compression

$$I_B = \frac{S_p - S_{min}}{S_p - S_o} \qquad [2.6]$$

b) triaxial extension

$$I_B = \frac{S_p - S_{min}}{S_p + S_o} \qquad [2.7]$$

where;

S_p= shear strength at peak ($q_p/2$)

S_{min}= minimum shear strength at ultimate steady state or quasi-steady state

S_o= static shear ($q_o/2$)

Work by Sladen *et al.*(1985) showed that undrained brittleness index of very loose sands is only a function of initial state defined by RSR= p'_o/p'_{uss}. Other researchers (Vaid *et al.*, 1995a) reported that brittleness index is a function of initial fabric, void ratio, confining stresses prior to shearing (i.e. p'_o), and stress path during undrained loading.

2.2 Shear Wave Velocity Measurement

The **small strain shear modulus (G_o)** is a fundamental soil parameter in many kinds of static and dynamic analyses involving deformation calculations. Torsional resonant column and cyclic torsional shear techniques are among the several laboratory methods that have been developed by Isenhower *et al.* (1987) to measure small strain shear modulus. Small strain shear modulus (G_o), also termed as the initial tangent shear modulus, is measured at strains generally less than 0.001% where measurements are in a linear elastic condition. Thus, G_o is independent of strain amplitude.

Since shear wave velocity can be measured in the field, and in the laboratory, there is an increasing interest in using shear-velocity to define the state of a soil. In the field, shear wave velocity can be measured by intrusive methods such as the Seismic Cone Penetration Test (SCPT) (Robertson *et al.*, 1986). Shear wave velocity is obtained by measuring the travel time of the wave over a known distance.

As the shear wave travels, particle motion occurs perpendicular to the direction of wave propagation. Thus, based on elastic theory, V_S can be related to small strain shear modulus (G_o) by the following relationship:

$$G_o = \rho \times V_S^2 \qquad [2.8]$$

where;

G_o= small strain shear shear modulus

ρ= mass density of the material

V_S = shear wave velocity

A similar procedure can be used for compression wave measurements (V_P) in the laboratory and the field. Compression waves involve no deformation perpendicular to the direction of wave propagation.

Hardin and Black (1968) showed that the small strain shear modulus is controlled by the following factors:

$$G_o = f(p', e, H, S_r, \tau_o, C, f, t, S_s, T) \qquad [2.9]$$

where:

p'= mean effective normal stress

e= void ratio

H=ambient stress history

S_r= degree of saturation

τ_o= octahedral shear stress

C= grain characteristics (shape, size, mineralogy, grading)

f= frequency of vibration

t= secondary effects that are functions of time and secondary loading

S_s= soil structure

T= temperature

Shear wave velocity is controlled primarily by void ratio, effective stresses, the grain characteristics (grain size distribution, grain shape, angularity, surface roughness, and mineralogical composition), and the soil structure (fabric, interparticle forces, and bounds). Unless significant grain crushing occurs, the intrinsic characteristics of the soil do not change with alterations in void ratio and effective confining stresses, although the soil structure can vary somewhat. (Robertson *et al.*, 1995).

De Alba *et al.* (1984) showed that for dense sands, the soil fabric created using different methods of sample preparation can affect shear wave velocity measurements. This is because of the orientation of sand particles and the distribution of normal contacts among them. Sasitharan *et al.* (1994) showed that for loose sands, soil fabric has only a small influence on shear wave velocity.

Using resonant column test results, Hardin and Richart (1963) proposed a relationship between V_S, e and p' in a general form of :

$$V_S = (m_1 - m_2 \times e)(p')^{0.25} \qquad [2.10]$$

Shear wave velocity constants, m1 and m2, are constant values for each soil and can be determined from laboratory studies. This equation was based on isotropically consolidated test results. A more general equation was suggested by Roseler (1979) using individual stresses in the direction of wave propagation and particle motion. Roseler found that these individual stresses control shear wave velocity. He proposed the following equation:

$$V_S = (m_1 - m_2 \times e)\,(\sigma'_a)^{na}\,(\sigma'_p)^{nb} \qquad [2.11]$$

where;

σ'_a = the effective stress in the direction of wave propagation

σ'_p = the effective stress in the direction of particle motion

na, nb, m_1 and m_2 are constants.

Yu and Richart (1984) and Stokoe *et al.* (1985) showed that the exponent m_a and m_b are generally close to 0.125.

For isotropic consolidation, these stresses are equal to the mean effective normal stress (p'), thus the following relationship applies:

$$\sigma'_a = \sigma'_p = \sigma'_c = p' = \text{mean effective normal stress}$$

where; σ'_c = the effective stress in the direction perpendicular to a and p

Robertson *et al.* (1992) suggested a normalized shear wave velocity given by:

$$V_{S1} = V_S\,(P_a/\sigma'_v)^{0.25} \qquad [2.12]$$

where:

V_{S1}= normalized shear wave velocity

V_S= shear wave velocity

P_a= atmospheric stress; typically 100 kPa

σ'_v= effective overburden pressure

Based on CPT and in-situ shear wave velocity measurements, Robertson *et al.* (1992) suggested a critical value of V_{S1} between 140 to 160 m/s, that separates contractive behavior from dilative behavior at large strains in clean, young, uncemented sands.

Equation [2.12] assumes that the coefficient of earth pressure at rest (K_o) equals unity. Hence, this equation should be modified as follows:

$$V_{S1} = V_S (P_a/\sigma'_v)^{0.25} (1/K_o)^{0.125} \qquad [2.13]$$

The normalization of shear wave velocity can also be done with respect to the mean effective normal stress (p′) for isotropic consolidation using the following relationship:

$$V_{S1} = V_S \times (P_a/p')^n \qquad [2.14]$$

where;

p′= mean effective normal stress (kPa)

n= stress exponent; typically n=0.25

2.2.1 Bender Element Technology:

Lawrence (1963) described one of the first applications of piezoelectric transducers in shear wave testing in sands, and later clays (Lawrence, 1965). He

used shear-plate transducers housed in the base pedestal and the top cap of a triaxial set up. Shirley and Anderson (1975) used bender transducers that were able to generate and detect shear wave. Bender transducers have been preferred to shear-plate transducers in recent work. De Alba *et al.* (1984) used bender elements that were incorporated in the ends of a triaxial testing device to relate shear wave velocity to liquefaction potential of saturated sands in cyclic triaxial tests. Dyvik and Madshus (1985) and Dyvik and Olsen (1991) measured shear wave velocity using bender elements in several geotechnical test devices such as triaxial cell, oedometer and direct simple shear. They also used a resonant column device to measure G_o, and compared these results with those obtained from bender elements, and found that these two shear moduli agree quite well with each other within the range of G_o from 5 to 140 MPa.

Using bender elements to measure shear wave velocity, is a sonic technique utilizing direct-transmission measurement. In this method, an elastic wave is generated by a piezoelectric transducer which is received by another piezoelectric transducer. A piezoelectric material is a material which generates electrical output when subjected to mechanical deformation or vice versa. The transducers for industrial applications, are often made of ceramic such as lead zirconate titanate, barium titanate and lead titanate (Brignoli *et al.*, 1995).

These transducers can be placed on both ends of a specimen (top cap and bottom pedestal in a triaxial testing device) and by measuring the distance between the two transducer (L), and the time required by the wave to travel this distance (t) the propagation velocity, V_S can be calculated.

2.2.2 The e-p′-Vs Relationship

Cunning (1994) showed the general relationship between normalized shear wave velocity (V_{Sl}) and void ratio can be expressed in a the form of:

$$V_{SI} = A - B \times e \qquad [2.15]$$

where:

A= the intercept of the V_{SI}-e relationship at e=0 (m/s)

B= slope of the V_{SI}-e relationship (m/s)

By substituting V_{SI} from equation [2.14] into equation [2.15], the following e-p′-V_S relationship can be developed for isotropic condition:

$$V_S = (A - B \times e) \times (p'/P_a)^n \qquad [2.16]$$

By making the following substitutions;

P_a= 100 kPa

n= 0.25

the final form of the equation will be:

$$V_S = (A - B \times e) \times (p'/100)^{0.25} \qquad [2.17]$$

Shear wave velocity parameters (A and B) can be determined from isotropic laboratory test results for each soil.

By using this relationship, and shear wave velocity measurements from the field, the in-situ void ratios can be estimated for uncemented, unaged sands, when stress conditions in the ground are known. The bulk density of the soil, ground water condition, and K_o are required to estimate the effective stress conditions in the ground.

Ultimate steady state parameters and then, the location of USSL in e-logp′ space can be determined from shear loading results. The in-situ state of the sand can be evaluated by plotting the field void ratios with respect to the USSL. Therefore; the large strain response of the sand can be estimated.

2.2.3 Using e-p′-V_S Relationship to Evaluate Flow Liquefaction:

To evaluate the susceptibility of a sand deposit for flow liquefaction the first step is to determine if the response of the soil under large strain is contractive or dilative. For contractive sands (strain softening), flow liquefaction is possible, however for dilative sands (strain hardening) flow liquefaction is not expected, but cyclic liquefaction or cyclic mobility should be investigated.

Since the ground condition is not isotropic, but anisotropic, a general relationship for e-p′-V_S is required to determine the contractive/dilative boundary of the soil deposit. This general form can be expressed as follows by using different stress exponents for individual stresses (Sasitharan, 1994; Robertson *et al.*, 1995):

$$V_S = (A\text{-}B\times e)\times(\sigma'_a/P_a)^{na}\times(\sigma'_p/P_a)^{nb} \qquad [2.18]$$

where:

$\sigma'_a = \sigma'_v$ = axial or vertical effective stress (kPa)

$\sigma'_p = \sigma'_h$ = horizontal effective stress (kPa)

This can be reduced with the introduction of coefficient of earth pressure at rest (K_o),

$$K_o = \sigma'_h/\sigma'v \qquad [2.19]$$

which gives the following form:

$$V_S = (A\text{-}B\times e)\times(\sigma'_v/P_a)^{na+nb}\times(K_o)^{nb} \qquad [2.20]$$

State parameter can describe the contractive or dilative response of the soil, and is given by:

$$\Psi = e - e_{uss} \qquad [2.21]$$

where:

e = in-situ void ratio

e_{uss} = void ratio at the ultimate steady state at the same stress level (Figure 2.5)

The equation of steady state line gives:

$$e_{uss} = \Gamma - \lambda_{ln} \times \ln(p'_{uss}) \qquad [2.22]$$

Combining the equations [2.21] and [2.22]:

$$\Psi = e - [\Gamma - \lambda_{ln} \times \ln(p'_{uss})] \qquad [2.23]$$

By rearranging equation [2.20], void ratio (e) can be written as:

$$e = \frac{A}{B} - \frac{V_{S\times}(P_a)^{na+nb}}{B(\sigma'_v)^{na+nb} \times (K_o)^{nb}} \qquad [2.24]$$

Substituting equations [2.22] and [2.24] into equation [2.21]:

$$\Psi = \frac{A}{B} - \frac{V_{S\times}(P_a)^{na+nb}}{B(\sigma'_v)^{na+nb} \times (K_o)^{nb}} - [\Gamma - \lambda_{ln} \times \ln(p'_{uss})] \qquad [2.25]$$

On the other hand p'_{uss} can be written in terms of σ'_v and K_o:

$$p'_{uss} = \frac{1}{3}(\sigma'_v + 2\times\sigma'_h) = \frac{\sigma'_v}{3}\times(1+2\times K_o) \qquad [2.26]$$

Substituting equation [2.26] into equation [2.25]:

$$\Psi = \frac{A}{B} - \Gamma - \left\{ \frac{V_S \times (P_a)^{na+nb}}{B\times(\sigma'_v)^{na+nb}(K_o)^{nb}} - \lambda_{ln}\times \ln\left[\frac{\sigma'_v}{3}(1+2K_o)\right]\right\} \qquad [2.27]$$

At the contractive/dilative boundary of sand $\Psi=0$. Applying this condition to the equation [2.27] and rearranging, it gives the following relationship for contractive/dilative boundary:

$$(V_S)_{\Psi=0} = \{A - B \times [\Gamma - \lambda_{ln}\times\ln(\sigma'_v\times(1+2\times K_o)/3)]\}\times(\sigma'_v/P_a)^{na+nb}\times(K_o)^{nb} \qquad [2.28]$$

making the following substitutions:

P_a =100 kPa

na=nb=0.125

results in the following equation:

$$(V_S)_{\Psi=0} = \{A - B\times[\Gamma - \lambda_{ln}\times\ln(\sigma'_v\times(1+2\times K_o)/3)]\}\times(\sigma'_v/100)^{0.25}\times(K_o)^{0.125} \qquad [2.29]$$

It can be seen that $(V_S)_{\psi=0}$ is a function of effective vertical overburden, K_o, and material constants, A, B, Γ, and λ. Four soil constants can be obtained by laboratory testing. By estimating K_o value and plotting V_S against σ'_v, the boundary between contrantive and dilative behavior can be shown. Thus, by measuring in-situ shear wave velocities and knowing the effective vertical

stress, the state of the soil can be estimated. This approach is only applicable to sands that are unaged, and uncemented, since aging and cementation also influence the shear wave velocity measurements.

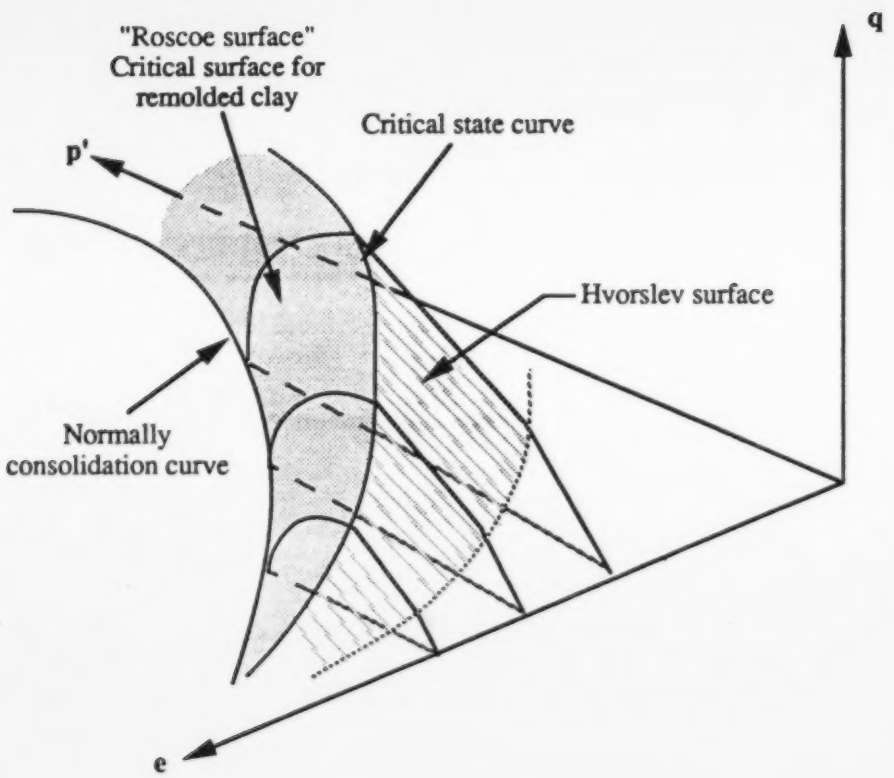

FIGURE 2.1 State Boundary Surface for Remolded Clay
(after Sasitharan, 1994)

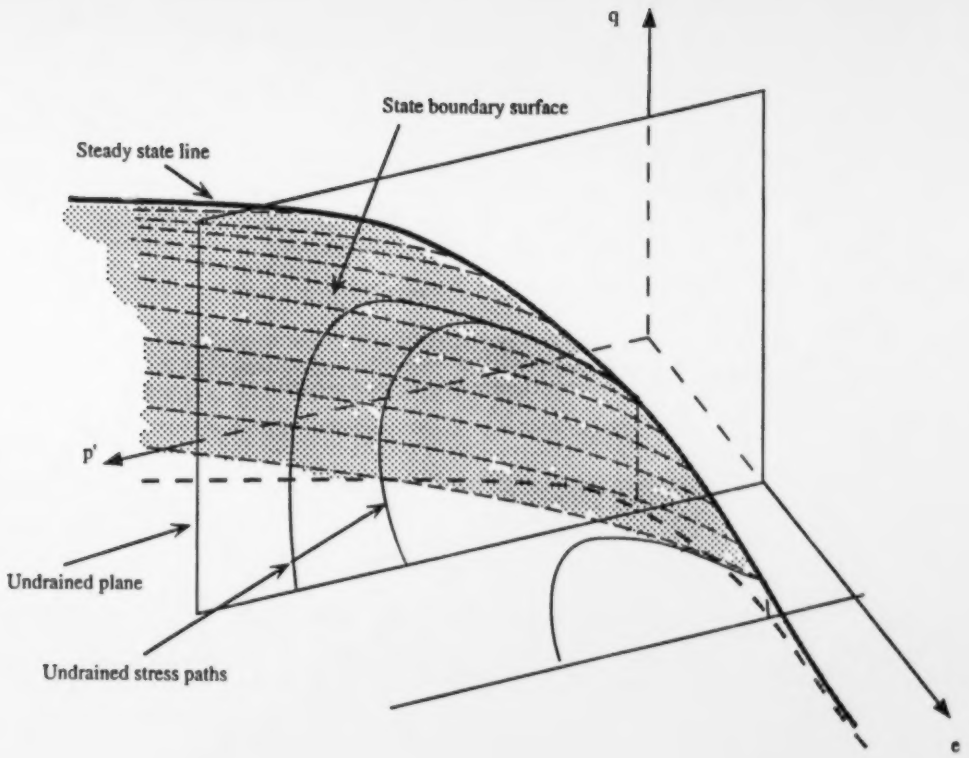

FIGURE 2.2 Schematic of State Boundary Surface for Very Loose Sand (after Chillarige, 1995)

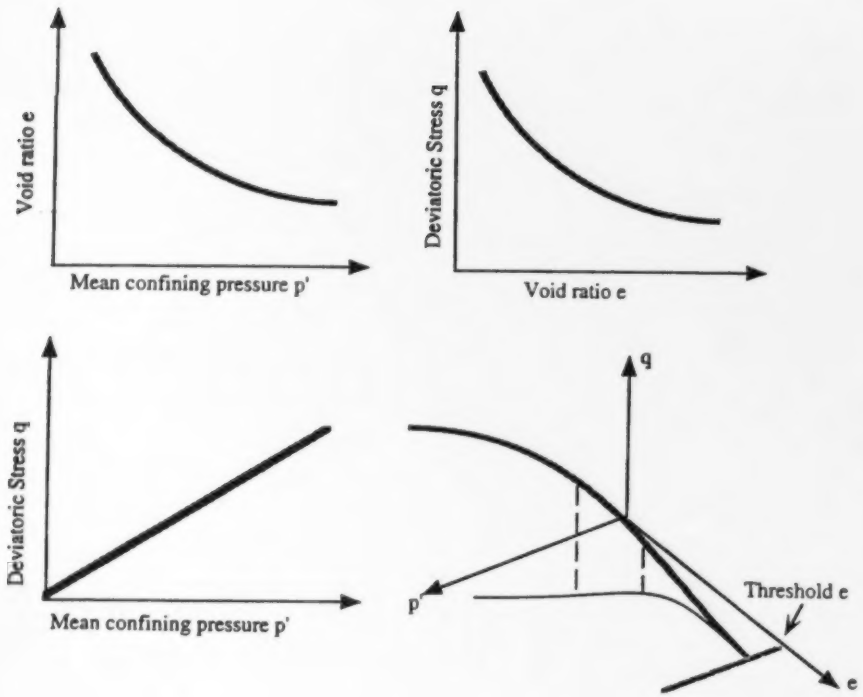

FIGURE 2.3 Ultimate Steady State Line along with the Projections on e-p′, q-e, and q-p′ Planes (after Chillarige, 1995)

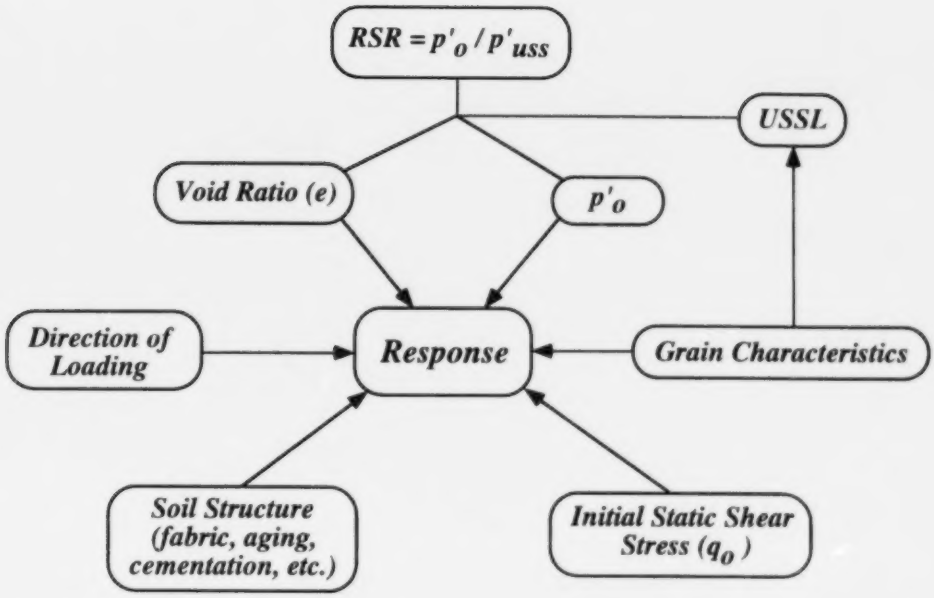

FIGURE 2.4 Factors Influencing the Undrained Monotonic Response (after Fear *et al.*, 1995)

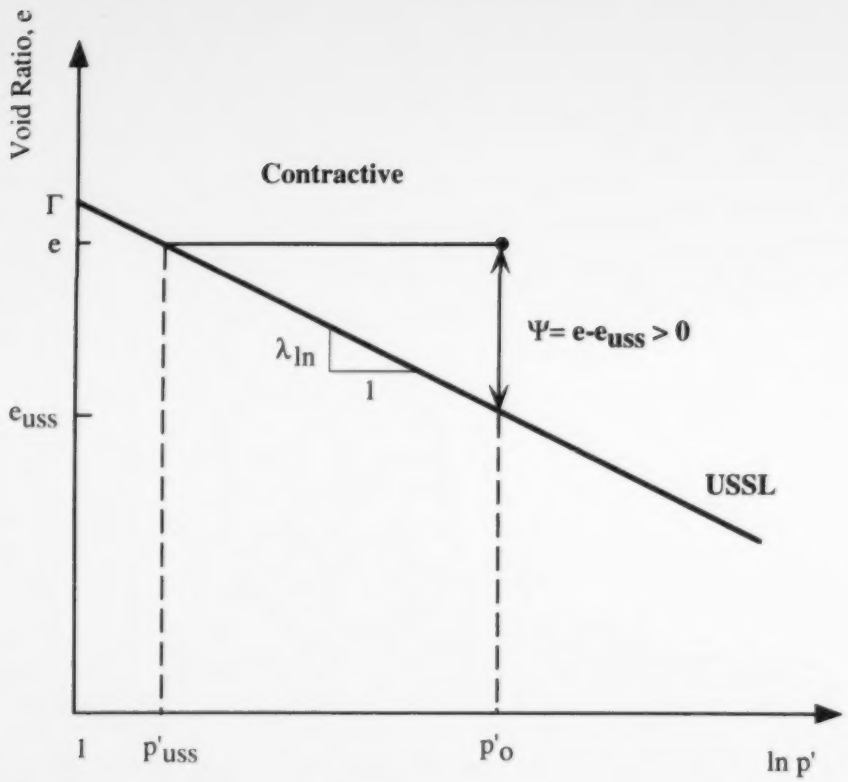

FIGURE 2.5 Relationship between State Parameter (Ψ) and soil behaviour

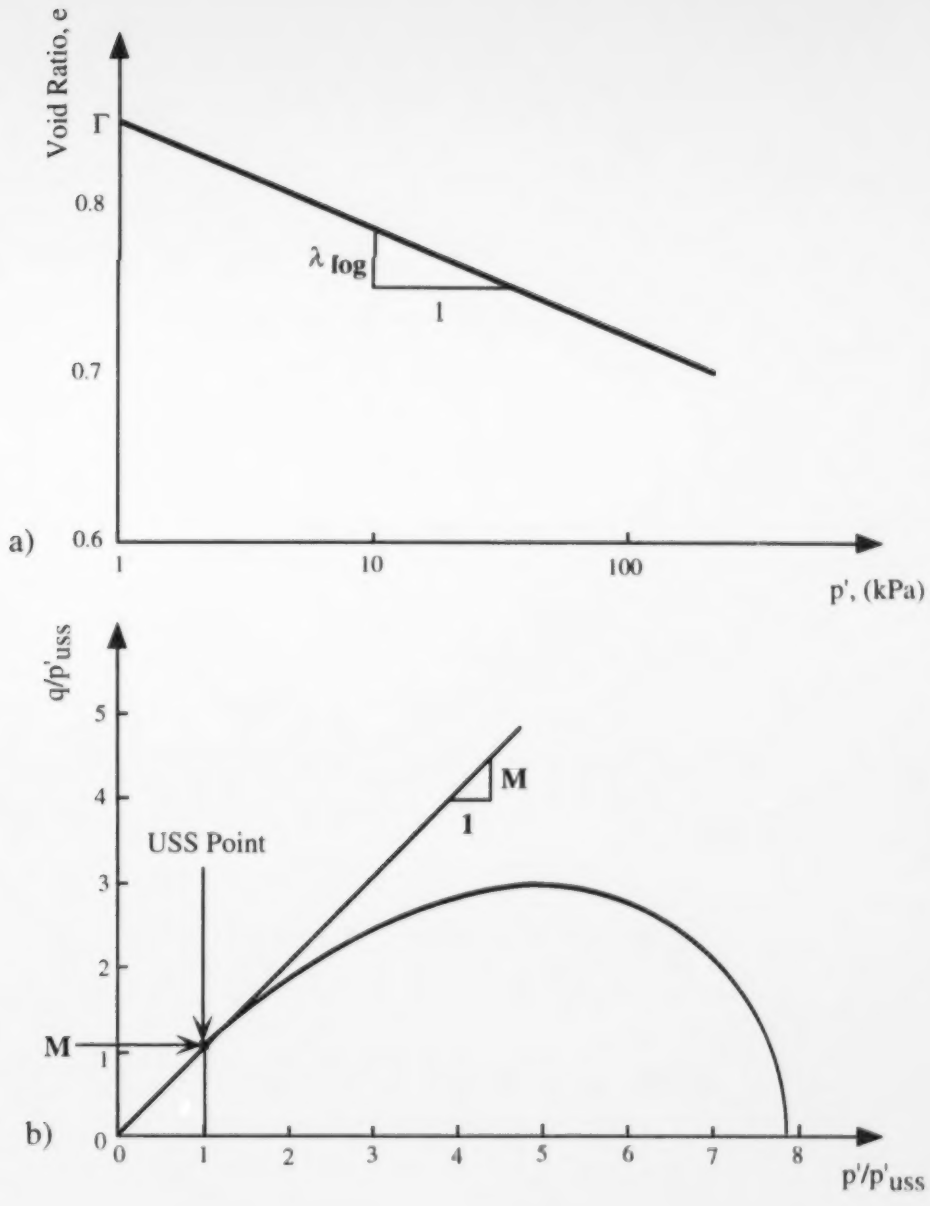

FIGURE 2.6 Definitions of USS parameters

a) e-log p' space

b) normalized stress path

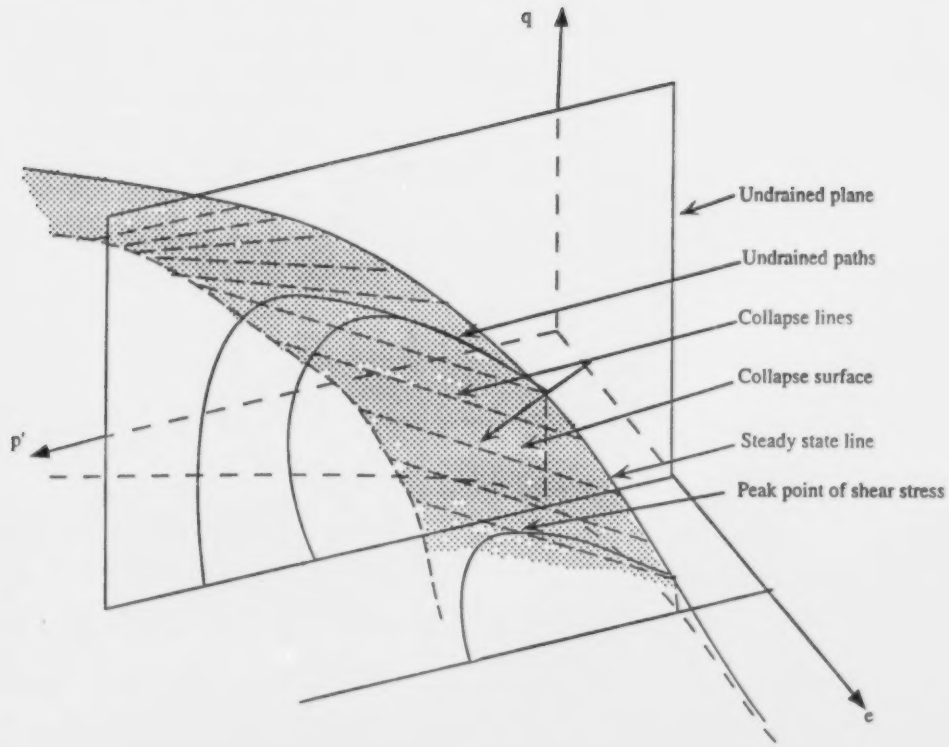

FIGURE 2.7 Collapse Surface in e-p′-q Space (Sladen *et al.*, 1985)

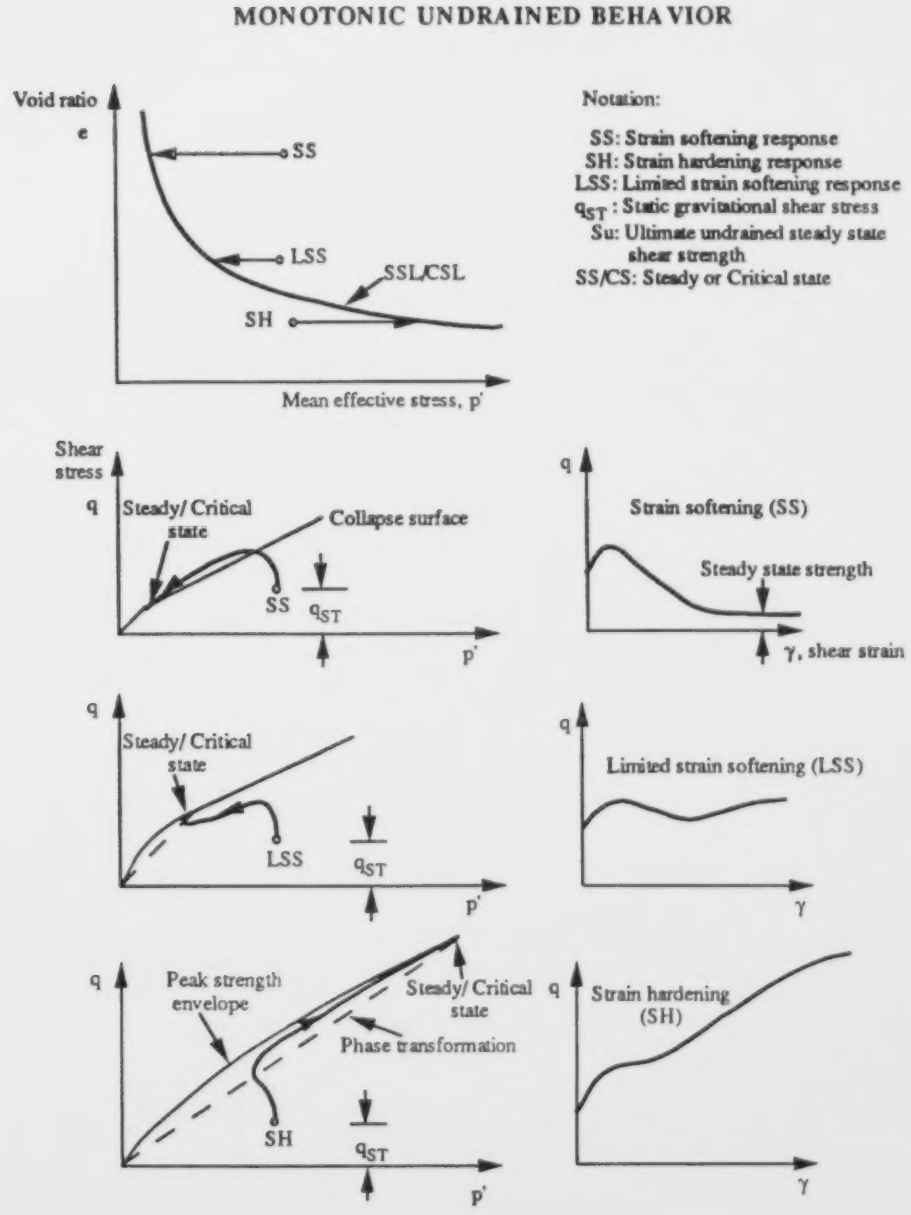

FIGURE 2.8 Schematic of Undrained Monotonic Behaviour of Sand in Triaxial Compression (after Robertson, 1994)

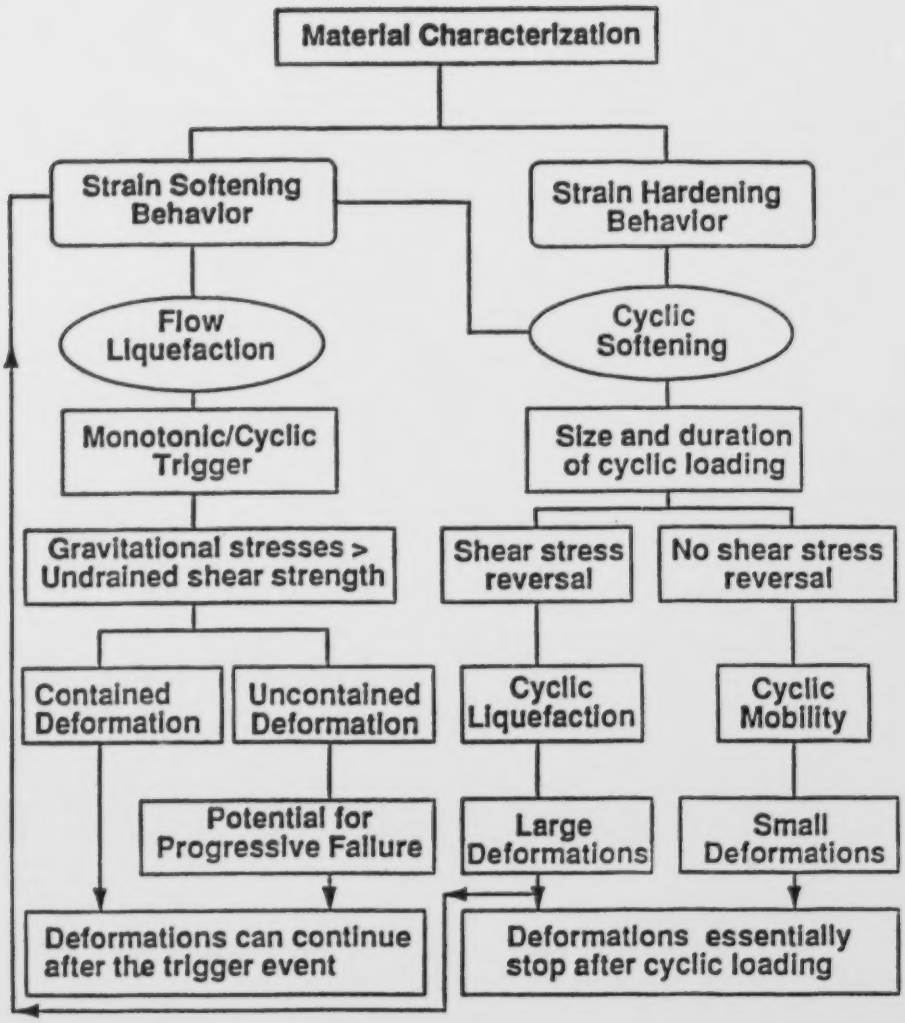

FIGURE 2.9 Suggested Flow Chart for Evaluation of Soil Liquefaction (after Robertson, 1994)

CHAPTER 3

EXPERIMENTAL WORK

3.1 Material Tested

Three different kinds of sands were tested in this study: Montana Sand (MS), Syncrude Sand (SS), and Fraser River Sand (FS).

3.1.1 Montana Tailings Sand

A laboratory testing program has been carried out to determine the parameters in equation [2.29] for Montana tailings sand. The sand is a uniform, rounded to subrounded sand with a specific gravity (G_s) of 2.62, and estimated maximum and minimum void ratio of 0.85 and 0.51, respectively, using ASTM D2049. The grain size distribution curve for this sand using wet sieve analysis is shown in Figure 3.1. The fines content (<74μm) is about 20% and the mean grain size (D_{50}) is 0.17 mm. C_u (coefficient of uniformity) and C_c (coefficient of curvature) are 3.8 and 0.95, respectively for Montana sand. The sand has a D_{20}=0.07 mm.

3.1.2 Syncrude Tailings Sand

Syncrude sand is a natural sand from the open pit mine at the Syncrude Canada Ltd. tailing storage facility near Fort McMurray, Alberta. The tailings

sand is the result of oil extraction from natural oil sand and is used to hydraulically construct the containment dykes and supporting beaches of the storage facility. Syncrude sand is a fine, uniform, angular to subangular sand with traces of silt and clay. It has a specific gravity of 2.64 and maximum and minimum void ratio of 1.07 and 0.632, respectively using ASTM D2049. The material is composed of quartz (95%), feldspar (2%), amphibole (1%), pyrite (1-2%), and muscovite (1%) (Sladen and Handford, 1987). For Syncrude sand, C_u=2.86 and C_c= 1.21. The mean grain size (D_{50}) is 0.18 mm and D_{20}= 0.09 mm. The sand has about 12% fines content. The grain size distribution of this sand is shown in Figure 3.2.

Reconstituted and undisturbed samples of Syncrude sand were tested in this study.

3.1.3 Fraser River Sand

Triaxial tests were performed on reconstituted and frozen samples of sand from Fraser River (Massey Tunnel) near Vancouver, British Columbia. The sand underlies the Fraser delta, which is a region of high seismicity. It is a uniform gray colored sand with subangular to subrounded particles. The material composition is 40% quartz, quartzite and chert, 11% feldspar, 45% unstable rock fragments (mainly volcanics), and 4% miscellaneous detritus (Thomas, 1992). The specific gravity of this sand is 2.68 and maximum and minimum void ratio are 1.102 and 0.715, respectively in accordance with ASTM D2049. The grain size distribution is shown in Figure 3.3. The sand has about 3% fines content. Fraser River sand has C_u= 2.17, and C_c= 1.04. The mean particle size (D_{50}) is 0.23 mm, and D_{20}= 0.16 mm.

3.2 Testing Apparatus

A modified triaxial apparatus was used for laboratory testing in this study. A Wykeham Farrance loading frame was used for loading the samples in shear. For Isotropically Consolidated (IC) tests the main modification of the triaxial cell was the incorporation of bender elements in the load head and the base of the cell for the measurement of V_S. As well, modifications were done to the loading frame to add dead weights to the loading ram to compensate for not having the cell pressure acting on the load head over the ram rod area. The modification to the cell included a top cap to allow the cell to be assembled with minimum disturbance to the sample. A schematic diagram of the test set up for IC tests is shown in Figure 3.4.

For Anisotropically Consolidated (AC) tests (compression and extension), the former set up was changed and some additional equipment was added for consolidating the samples along the K_o line. These included a Double Acting Piston (DAP), and a pressure regulator to apply vertical load through the DAP and also an External Load Cell (ELC) for measuring the applied load more accurately.

The DAP was saturated with oil instead of air, because oil is an incompressible liquid. By locking the valves on the DAP at the start of loading, no movement at the load head (top of the sample) will occur if the DAP container is properly saturated. As a result, the sample can be loaded at a pre-selected strain rate using the loading frame after the application of an initial deviatoric stress.

However, to avoid any kind of movement during loading (probably because of the existence of some air bubbles in DAP container) a Supporting Frame (SF) was added to the top portion of the set up. The SF consists of two vertical rods and a horizontal plate surrounding the ELC. It was used

successfully in both compression and extension direction of loading to give extra support when shearing the sample. Eight restricting nuts were used to keep the SF rigid and stable.

For consolidating the sample under K_o condition (K_o<1.0), the vertical stress is higher than the horizontal stress. Thus, a higher vertical force is required compared to isotropic consolidation. Such a high force can not be achieved by adding dead loads on top of the loading ram, therefore; the DAP system was employed and worked quite well. The calculated vertical force was applied by a pressure regulator, and measured accurately by a pressure transducer. During consolidation, the vertical load applied on the sample was measured by the ELC and this force was found to be always a few kilograms less than the initial measured force based on the regulator and the corresponding transducer. This loss of force was the result of the friction in the DAP system, specifically the friction between the ram and the container. Thus, the applied initial force was a few kilograms higher than the calculated vertical force to compensate for the friction loss in the system. A schematic diagram of the test equipment for AC tests is shown in Figure 3.5.

The axial force used to calculate the deviatoric stress (q) during shearing was measured by an Internal Load Cell (ILC). This load cell was in the triaxial cell, therefore; no correction was required for the friction of the loading ram rod.

Consolidation of the samples was performed by a gradual increase in cell pressure and vertical stress. The readings on the ILC are effected by any change in cell pressure therefore; the ILC was not employed to measure the axial force for anisotropic consolidation.

All tests in this research were strain controlled tests. The gearing system in the loading frame maintains the axial strain rate constant regardless of the load.

One of the objectives of this research was to develop the e-p′-V_S relationship for Montana sand. Bender element technology was used to measure

shear wave velocity. The initial bender element system was developed using single protruded benders incorporated in the loading head and the base pedestal (Sasitharan, 1994). This system was modified and flush mounted bender elements were developed mainly for testing frozen undisturbed samples (Cunning, 1994). As a part of this study, the flush mounted system was modified to make it more appropriate for testing undisturbed-frozen, and reconstituted samples.

Cell pressure, pore pressure, back pressure, and also initial vertical force were measured using electronic pressure transducers. A Linear Voltage Displacement Transducer (LVDT) was used for the measurement of axial displacement. Volume change during consolidation and drained loading was measured by electronic Volume Change Device (VCD). This device consists of a cylinder with a moving internal diaphragm. When the volume changes in the saturated sample, the diaphragm is displaced upwards or downwards, depending on the orientation of the valve on the front. The movements of the diaphragm is recorded by a LVDT attached to it. By calibrating the LVDT to the volume change of the cylinder, accurate volume changes in the sample can be measured.

Axial force during shearing was measured by the ILC for both IC and AC tests, and axial load during anisotropic consolidation was measured by the ELC.

All transducers, load cells, LVDT and VCD were coupled to a data acquisition system interfaced with a microcomputer. All data were recorded by a Fluke 2400 data logging system and stored in an IBM computer.

3.3 Sample Preparation Method

3.3.1 Reconstituted Samples

The reconstituted soil samples in this research were prepared by moist tamping method to obtain the loosest state. In order to achieve such a loose structure prior to shearing, it was necessary to prepare specimens in an unsaturated state and then saturate and consolidate them to the desired stress levels. For moist tamping, the mass of dry sand was thoroughly mixed with water to achieve a moisture content of about 5%. This low moisture content provides an apparent cohesion to prepare loose samples due to capillary tension forces acting between the grains. At low confining stresses, capillary tension forces are larger than self weight forces and thus, particle contacts are random because water tension forces are independent of direction (Kuerbis 1989).

An aluminum split mold and a small drop hammer were used to prepare reconstituted samples. To ensure a uniform density distribution in the sample and to minimize the void ratio variation, the sands were placed in four layers and compaction energy was increased with each layer by increasing the number of drops of the hammer (Mulilis *et al.*, 1977).

After the top layer of sand was placed and leveled, the top loading ram was placed on top of the sample and the top and bottom benders were aligned to ensure a strong shear wave. A suction of about 25 kPa was applied to the specimen for preparation. After removing the mold, direct measurements of the sample diameter were made. At this stage a vacuum was applied through the drainage port of the sample. The cell was then assembled and the final height of the sample was measured. After placing the cell in the loading frame, it was filled with water.

Final measurement of the sample height was done together with the first reading on the LVDT. This reading was used as the initial value representing

the initial height of the specimen. Any changes in the height was monitored by LVDT so that all the changes in void ratio due to cell assembly and back pressure saturation could be measured. A discussion of the void ratio calculation will be presented in section 3.7.

A cell pressure of about 30 kPa was applied to the sample before turning the vacuum off and starting the saturation procedure.

The more dilative the soil response, the higher the difference between rough and frictionless ends. In this study most samples were loose therefore, end effects do not come into the play (Georgiannou, 1988).

There is a debate among several researchers about the proper method for sample preparation. Previous studies show that soil behavior is significantly dependent on the preparation method (Been *et al.*, 1991; Kuerbis, 1989; Mulilis *et al.*, 1977). Many investigators (Lee and Seed, 1967; Vaid and Negussey, 1984) describe the water pluviation method for sample preparation. They suggest that this technique simulates the deposition of sand through water found in alluvial soils and hydraulically placed fills. However water pluviating can not produce very loose samples in the laboratory, and also is difficult to use for sands with a high fines content.

Sasitharan (1994) and Pitman (1993) have shown that samples prepared by moist tamping method have uniform void ratio and consistent fines content with that of the input material.

3.3.2 Frozen Undisturbed Samples

As a part of this research, a procedure for thawing frozen undisturbed samples was developed. More information about this method and obtained results are presented in the "Preliminary Report on Thawing of Undisturbed Frozen Specimens for Triaxial Testing" (Ayoubian and Hofmann, 1995; CANLEX internal report).

The triaxial apparatus was placed in the cold room at a temperature of about 1 to 2 °C for about an hour prior to assembling the sample. The frozen samples tested in this study were assembled in the triaxial cell, in the cold room, and then the cell was filled with ice water.

After filling the cell, the in-situ stresses were applied to the specimens while they were frozen. The applied vertical stress, cell pressure and back pressure were almost equal to the in-situ vertical stress, horizontal stress, and pore pressure that existed in the ground prior to ground freezing, respectively. These stresses were calculated knowing the depth of the samples, ground water condition, K_o, and the bulk density of the sands.

After the application of in-situ stresses, thawing was induced by circulating warm water through the bottom of the triaxial cell. Thus, the samples were thawed unidirectionally from the bottom of the specimens, upwards. It is important to allow the specimens access to water during thawing by opening the drainage valve, so that water can be taken in to replace the 9% pore water volume decrease due to phase transformation of the ice filled voids. An LVDT was mounted to measure the changes in the height of the samples during each stage of the test. As well, volume changes were monitored by the VCD.

The Fraser River sand samples were initially fully saturated, but the Syncrude samples were partially saturated. These specimens were not saturated using back pressure method in order to maintain the saturation condition that existed in the field.

3.4 Back Pressure Saturation

To facilitate later back pressure saturation, carbon dioxide (CO_2) was percolated through the reconstituted samples for about 15 to 20 minutes from each of the two drainage ports. This allowed the air bubbles to be replaced by

CO_2. Then distilled-deaired water was flushed through the specimen to let carbon dioxide enter the solution under lower back pressure.

The pressure for flushing water through the sample was provided by the head difference between the triaxial cell and a water tank. This head difference must be chosen carefully for each material. If the head difference is too high, the upward flow will cause finer material to migrate from the bottom of the sample to the top and therefore, the distribution of fines content will not be consistent with that of the input material. Such a consideration was also taken into account for the CO_2 flushing.

Samples were saturated by back pressure system until a Skempton's B value of no less than 0.96 was achieved. During back pressure saturation, cell pressure and back pressure were increased in increments and a 25 kPa difference between cell and back pressure was always maintained.

Sladen and Handford (1987) pointed out that the volume changes during saturation are to be considered otherwise the calculated void ratios are overestimated and there can be a systematic error in calculations. This issue will be discussed in section 3.7.

3.5 Consolidation

3.5.1 Isotropically Consolidated (IC) Tests

All the reconstituted samples of Montana sand were consolidated isotropically (K_o=1) to the desired stress levels between p′= 120 to 500 kPa. Consolidation was done by step wise increase of cell pressure and appropriate compensating weights to ensure an isotropic stress condition. Enough time was allowed in each step for full consolidation of the specimen. Then, shear wave velocities were measured across the sample at each stress level and void ratio.

3.5.2 Anisotropically Consolidated (AC) Tests

The reconstituted specimens of Syncrude sand (SS), Fraser River sand (FS), and frozen undisturbed samples of Fraser River sand (FSF) and Syncrude sand (SSF) were consolidated anisotropically under $K_o \approx 0.5$ condition.

The e-p′-V_S relationship for Syncrude sand, and Fraser River sand based on isotropic, triaxial compression testing on reconstituted samples have already been developed (Cunning, 1994 and Chillarige 1995). The goal of this part of the study was to describe the behavior of these materials under anisotropic consolidation in both compression and extension direction of loading.

3.5.2.1 Reconstituted Samples

The reconstituted specimens were prepared in a very loose state and consolidated to high stresses to ensure a strain softening response.

Two specimens of Syncrude sand, prepared by moist tamping method, were consolidated anisotropically to a similar void ratio (about 0.88) and stress levels (about p′=330 kPa, q=240 kPa). Then the samples were sheared in undrained loading one in compression and another one in extension loading until they reached ultimate steady state.

For Fraser River sand, similar experiment was carried out. Two samples were consolidated anisotropically to an almost identical void ratio (about 1.01) and stress conditions (about p′=430 kPa, q=315 kPa) and then sheared one in compression and one in extension shear under undrained condition.

3.5.2.2 Frozen Undisturbed Samples

High quality undisturbed frozen samples of Fraser River sand, and Syncrude sand were tested to compare the results with those of reconstituted specimens. One frozen Syncrude, and one frozen Fraser River specimen were thawed unidirectionally and then consolidated along $K_o \approx 0.5$ line. The Syncrude sample was taken from the Syncrude site (Phase 1, CANLEX Project), and the Fraser River specimen was obtained from Massey site (Phase 2, CANLEX Project). The samples were consolidated to their field stresses (based on their depth in the ground, K_o condition, and ground water table level). It was important to test these undisturbed samples under in-situ stresses and void ratios, and this was achieved when they were thawed and consolidated under in-situ pressures. Since the Syncrude specimen was not initially fully saturated, some contraction took place during setup and thawing, but no considerable contraction was observed for the Fraser River sample.

For SSF, p'=348 kPa and q=226 kPa prior to shearing. FSF was consolidated up to p'=96 kPa and q=59 kPa. Both specimens were sheared in compression.

Shear wave velocities at the end of consolidation were measured to compare them with in-situ V_S measurements.

3.6 Shear Wave Velocity Measurements

Bender element technology provides a simple and inexpensive method of measuring V_S in the laboratory.

After each stage of consolidation, shear wave velocity was measured at that stress condition and void ratio to develop the e-p'-V_S relationship for Montana sand. The shear wave is assumed to propagate from the tips of the

generating benders to the tips of the receiving benders, and thus, the length of travel is equal to the distance between the tips of the bender elements. The travel time is the time difference between the trigger wave (input wave) and the first intense energy excursion at the received wave (output wave).

The generating benders were excited with a 20 Hz square wave (input wave) by the wave generator. Upon receiving this energy, bender elements behave as a fixed end cantilever moving back and forth and also the soil which is in direct contact with the benders. This generates a shear wave that travels through the sample and is received by the other set of bender elements at the other end of the specimen. Both the input and output waves were amplified by a dual amplifier and displayed on the oscilloscope.

Shear wave velocity measurements require careful signal analysis, because the wave form is sometimes complex and is not composed of only shear wave at the arrival time. Brignoli *et al.* (1995) showed that in some cases the shear wave is preceded by a compression wave in the fluid-soil system. Sometimes the shear wave is effected by "near-field effects" and the near-field component of the wave is measured. Near-field energy creates motion with initial polarity opposite to the component propagating with the shear wave. This energy is a function of the number of wavelengths between the generator and the receiver or H/λ ratio, where;

H= the distance between the tips of the bender elements (receiver and generator)

λ = the wavelength of the shear wave ($= V_S / f_{out}$)

V_S= shear wave velocity

f_{out}= the predominate frequency of the measured shear wave

Near-field effects decay with increasing H/λ. Brignoli *et al.* (1994) have also reported that if this ratio is less than 5, the form of the shear wave can be affected by the near-field component. Some of the velocity measurements in this study had the H/λ as low as 2. At least two wavelengths should be kept

between the transmitter and the receiver in order to perform the measurements in the far field (Sanchez-Salinero *et al.*, 1986).

Calibration of the system was necessary to determine any delay time introduced in the velocity measurements. Calibration was done by placing the bender elements in direct contact with each other and measuring the delay time between the input wave and the initial arrival of the wave recorded by the receivers.

3.6.1 Bender Element System

The equipment used in this study were piezoceramic bender elements, a Wavetek 148 A-20 MHz AM/FM/PM generator, a Kistler 5004 Dual mode Amplifier, a Philips PM 3365A 100 MHz 100MS/s oscilloscope and a Hewlett Packard HP Color Pro pen plotter. Figures 3.4 and 3.5 show a schematic of the shear wave system.

Shear wave velocities were measured using flush mounted bender elements. Both the shear wave generators and receivers consisted of an array of four bender elements wired together in series and mounted cantilever with epoxy at their base in PVC chambers. These chambers were incorporated in the top loading head and bottom pedestal. Each bender element was 25.3 mm long, 6.3 mm wide and 0.5 mm thick.

A layer of flexible membrane, separating the soil and the bender elements, was placed between the porous stone and these elements. The porous stones had holes in the center with diameters equal to that of the PVC chamber and were screwed to the top loading head and bottom pedestal. This provides a level surface to place both the frozen and reconstituted samples.

Since the membrane separating the bender elements, and the specimens was quite thin, the shear wave could be transferred to the soil and be received by the other set of bender elements. It is important to make sure that the tips of the

bender elements are in contact with the sample so that a strong shear wave can be obtained. Figure 3.6 shows a schematic diagram of the flush mounted bender elements used in this research.

By viewing the input and output waves, the shear wave velocity can be calculated using the first pulse arrival method. The travel length of the wave is equal to the current height of the sample and therefore the velocity is calculated using the following simple relationship:

$$V_S = H / \Delta t \qquad [3.1]$$

where;

V_S= shear wave velocity (m/s)

H= current height of the sample (m)

Δt= travel time of the shear wave throughout the sample (seconds)

It is important to consider the changes in the height of the specimens, and calculate the current height to obtain the accurate velocity.

A typical shear wave signal and trigger wave obtained from the tests on Montana sand is shown in Figure 3.7.

The PVC chambers were thoroughly saturated with silicon oil to withstand the high compressive forces during the tests. This oil was a non-conductive liquid to avoid any electrical shorting of the bender elements.

3.7 Void Ratio Calculation

3.7.1 Reconstituted Samples

For moist tamped samples the void ratio calculation is based on the initial dimensions and dry soil mass of the sample. The calculated void ratio is very

sensitive to height and accurate circumference measurements (Vaid, 1994). To minimize the error in void ratio calculation, proper care was taken when measuring diameter and height of the samples.

For diameter measurements, the height of the sample was divided into four regions (samples were placed in four layers), and at each region two to six measurements (in directions perpendicular to each other) were registered. All the measurements were corrected for the membrane thickness.

The initial height of the samples were measured by using the reference height of a "dummy" sample, 127 mm in height (Sasitharan, 1994 and Pitman, 1993). A ring stand dial gauge was used to make readings for both the dummy sample, and sand samples. Thus, the height of the sample was measured accurately when the difference between these two measurements was known.

After preparation, changes in void ratio were monitored and calculated during both saturation and consolidation. Volume changes can potentially occur during cell assembly, back pressure saturation, and consolidation. Volume changes during cell assembly and back pressure saturation can not be measured directly. These changes were calculated by measuring axial deflection of the sample. For sands with higher percentage of fines content, volume changes during cell assembly and back pressure saturation were higher. Such a result was also reported by Sladen and Handford (1987). Volume changes during consolidation were measured by the VCD.

Sladen and Handford (1987) showed that changes in void ratio during back pressure saturation should not be ignored otherwise serious errors can occur in void ratio calculation. To calculate the volume changes during saturation, they assumed an elastic response in the sample and suggested the following relationship to relate the axial strain to the volumetric strain:

$$\varepsilon_v / \varepsilon_a = 3 \qquad [3.2]$$

where;

ε_v = volumetric strain (%)

ε_a = axial strain (%)

Axial strain can be measured using the LVDT and initial height of the sample after preparation. The above equation was used to calculate volume changes during saturation for the tests in this research.

Nicholson *et al.* (1993) proposed a relationship to correct the calculated void ratio for the membrane penetration into the soil voids. They reported that the most dominant factors affecting membrane compliance were soil gradation and effective confining stress. They also found out that D_{20} was a representative grain size and provided a better correlation between material particle size and membrane compliance than the mean grain size, D_{50} (suggested by Vaid and Negussey, 1984; Sladen and Handford, 1987). Based on their results for material with D_{20}< 0.1 mm, the membrane compliance induced volume change can be negligible. Therefore, the effect of membrane penetration was neglected for Montana sand and Syncrude sand, but was taken into account for Fraser River samples. A value of S= 0.0034 was considered for FS, where S is the membrane compliance induced volume change per unit area (ml/cm^2) of membrane per log-cycle change in effective confining stress (σ'_3).

The following relationship was used to calculate the void ratio:

$$e = [G_s \times (V_{initial} - \Delta V_{sat.} - \Delta V_{cons.} - \Delta V_{mem.}) \times \rho_w / M_s] - 1 \qquad [3.3]$$

where;

$V_{initial}$ = initial volume of sample (cm^3)

$\Delta V_{sat.}$ = volume change during saturation and cell assembly (cm^3)

$\Delta V_{cons.}$ = volume change during consolidation (cm^3)

$\Delta V_{mem.}$ = volume change due to membrane penetration (cm^3)

G_s = specific gravity of the soil

M_s = dry mass of soil (gr)

ρ_w = density of water (1 gr/cm^3)

3.7.2 Frozen Undisturbed Samples

If the frozen specimen is known to be initially saturated, such as the Fraser River sample, the initial void ratio will be calculated by using weight relationship (Vaid 1994):

$$e_i = (W-W_s) \times G_s/(0.917W_s) \qquad [3.4]$$

(assumed specific gravity of ice= 0.917)

where;

W= initial frozen specimen weight

W_s= final weight of dry soil

G_s= specific gravity of soil

For partially saturated frozen samples, such as the Syncrude sample, initial void ratios will be obtained by measuring physical dimensions of specimens (diameter and height), and using the following relationship:

$$e_i = V-V_s/V_s \qquad [3.5]$$

where;

V= initial frozen specimen volume

V_s= volume of dry mass of soil (= W_s/G_s)

W_s was measured at the end of the test.

The Void ratio at the end of consolidation (start of shearing) is calculated from the following equation:

$$e_c = e_i - (\Delta V_{thaw})/V_s - (\Delta V_{cons.})/V_s \qquad [3.6]$$

where;

e_c= void ratio at the end of consolidation

e_i= initial void ratio from [3.4] or [3.5]

ΔV_{thaw}= volume change during thawing and set up (decrease +ve)

$\Delta V_{cons.}$= volume change during consolidation (decrease +ve)

Since all the tests were undrained, void ratio at the end of consolidation was the same as final void ratio (e_f).

3.8 Monotonic Loading

All the samples were sheared to large strains under monotonic loading until they reached ultimate steady state. The tests were strain controlled at a constant rate of 0.15 mm/min (≈0.13%/min).

Most of the tests carried out in this study were undrained and no volume change was allowed during loading. Contraction and dilation for these tests were described by increase or decrease in pore pressure, respectively during shearing.

3.8.1 Isotropically Consolidated (IC) Tests

A total number of six triaxial compression (drained and undrained) tests were carried out on Montana sand. Only one drained test was undertaken on

this sand to obtain information for ultimate steady state at higher stress levels, and the rest of the tests were undrained.

3.8.2 Anisotropically Consolidated (AC) Tests:

A total number of six AC tests were carried out in this study. All the tests were undrained.

Two tests were done on reconstituted samples of SS, one in compression and one in extension. Also two reconstituted specimens of FS were tested in compression, and extension direction of loading.

Two compression tests were carried out on undisturbed samples of Syncrude and Fraser River sand.

3.9 Resolution of Measurements

Axial stresses were corrected for membrane strength (Kuerbis and Vaid, 1990). Membrane forces can become significant, particularly in tests on soft sediments, and undrained tests on loose sands that undergo liquefaction causing deformations at low confining stresses.

For isotropic consolidation, a proper amount of dead weights were added to the top of the loading ram to compensate for not having the cell pressure acting on the ram rod area.

Void ratio calculations were corrected for membrane compliance effect (Nicholson *et al.*, 1993).

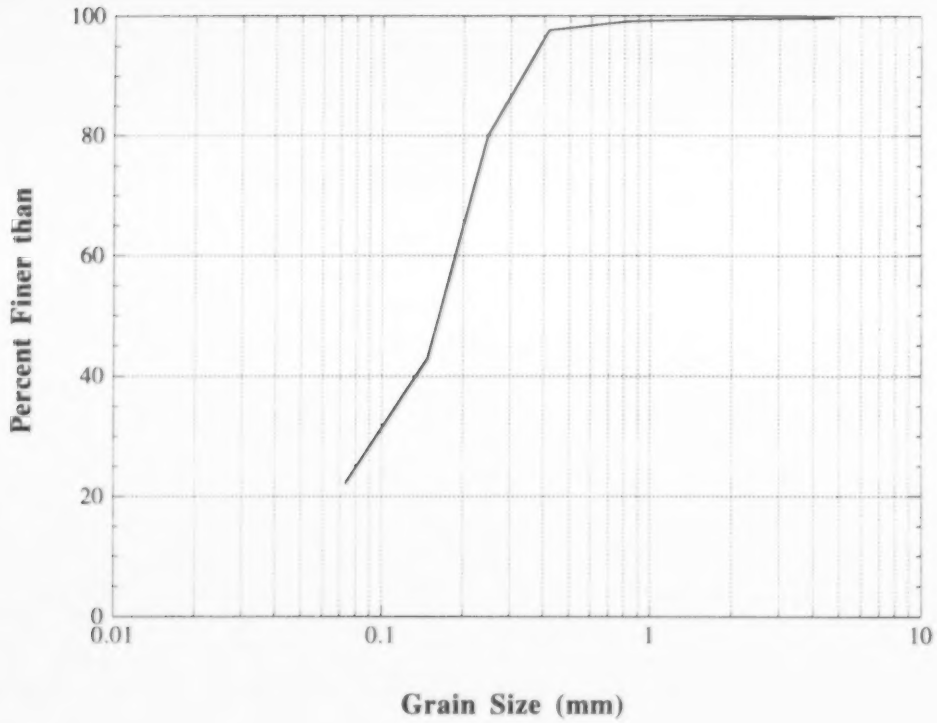

FIGURE 3.1 Grain Size Distribution for Montana Sand

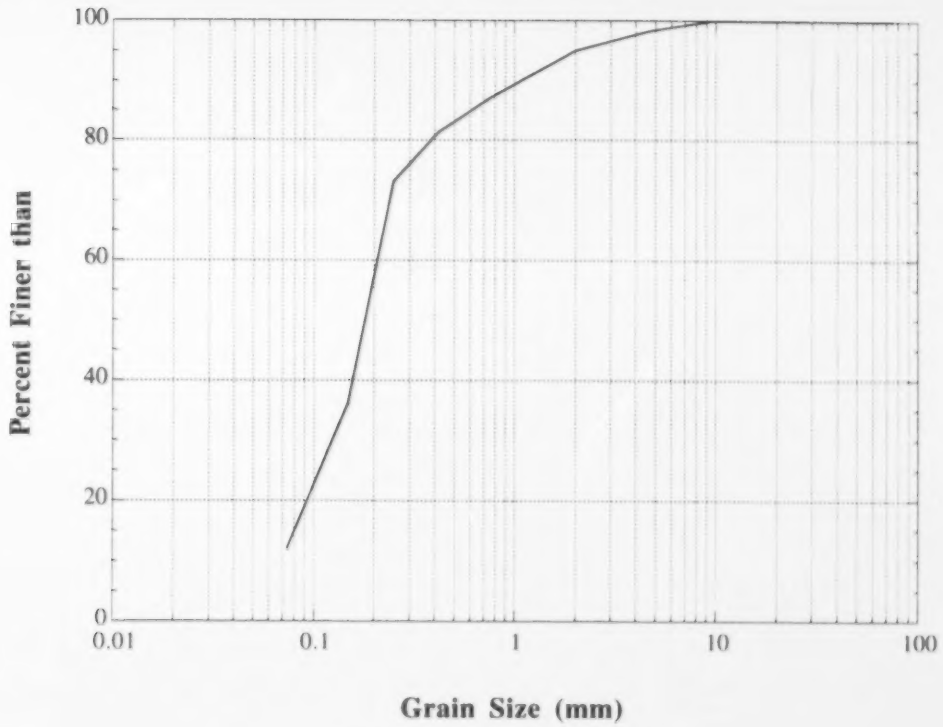

FIGURE 3.2 Grain Size Distribution for Syncrude Sand

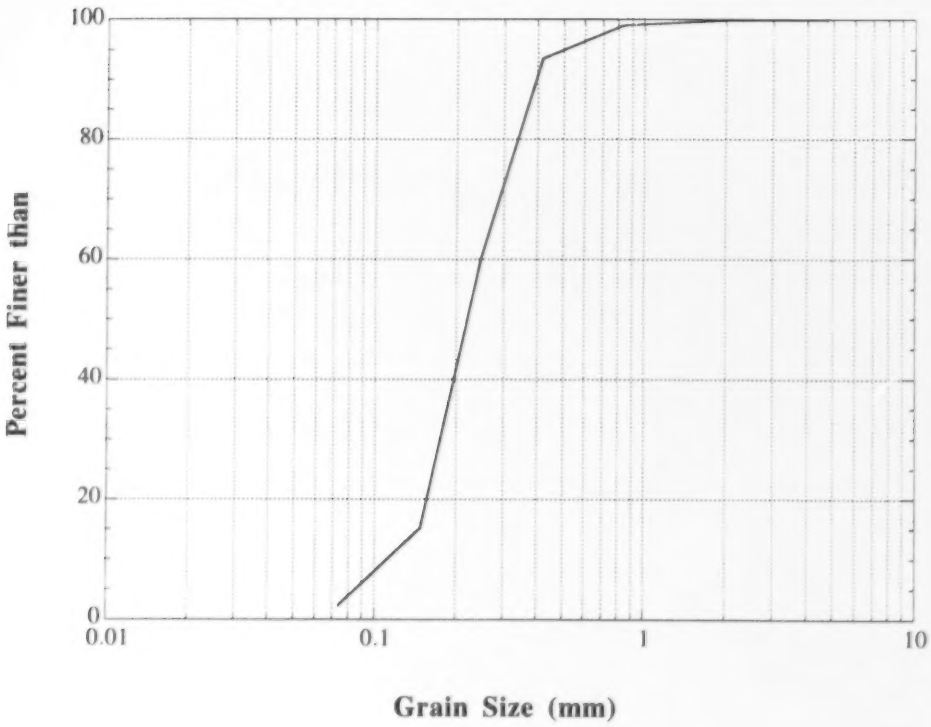

FIGURE 3.3 Grain Size Distribution for Fraser River Sand

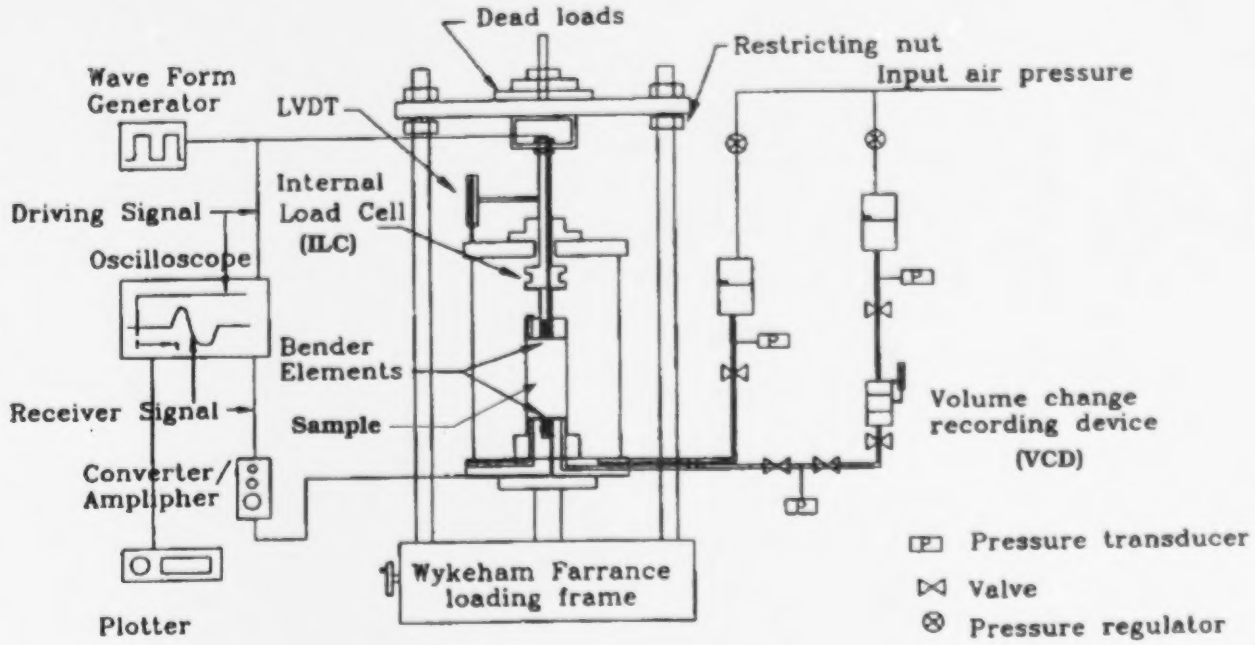

FIGURE 3.4 Schematic Diagram of the Test Setup for Isotropically Consolidated Tests (after Cunning, 1994)

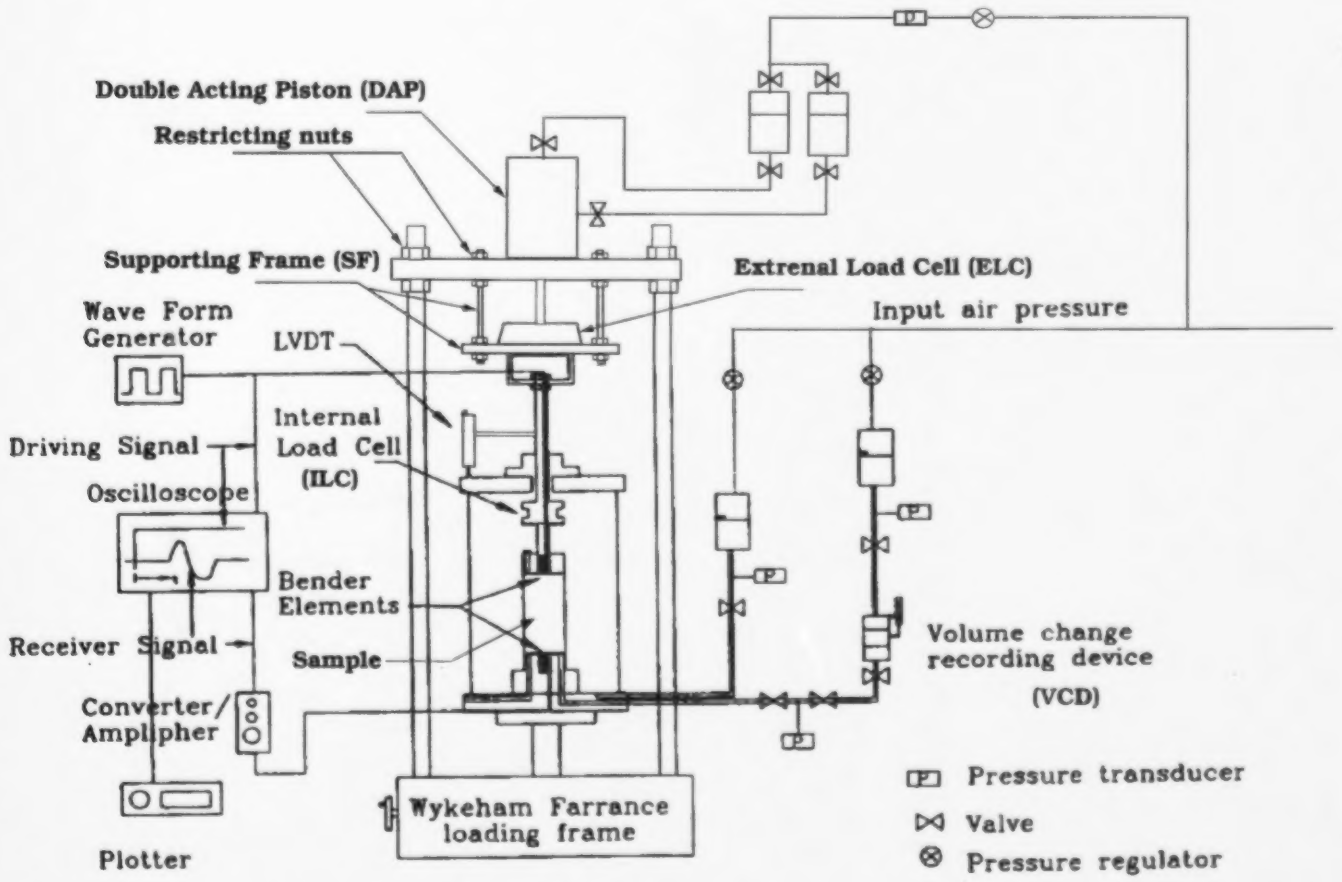

FIGURE 3.5 Schematic Diagram of the Test Setup for Anisotropically Consolidated Tests

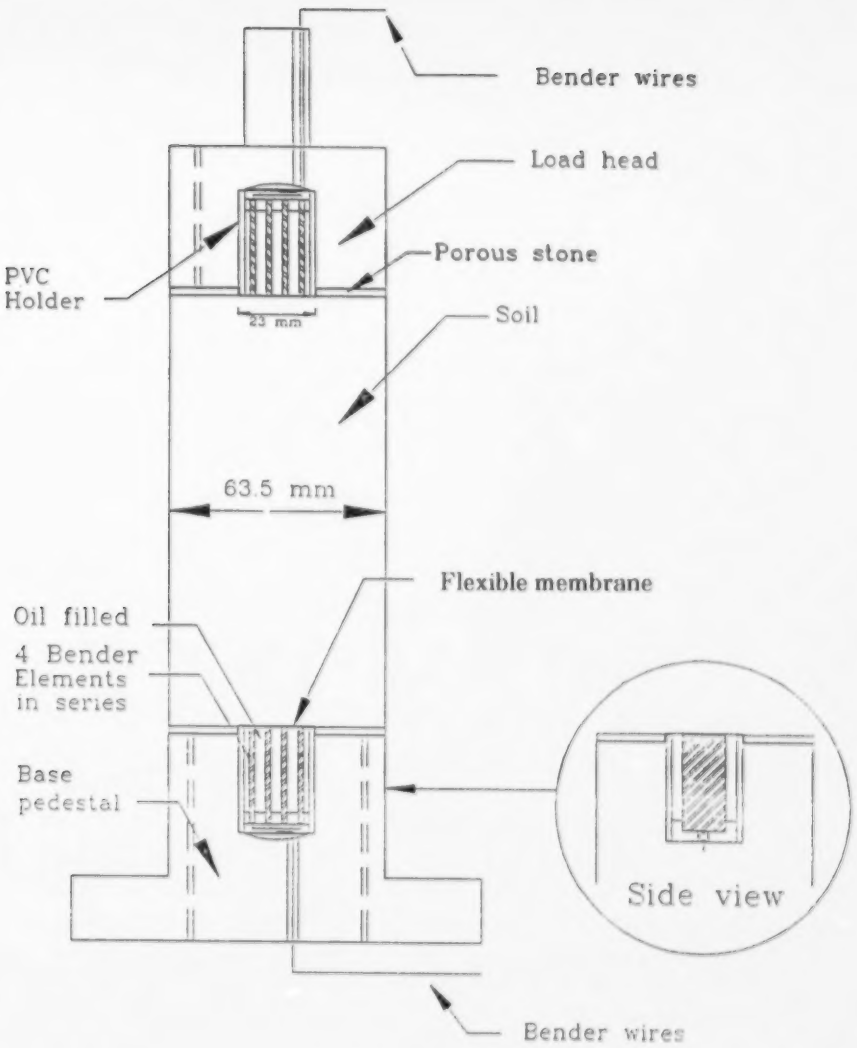

FIGURE 3.6 Flush Mounted Bender Element System in Triaxial Load Head and Base Pedestal (after Cunning, 1994)

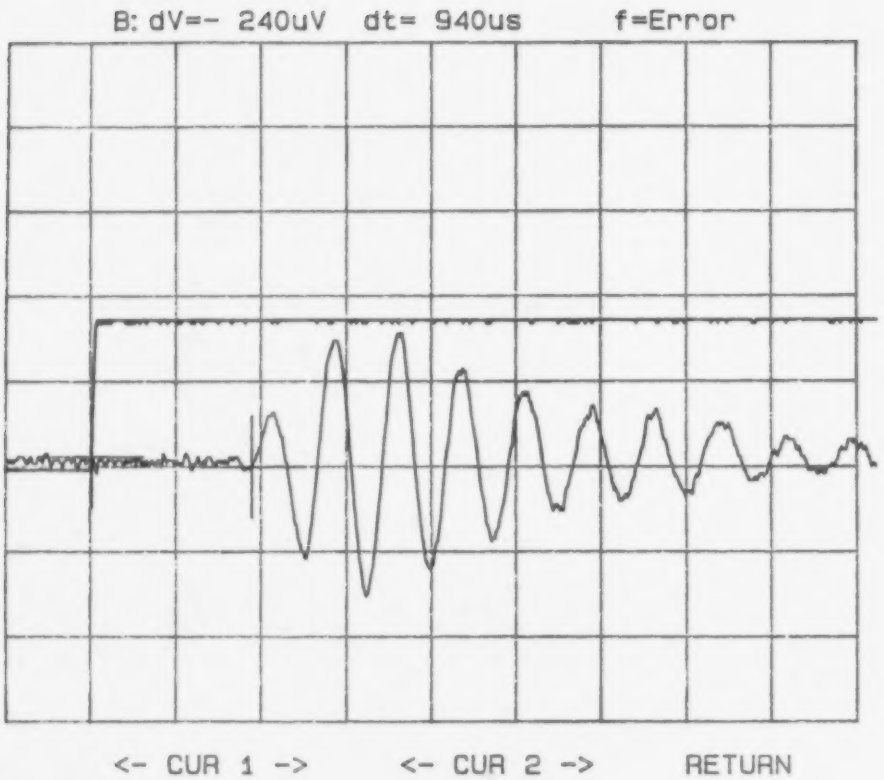

FIGURE 3.7 Typical Shear Wave Signal and Trigger Wave Obtained from the Tests on Montana Sand

CHAPTER 4

TEST RESULTS

In triaxial compression, the major principal stress (σ'_1) is the vertical stress (σ'_v) and the minor principal stress (σ'_3) is the horizontal stress (σ'_h). However in triaxial extension, the vertical stress (σ'_v) becomes the minor principal stress (σ'_3), and the horizontal stress (σ'_h) becomes the major principal stress (σ'_1). The test results are presented in terms of deviatoric stress ($q= \sigma'_v-\sigma'_h$) and mean effective normal stress ($p'=(\sigma'_v+2\sigma'_h)/3$). For the compression tests, deviator stress is positive and for extension tests it becomes negative.

4.1 Isotropically Consolidated (IC) Tests

Test results from experiments performed on reconstituted samples of Montana sand (MS) are presented in this section. All samples were prepared by moist tamping technique (Sasitharan, 1994).

4.1.1 V_S measurements and e-p'-V_S Relationship

Table 4.1 gives a summary of V_S measurements at different consolidation stresses and void ratios for the triaxial tests on Montana sand. All the tests

except test 4 were undrained. Undrained tests are identified by "U" and the drained test is shown by "D". For test 1 and test 6, bender elements were not working properly. Thus, no shear wave velocities were measured for these tests.

Sometimes V_S measurements at low consolidation stresses (lower than 100 kPa) did not give consistent results with other V_S measurements. This was also reported by Hardin and Richart (1963). They proposed that there is a different relationship for e-p′-V_S for consolidation stresses less than 100 kPa. One of the reasons for such an observation could be the lack of proper contact between the tips of the bender elements and the soil specimen at relatively low stresses. Thus, this group of velocities was not considered when developing the e-p′-V_S relationship for Montana sand.

Since all the tests on this sand were IC tests, shear wave velocities were normalized with respect to the mean effective consolidation stress (p′) using equation [2.14]. This equation can be re-written by substituting the atmospheric pressure (P_a) and stress exponent (n) with 100 kPa and 0.25, respectively, as follows:

$$V_{S1} = V_S \times (100/p')^{0.25} \qquad [4.1]$$

Figure 4.1 shows the normalized shear wave velocity (V_{S1}) against void ratio (e) during isotropic consolidation. Three different ranges of void ratios (i.e. dense, medium and loose) are shown on this plot. The average tailings sand V_{S1}-e equation was determined from linear regression and can be expressed as;

$$V_{S1} = 240\text{-}116\ e \qquad [4.2]$$

The average equation [4.2] (V_{S1} versus e) was combined with the normalization equation [4.1] to give the average e-p′-V_S equation for Montana Sand as;

$$V_S = \{240\text{-}116\ e\} \times (p'/100)^{0.25} \qquad [4.3]$$

Based on equation [4.3] contours of V_S were developed and shown on a plot of e against log p′ (Figure 4.2). Also shown on Figure 4.2 are some of the consolidation data for the tailings sand in the dense and loose ranges and the ultimate steady state line (USSL) derived from shear loading tests that are described in a later section. Figure 4.2 shows that Montana sand has a moderate compressibility reflected in the relatively large change in void ratio during consolidation of the very loose sand. Each consolidation state is marked with its laboratory measured V_S and reasonable agreement with the contours can be noted.

4.1.2 Shear Loading Results and Ultimate Steady State Parameters

After consolidation all samples were loaded in shear, either undrained or drained and USS parameters for the tailings sand were determined. Table 4.2 summarizes the e and p′ at USS for these tests on Montana sand.

A summary of the results of the undrained and drained triaxial compression tests from this study are shown in Figures 4.3 and 4.4. Figure 4.3 shows a plot of e against log p'_{uss} and Figure 4.4 shows the data in q_{uss} against p'_{uss}. From these two plots, the intercept of the USSL at p′=1 kPa (Γ) and the slope of this line (λ) can be defined. The USS parameters are presented at the end of this section.

Figure 4.5 shows a summary of the test results in terms of the consolidation curves, initial void ratio and final void ratio at ultimate steady state. For the undrained tests the void ratios remained constant and the effective stresses decreased due to a tendency for contraction. For the drained test the

void ratio decreased due to contraction during shear. Also from this plot it can be noted that the loosest sand was very compressible relative to other quartz sands.

Figure 4.6 shows the normalized stress paths in terms of q/p'_{uss} against p'/p'_{uss} for the tests from this study. The stresses are normalized by the mean effective normal stress at the ultimate steady state (p'_{uss}) for the given void ratio. For the drained test, as the void ratio changes during the test it is necessary to divide by the instantaneous value of p′ corresponding to the actual void ratio at any stage of the test. By this normalization the effect of void ratio is removed and the response of different tests at different void ratios can be directly compared. In the normalized plot the USS line becomes a point and is defined at a ratio of $p'/p'_{uss}=1$ and $q/p'_{uss}=M$. For Montana sand the value of M=1.5, which corresponds to an ultimate friction angle $\phi'=37°$. Figure 4.6 clearly shows the strain softening nature of the undrained tests on very loose sand samples. It also shows that this strain softening (ss) response becomes a limited strain softening (LSS) response and ultimately a strain hardening behavior (SH) as the sand becomes denser. Test 1 and 5 show strain softening behavior, whereas test 6 shows a limited strain softening response, and test 3 has a clear hardening response at the end of the test even though it showed some strain softening behavior initially.

Figure 4.7 shows the stress-strain plots for each test in terms of deviatoric stress (q) and axial strain and Figure 4.8 is a plot of pore pressure against axial strain (only for undrained tests). The stress-strain plot shows that all the undrained tests (test number 1, 3, 5 and 6) have clearly defined peaks that are reached within 0.5% to 1 % of axial strain. It can be noted that the strain softening tests (tests 1 and 5) reached ultimate steady state at about 15% axial strain and the LSS tests (tests 3 and 6) and the drained tests (test 4) reached their ultimate condition at higher strain level, about 25% axial strain.

The only drained test (test 4) reached a peak deviatoric stress at a much higher stress level and axial strain relative to the undrained tests. In the drained test the deviator stress rose very slowly with increasing axial strain and at almost 25% strain reached the peak shear resistance. The peak point for the drained test is actually the ultimate steady state condition for the sand.

Figure 4.8 shows a continuous increase in pore pressure for all the undrained tests until they leveled off at about 10% axial strain.

Figure 4.9 shows the volume change versus axial strain for the drained test on Montana sand. The volume change during shearing showed a continual contraction until it reached a constant value at 25% axial strain.

From the results in Figures 4.3 and 4.4 the following USS parameters were determined for Montana tailings sand;

$\Gamma = 0.847$

$\lambda_{1n} = 0.055$ ($\lambda_{log} = 0.126$)

$M = 1.5$ ($\phi' = 37°$)

These values are valid over a stress range of $p' = 10$ to 500 kPa.

The results are summarized in Table 4.3 for the V_S parameters, (A, B and n) and USS parameters (Γ, λ_{1n} and M). Also contained in Table 4.3 are typical values for other sands (Ottawa, Alaska, Syncrude and Fraser River sand). It should be noted that the USS parameters for Montana tailings sand are slightly different from those of other quartz sands (Ottawa, Syncrude, and Fraser River sand). Based on these test results it would appear that Montana tailings sand is moderately compressible since both the slope of consolidation line for loose samples (see Figure 4.5) and the slope of the ultimate steady state line (λ_{1n}) are greater than those of predominately quartz sands. Fear and Robertson (1995) noted that the USS parameters for Alaska and Ottawa sand appear to bound most sands, with the Alaska sand representing a very compressible sand and

Ottawa sand representing a relatively incompressible sand. The Alaska sand is a tailings with 30% fines content and a high proportion of shell fragments within the fines.

4.2 Anisotropically Consolidated (AC) Tests

The test results on reconstituted samples of Syncrude and Fraser River sand and frozen undisturbed specimens are presented in this section. All the tests were undrained.

The results are tabulated in the form of TCA (Triaxial Compression Anisotropic) or TEA (Triaxial Extension Anisotropic).

4.2.1 Reconstituted Samples

The reconstituted samples were all prepared by moist tamping method and were consolidated along $K_o \approx 0.5$ line by a step wise increase in cell pressure and vertical stress. The in-situ K_o conditions were estimated from high quality self-boring pressuremeter tests (Hughes *et al.*, 1995) and found to have a value close to 0.5. These samples were generally consolidated to high effective stresses to observe the contractive response during undrained shear.

4.2.1.1 Syncrude Sand (SS) Test Results

Two tests were carried out on Syncrude sand in both compression and extension directions of loading. The stresses and void ratios at the end of consolidation are summarized in Table 4.4.

Figure 4.10 is a plot of the anisotropic consolidation curves in terms of e against log p′. The consolidation curves and the ultimate states of the specimens are shown relative to the Reference USSL. The Reference USSLs for Syncrude sand and Fraser River sand were determined as parts of research works for the CANLEX project based on triaxial compression tests on isotropically consolidated moist tamped samples of the same sand (Cunning 1994; Chillarige 1995). These lines have been used as reference lines representing the actual USSLs. The parameters for these lines are summarized in Table 4.3.

Figure 4.10 shows that the two tests were consolidated to the same location in the e-log p′ plot, with similar state parameters ($\Psi \approx 0.05$) for these tests.

Figure 4.11 shows the stress paths in p′-q plot for these tests. Each test started at almost the same effective stress levels and strain softened to their ultimate steady state values. It is interesting to note that the sample sheared in compression is much more brittle than the one loaded in extension. Also it can be seen that both tests (especially the extension test) almost reached the state of zero effective stresses and zero shear resistance. This implies that these samples behaved similar to a liquid at ultimate state. This is consistent with the results reported by Ishihara (1993) where very loose samples of Toyoura sand reached the condition of zero effective stresses under undrained monotonic loading at large strains.

For the extension test, at large strains, necking of the sample was observed. The same observation was reported by other researchers for extension tests on loose samples (Wu and Kolymbas; 1991).

Figure 4.12a shows the stress-strain curves for these two tests and Figure 4.12b shows the change in pore pressure with axial strain. The stress-strain plot for the compression test shows that the peak shear resistance was reached at almost 0.06% axial strain, however for the extension test the sample reached its

peak deviator stress at 0.7% strain (about 12 times bigger than compression test). The compression test reached USS at about 10% strain, where for the extension test ultimate steady state took place at about 8% axial strain.

The plot of pore pressure versus strain indicates that for both tests pore pressure increased continuously to about 6% to 8% strain and then leveled off.

Both samples showed a similar change in pore pressure.

4.2.1.2 Fraser River Sand (FS) Test Results

One compression and one extension test were performed on reconstituted samples of Fraser River sand. A summary of the consolidation stresses and void ratios are presented in Table 4.4.

The consolidation curves, and the Reference USSL for Fraser River sand are shown in Figure 4.13. Both specimens were consolidated to almost identical stresses and densities prior to shearing ($\Psi \approx 0.078$). Figure 4.14 shows the stress paths for these two tests. Both samples strain softened to their ultimate steady states, but the sample in compression showed a more brittle response relative to the sample in extension.

The stress-strain curves are shown in Figure 4.15a, and Figure 4.15b shows the change in pore pressure with strain during shear for the two tests on reconstituted Fraser River samples. The sample in compression reached the maximum shear stress at 0.09% axial strain whereas the extension test reached the peak deviatoric stress at 0.91% strain (about 10 times bigger than the compression test). The ultimate steady state for the compression test was at 18% axial strain, and for the extension test at about 14% strain.

It is interesting to note the slight hardening behavior at the end of the extension test that is shown as a decrease in pore pressure or small increase in deviatoric stress at large strains. Also this phase transformation from

contraction to dilation can be noticed in the corresponding stress path (Figure 4.14) as a small elbow at the end of the test.

From the AC test results on Syncrude sand and Fraser River sand, It can be concluded that the anisotropically consolidated compression tests reached the peak deviator stress at a much lower strain level relative to the extension tests. This is because the samples have already been sheared (static shear) along K_o consolidation line. The compression loading (strain controlled shear) continues in the same direction, and the peak shear stresses were achieved at very small axial strains. For the extension tests, the specimens were sheared in the opposite direction and the sample is essentially unloaded. Thus, the strain is larger to reach peak resistance in extension.

The pore pressure plots (Figures 4.12b and 4.15b) show that the changes in pore pressure are similar or larger for the compression loading than those for extension shearing.

4.2.2 Undisturbed Frozen Samples

Laboratory testing on undisturbed samples is becoming more important, since the soil structure can be difficult to replicate using reconstituted samples. Ground freezing is one of the main methods for obtaining undisturbed samples of sands. However due to the high cost and difficulty of ground freezing, laboratory testing on reconstituted specimens and in-situ tests will remain popular for routine engineering projects.

One Syncrude and one Fraser River frozen sample were thawed uni-directionally under in-situ stresses and then allowed to consolidated under these conditions. It was observed that when these samples were thawed and then consolidated under field condition ($K_o \approx 0.5$) some water flowed into the samples during the thawing, and later a little volume of water was expelled from the

specimens during consolidation. Hence, the initial in-situ void ratio did not change significantly during the thaw-consolidation process.

The frozen undisturbed samples were tested undrained in compression to compare their results with those of the reconstituted samples. The main purpose of testing the undisturbed samples was to test them under in-situ conditions, at in-situ void ratio, vertical and horizontal stresses, and also in-situ fabric to determine the actual soil response.

Testing on reconstituted samples could be useful when the in-situ soil fabric could be reasonably reproduce. One way to check the quality of reconstituted (and also undisturbed) samples is by measuring small strain shear modulus or shear wave velocity (Takimatsu and Hosaka, 1986). Samples can be reconstituted in the laboratory in such a way that their small strain stiffnesses (i.e. shear wave velocities) and densities are equal to the in-situ values. For the undisturbed samples tested in this study, shear wave velocities were measured at the end of consolidation to compare them with the in-situ velocities measurements.

By thawing the frozen samples under in-situ stresses, the field void ratios were kept sufficiently unchanged. As an indication of this achievement, for FSF sample, the amount of water flowed in (measured by Volume Change Device) was approximately equal to the calculated amount of water expelled during freezing. This means that the void ratio of the FSF was not altered during thawing.

The volume of expelled water during freezing was calculated based on 9% expulsion of water (McRoberts and Morgenstern, 1975) from the following relationship:

$$V_{exp.} = [0.09\ S_r /(1+1/e)] \times (\pi HD^2/4) \qquad [4.4]$$

where;

$V_{exp.}$ = volume of expelled water during freezing (cm^3)

S_r = degree of saturation

e= void ratio

H= height of the sample (cm)

D= diameter of the sample (cm)

For the Syncrude sample, the initial degree of saturation was not known.

Details of the in-situ ground freezing and sampling for the CANLEX sites are given in Hofmann *et al.* (1995).

4.2.2.1 Syncrude Sand (SSF) Test Results

The summary of consolidation stresses and void ratio at the start of shearing for the SSF test are presented in Table 4.5. Figure 4.16 shows the state of the sand at the start and end of shearing relative to the Reference USSL. Figure 4.17 is a plot of the stress path for this test. The behavior of the sand was dilative as it strain hardened from the initial consolidation stress to its ultimate steady state. Since the initial state of the sand before loading was lower than the Reference USSL (Ψ= -0.077, RSR=0.66), the sand gained strength to reach USS at large strains. In other words the state of the sample was dense of steady state with a negative state parameter. The development of a shear plane was clearly observed at large strains because of the initial high density of the specimen.

Figure 4.18a shows the corresponding stress-strain plot for this test. Shear stress continuously increased until reached the peak strength at almost 15% axial strain. The plot of pore pressure against strain shows an initial increase in pore pressure up to 4.5% axial strain, and then a continuous decrease until USS (Figure 4.18b). Although the response of the sand was dilative from the beginning of the test, an increase in pore pressure was observed at small strains

(ε_a< 5%). A sudden drop in shear strength at large strains was noticed due to the development of the shear plane.

4.2.2.2 Fraser River Sand (FSF) Test Results

Table 4.5 contains the information regarding the consolidation stresses and void ratio at the end of consolidation for this test. Figure 4.19 shows the initial and ultimate state of the sand with respect to the Reference USSL for Fraser sand. The sand had an initial state close to the Reference USSL (Ψ= -0.015, RSR=0.60), and as a result, a limited strain softening (LSS) response was observed. The stress path for this test (Figure 4.20) shows a softening (contraction) behaviour at the beginning, but at large strains, the response became strain hardening to the ultimate state. The stress-strain plot for this test (Figure 4.21a) shows deviatoric stress (q) reached an initial peak at 1% axial strain following by a slight softening behavior up to 3% strain. Then the hardening response started at this point and continued till the end of the test at ultimate steady state. Figure 4.19b shows the excess pore pressure against axial strain. Initially pore pressure increased to its maximum value at 5% strain and then started to decrease until USS at large strains.

Test No. & Type	p′ (kPa)	Void Ratio (e)	V_S (m/s)
Test 2 (U)	98.3	0.792	147
	147.4	0.785	165
	196.1	0.773	177
	246.7	0.764	196
	303.1	0.693	227
Test 3 (U)	75.2	0.637	149
	99.6	0.629	168
	124.5	0.623	181
	149.5	0.617	191
	173.4	0.608	204
Test 4 (D)	98.4	0.673	159
	120.2	0.655	184
Test 5 (U)	147.4	0.660	167
	171.8	0.654	176
	197.2	0.648	185
	247.3	0.637	208
	295.9	0.620	222

TABLE 4.1 Shear wave velocity measurements (V_S) during consolidation for the triaxial tests on Montana sand

Test No. & Type	p'_{uss} (kPa)	Void Ratio (e)
Test 2 (U)	26	0.693
Test 3 (U)	79	0.608
Test 4 (D)	243.4	0.548
Test 5 (U)	37	0.620
Test 6 (U)	111.8	0.597

TABLE 4.2 Mean effective normal stress (p′) and Void ratio (e) at USS for the triaxial tests on Montana sand

U: Undrained

D: Drained

Material	Ultimate Steady State Parameters			V_S Parameters			Grain Characteristics			
	Γ	λ_{in}[5]	M	A	B	n	e_{max}	e_{min}	G_s	%<74μm
Syncrude Sand[1]	0.919(e>0.829) 1.920(e<0.829)	0.015(e>0.829) 0.182(e<0.829)	1.31	311	188	0.26	1.07	0.632	2.64	12
Ottawa Sand[2]	0.926	0.032	1.20	381	259	0.26	0.82	0.50	2.67	0
Montana Sand	0.847	0.055	1.5	240	116	0.25	0.85*	0.51*	2.62	20
Fraser Sand[3]	1.11	0.029	1.4	295	143	0.26	1.102	0.715	2.68	3
Alaska Sand[2]	1.485	0.117	1.48	307	167	0.26	1.78	0.70	2.90	32
Hong Kong[4]	1.019	0.056	1.23	356	253	0.25	0.78	0.41	2.64	5

TABLE 4.3 Summary of ultimate steady state parameters and shear wave velocity parameters for Montana tailings sand as well as, Syncrude, Ottawa, Fraser River, Alaska, and Hong Kong sand.

1) Γ and λ_{in} for Syncrude sand were obtained by Fear *et al.* (1995). M value and the shear wave velocity parameters for this sand were introduced by Cunning (1994).

2) Cunning (1994) 3) Chillarige (1995) 4) Skirrow (1996)

5) p′ in kPa * estimated value

Test	σ'_v	σ'_h	p'_o	q_o	e_c
SS-TCA	489	257	334	232	0.879
SS-TEA	484	241	322	243	0.889
FS-TCA	644	329	434	315	1.010
FS-TEA	638	323	428	316	1.013

TABLE 4.4 Summary of consolidation stresses and void ratios for AC tests on **reconstituted** samples of Syncrude sand (SS) and Fraser River sand (FS).
(stresses in kPa)

Test	σ'_v	σ'_h	p'_o	q_o	e_c
SSF-TCA	499	272	348	226	0.778
FSF-TCA	136	76	96	59	0.963

TABLE 4.5 Summary of consolidation stresses and void ratios for AC tests on **undisturbed** samples of Syncrude sand (SSF) and Fraser River sand (FSF).
(stresses in kPa)

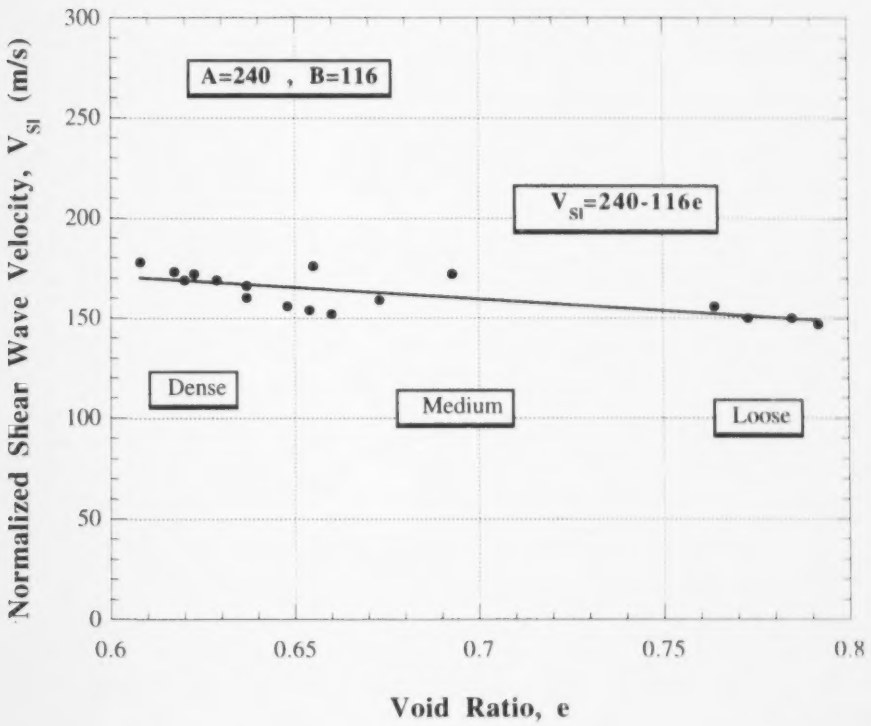

FIGURE 4.1 Normalized Shear Wave Velocity (V_{SI}) vs Void Ratio (e) for Montana Sand

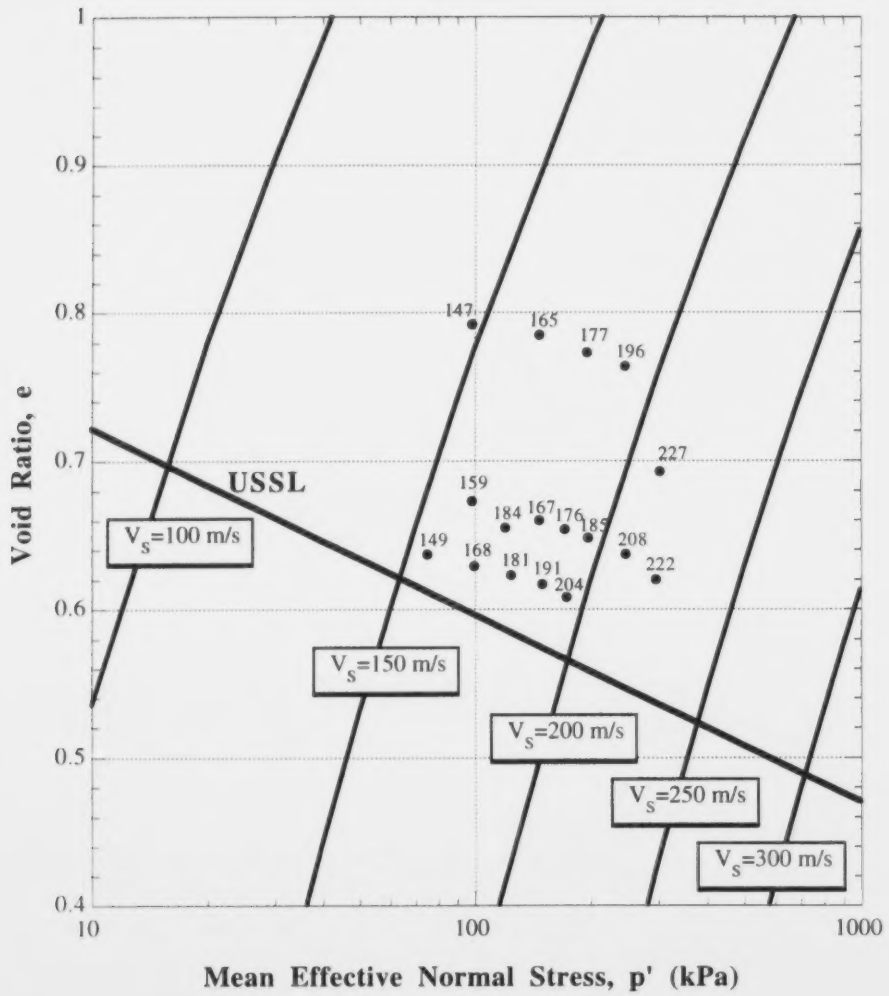

FIGURE 4.2 Shear Wave Velocity Contours and Consolidation States for Selected Samples of Montana Sand (Each Point Shows the Measured Shear Wave Velocity in m/s)

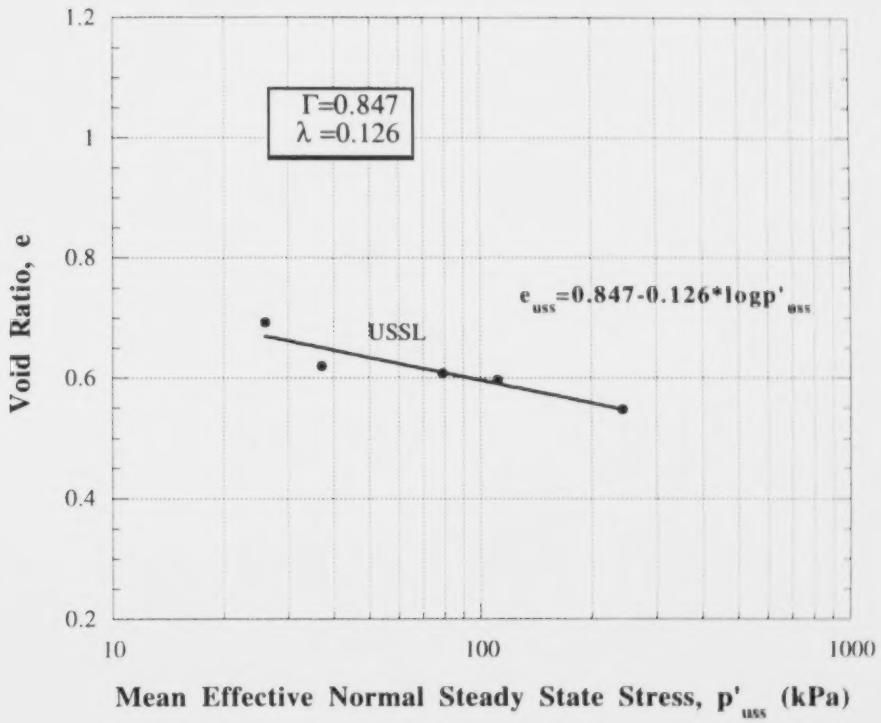

FIGURE 4.3 Void Ratio (e) vs p'_{uss} and Ultimate Steady State Parameters for Montana Sand

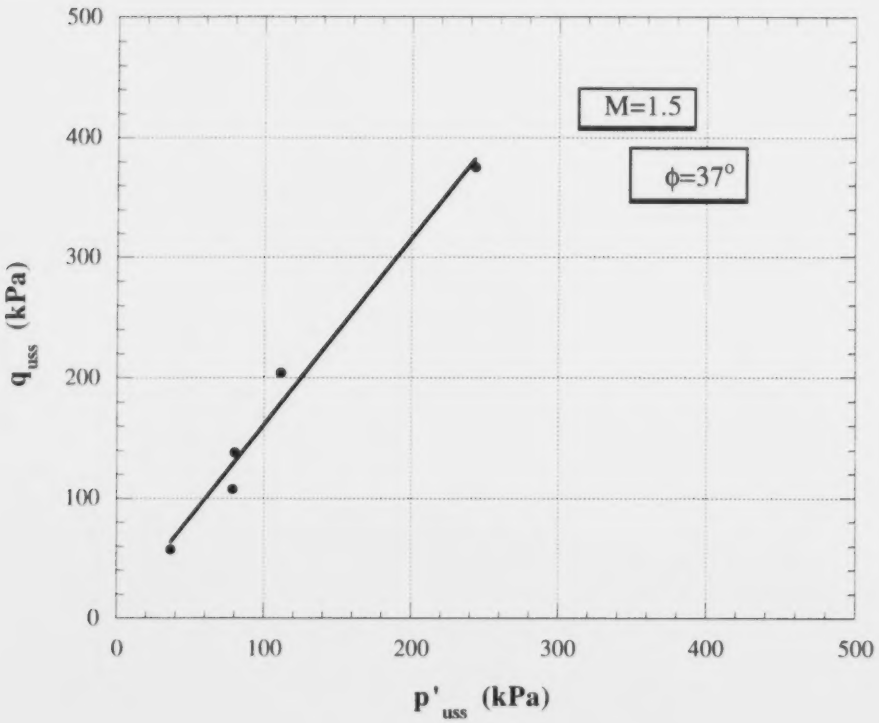

FIGURE 4.4 q_{uss} vs p'_{uss} and Ultimate Steady State Parameters for Montana Sand

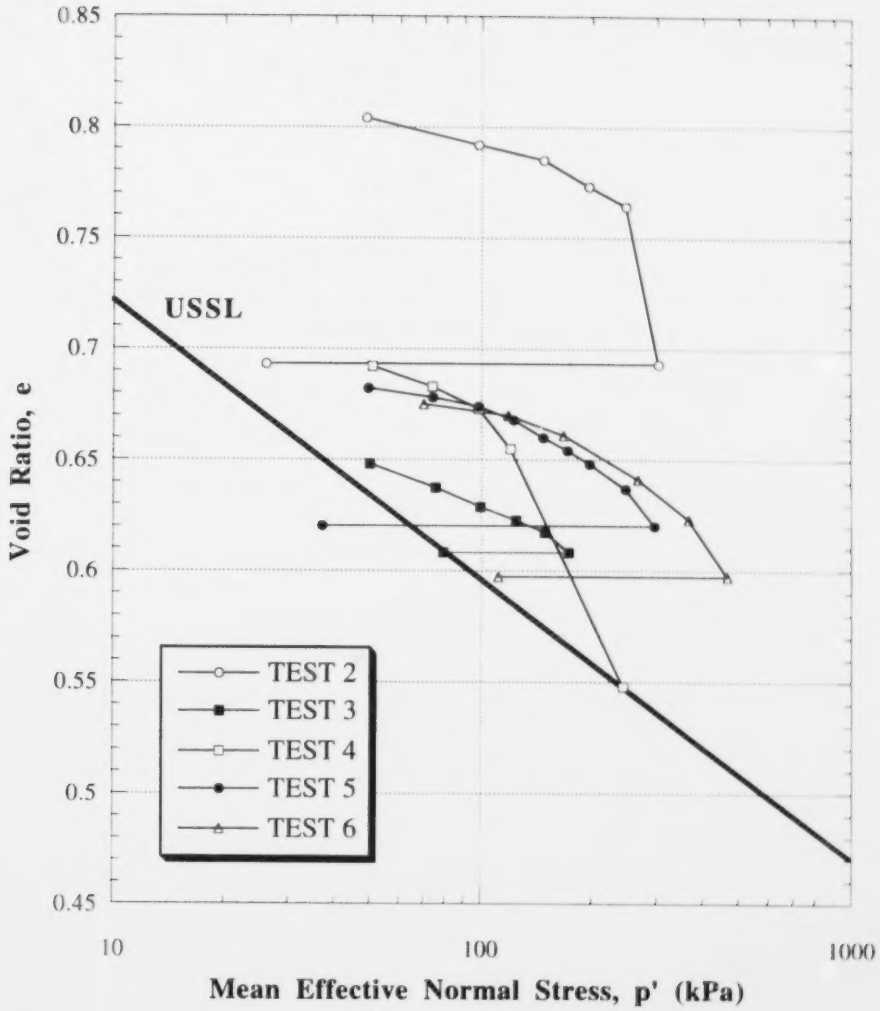

FIGURE 4.5 Consolidation Curves and Ultimate Steady States for Triaxial Tests on Montana Sand

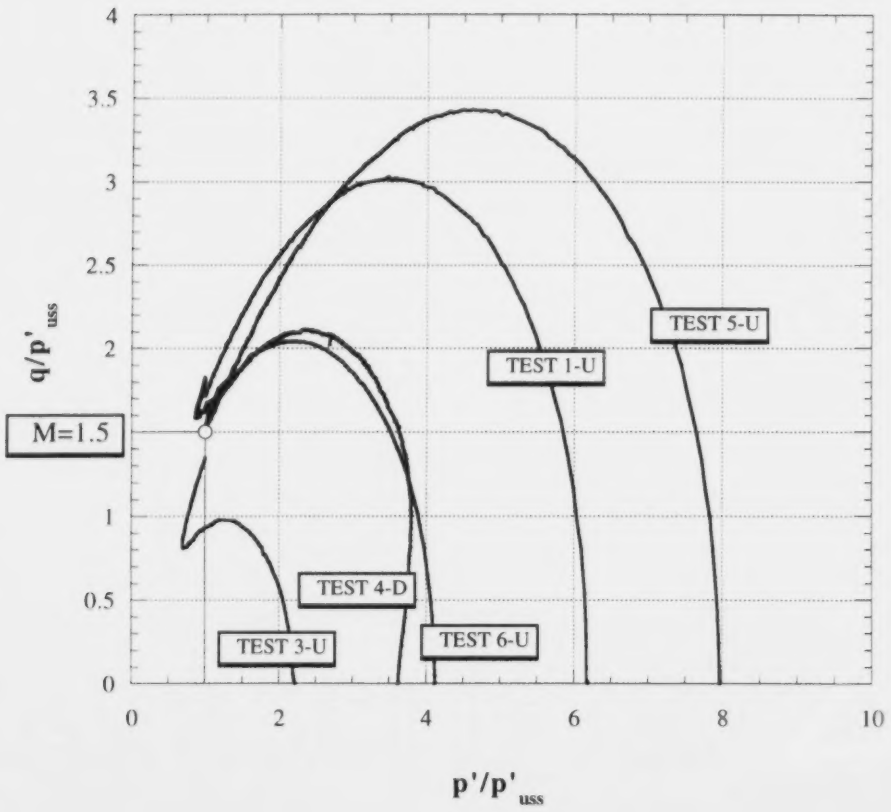

U: Undrained
D: Drained

FIGURE 4.6 Normalized Stress Paths for Triaxial Tests on Montana Sand

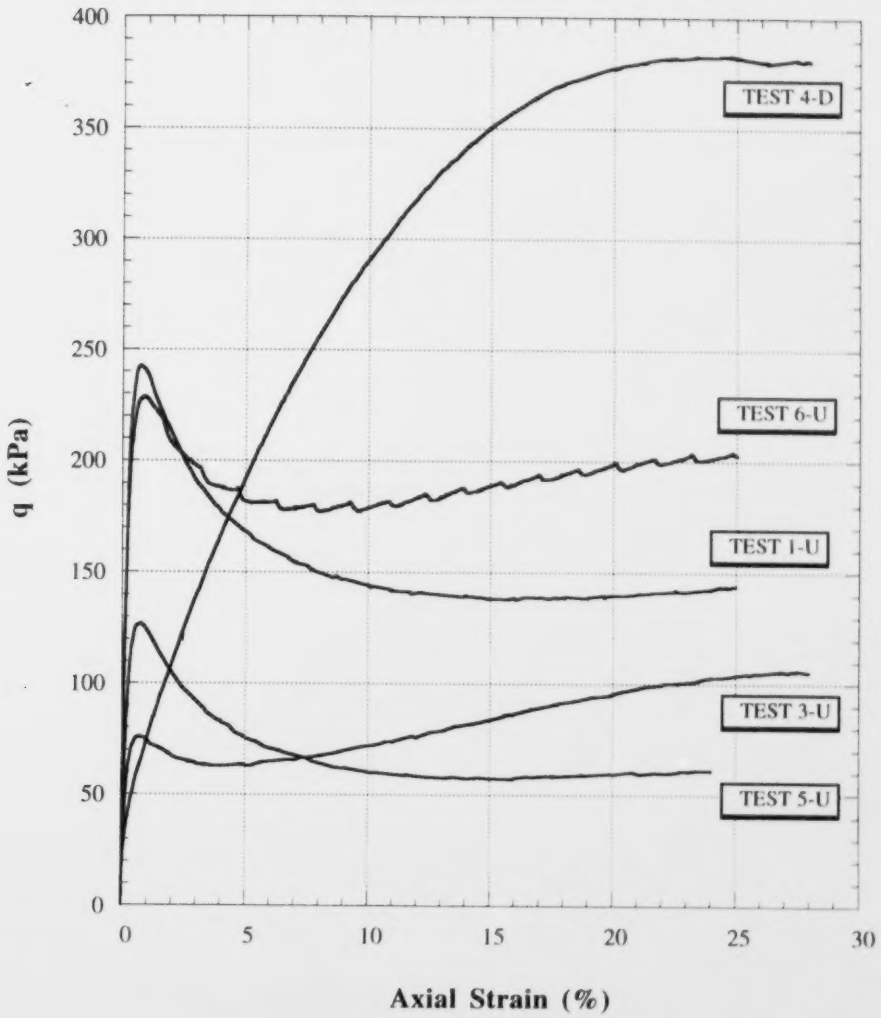

U: Undrained
D: Drained

FIGURE 4.7 Deviator Stress (q) vs Axial Strain for Triaxial Tests on Montana Sand

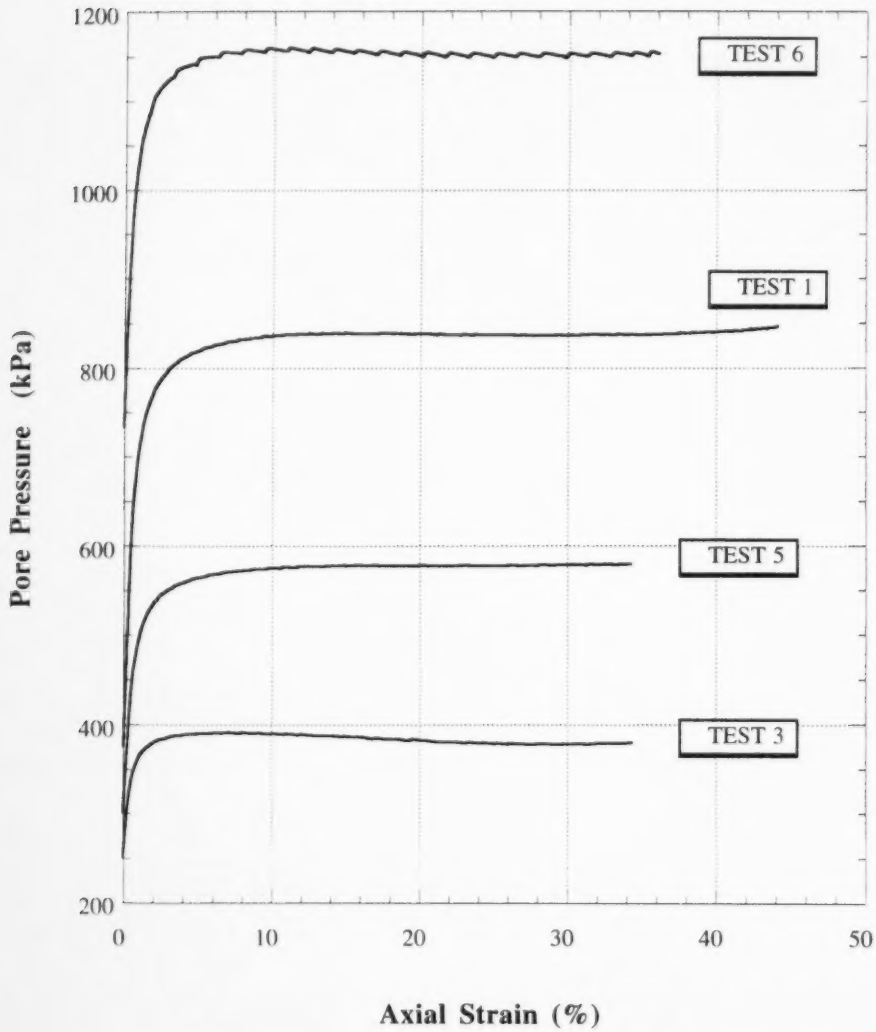

FIGURE 4.8 Pore Pressure during Undrained Shear vs Axial Strain for Triaxial Tests on Montana Sand

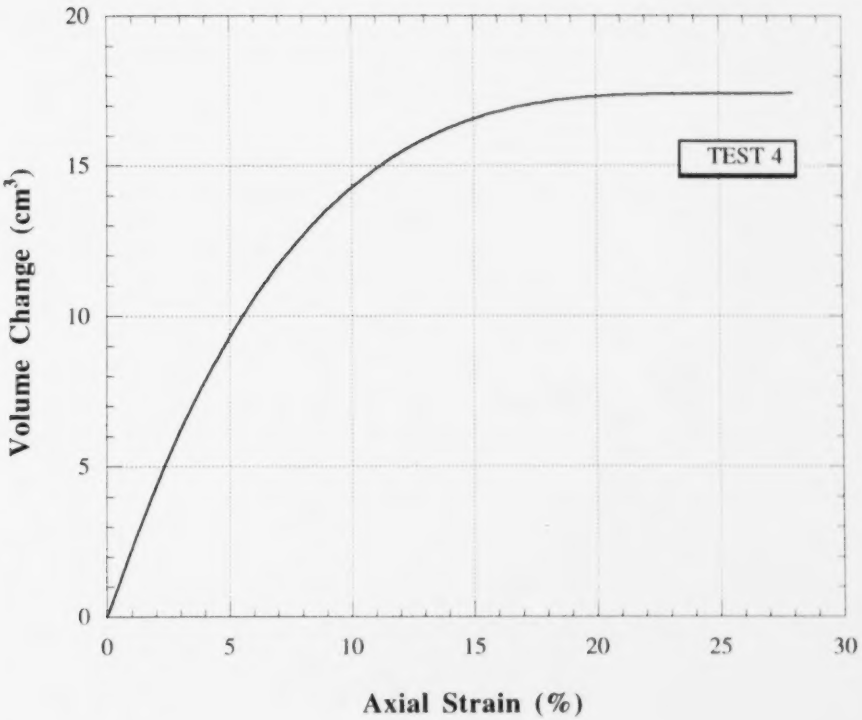

FIGURE 4.9 Volume Change (decrease +ve) vs Axial Strain for the Drained Test on Montana Sand

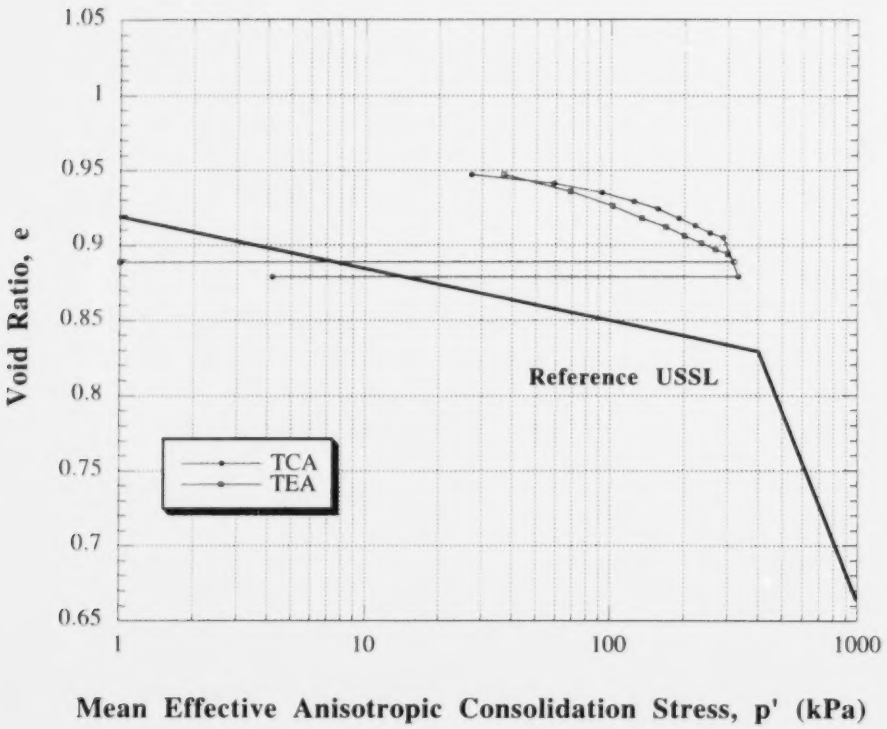

FIGURE 4.10 Consolidation Curves and Ultimate Steady States for AC Tests on Syncrude Sand

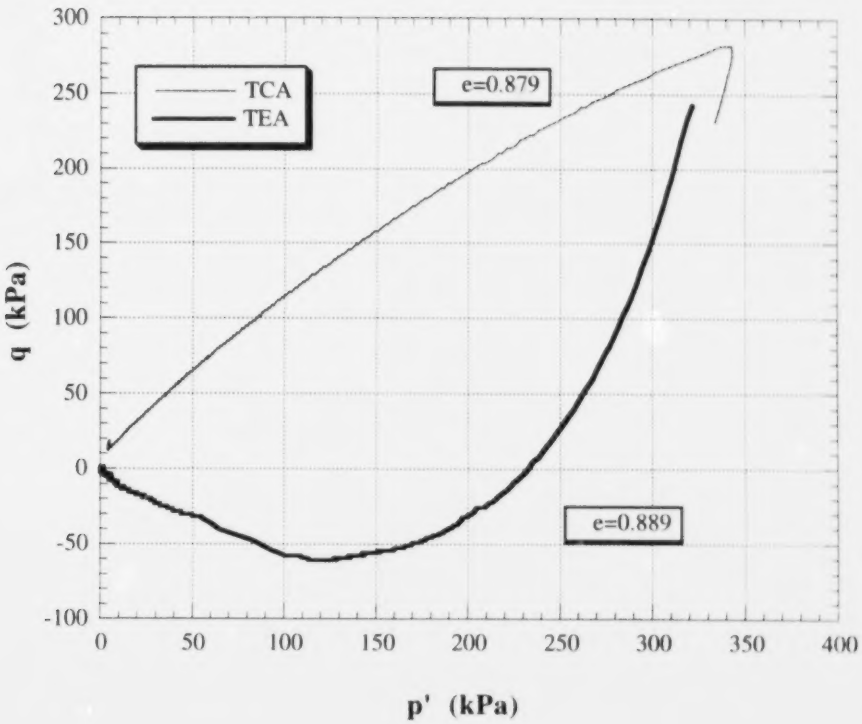

FIGURE 4.11 Stress Paths for AC Tests on Syncrude Sand

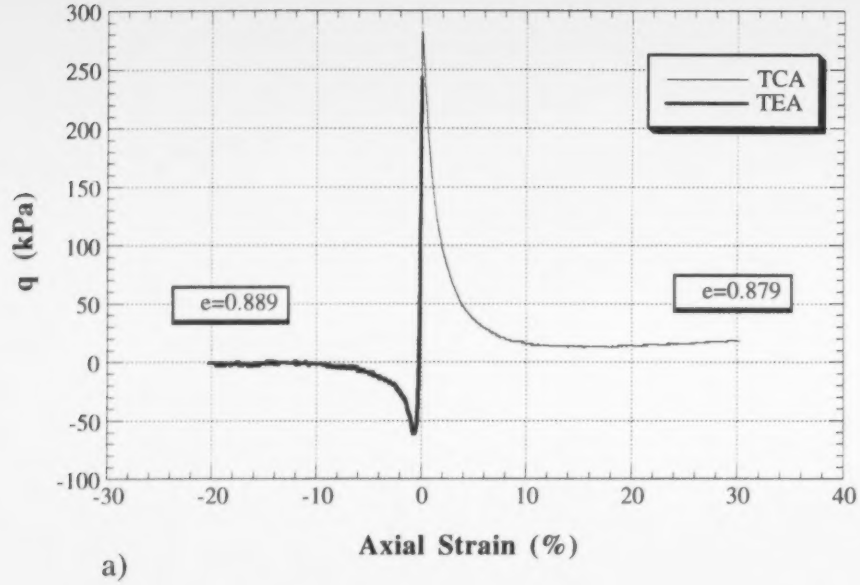

a)

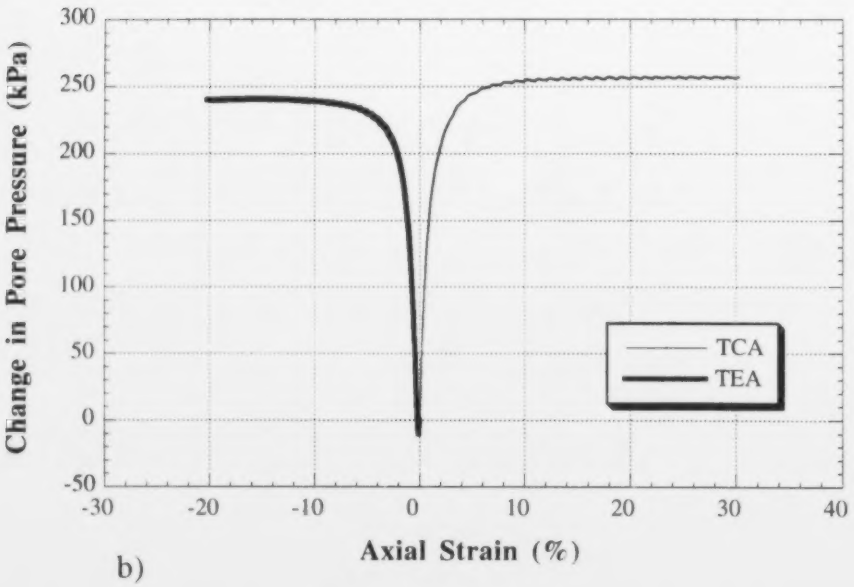

b)

FIGURE 4.12 Syncrude Sand AC Test Results
a) Deviator Stress (q) vs Axial Strain
b) Change in Pore Pressure vs Axial Strain

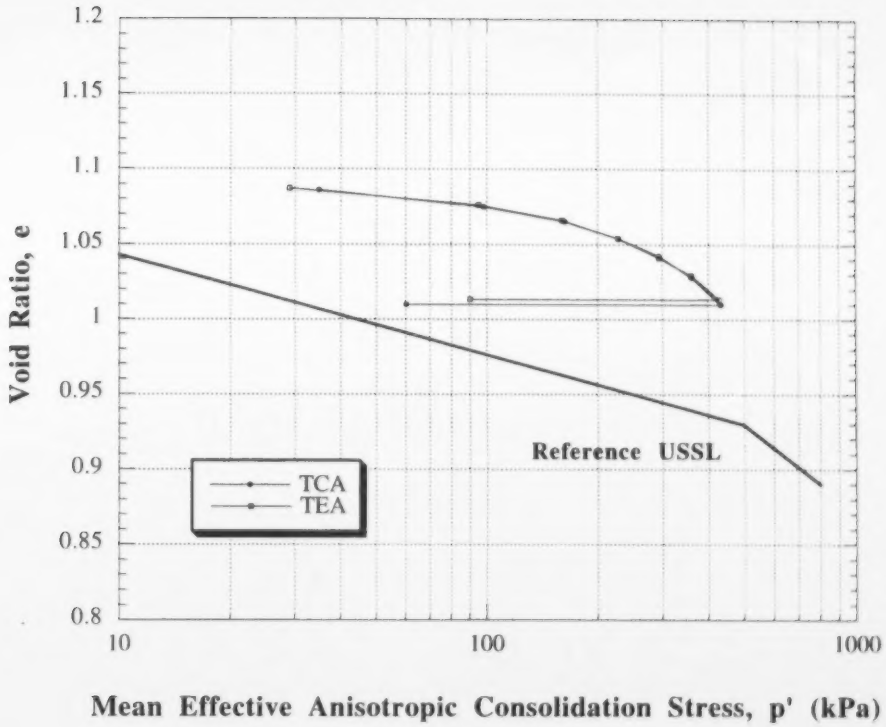

FIGURE 4.13 Consolidation Curves and Ultimate Steady States for AC Tests on Fraser River Sand

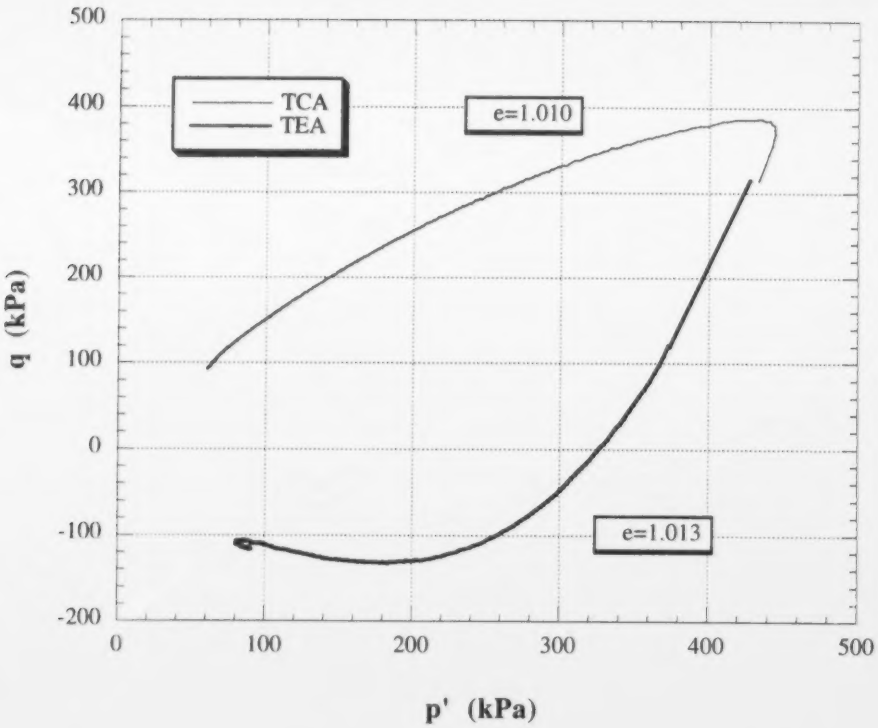

FIGURE 4.14 Stress Paths for AC Tests on Fraser River Sand

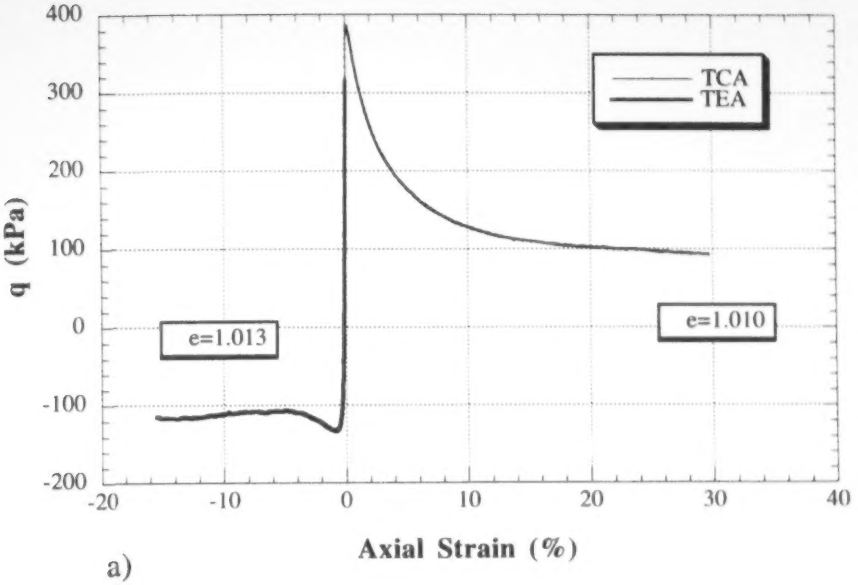

a)

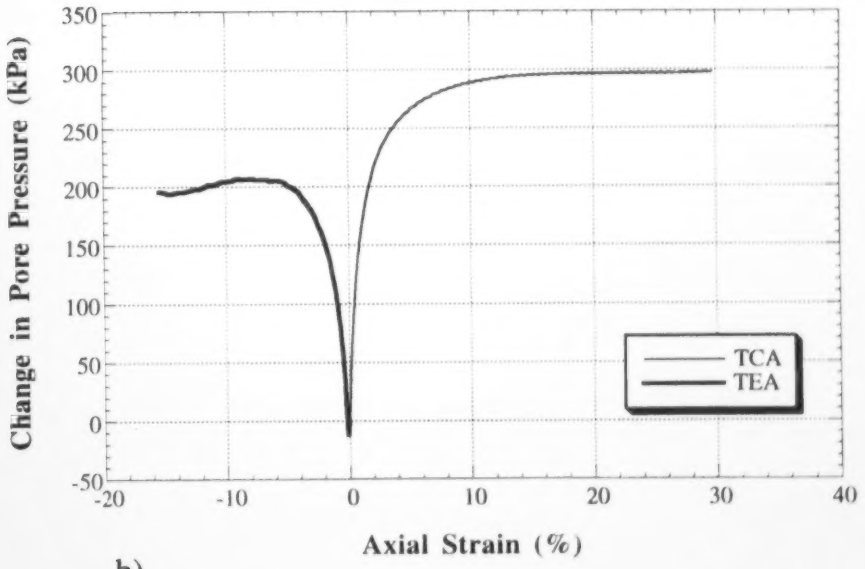

b)

FIGURE 4.15 Fraser River Sand AC Test Results
a) Deviator Stress (q) vs Strain
b) Change in Pore Pressure vs Strain

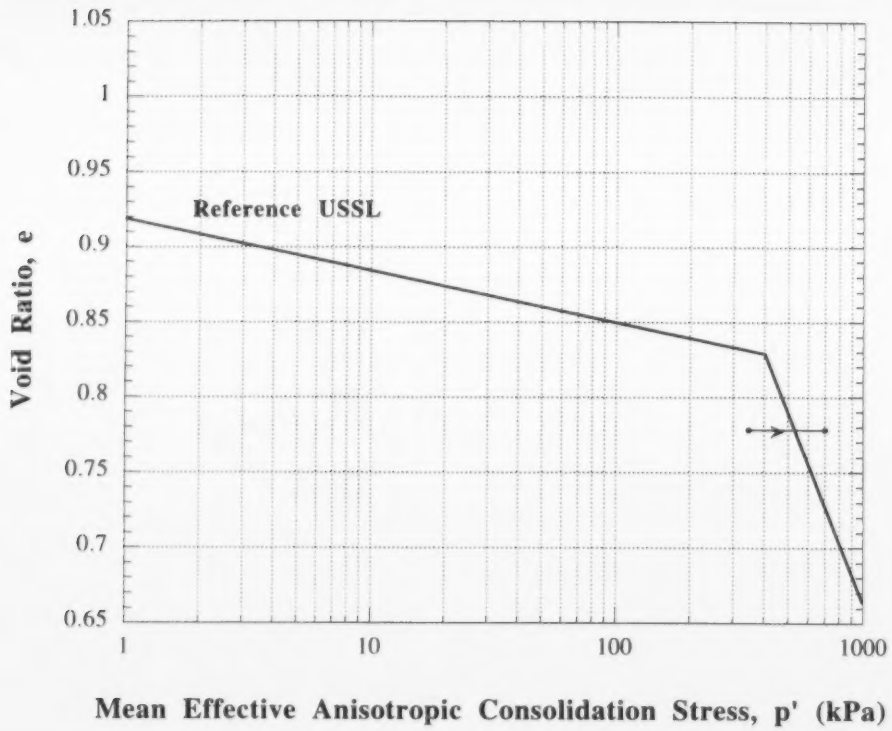

FIGURE 4.16 In-situ and Ultimate Steady State for AC Test on Undisturbed Sample of Syncrude Sand

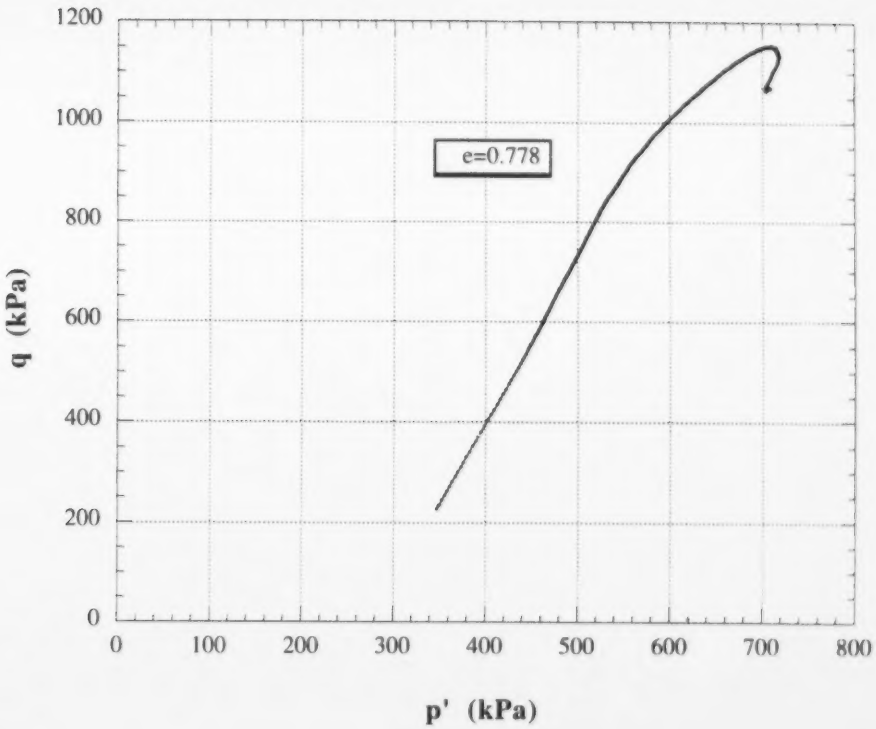

FIGURE 4.17 Stress Path for AC Test on Undisturbed Sample of Syncrude Sand (SSF)

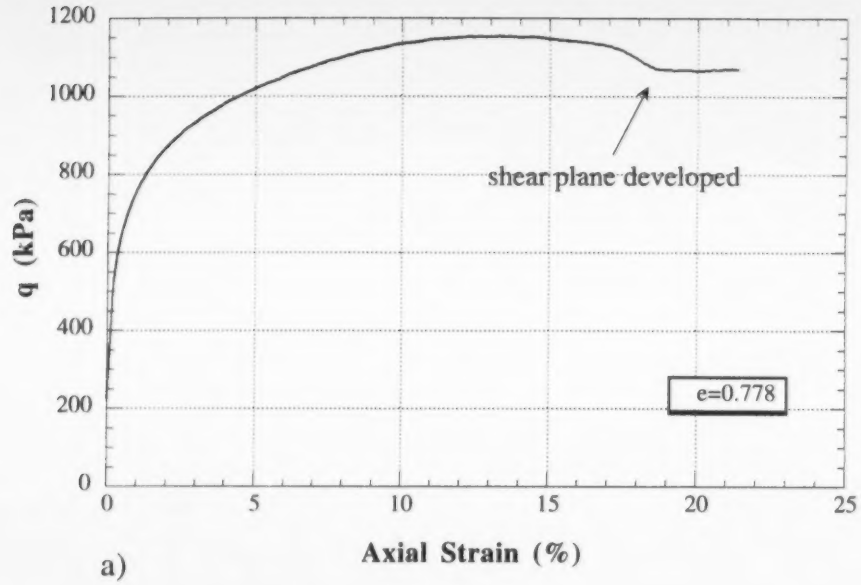

a)

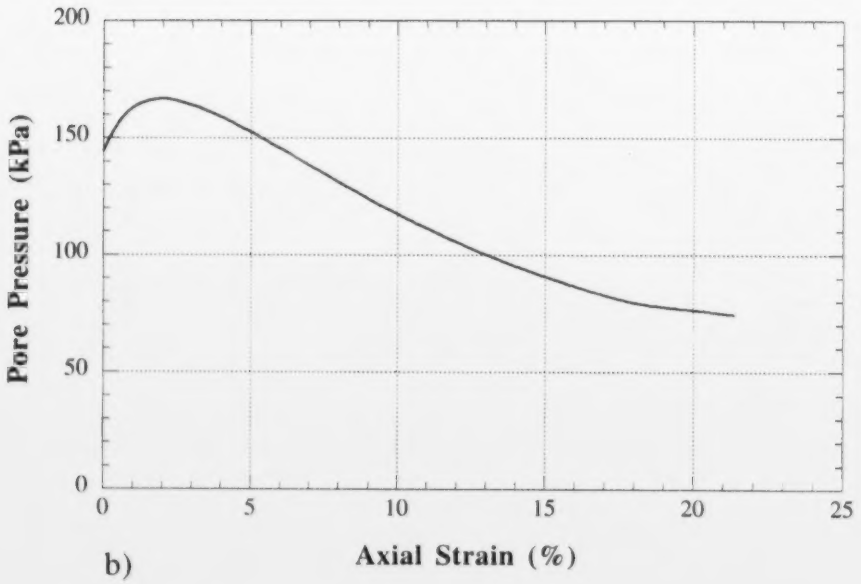

b)

FIGURE 4.18 Syncrude Sand AC Test Rsults
(Undisturbed sample)
a) Deviator Stress (q) vs Axial Strain
b) Pore Pressure vs Axial Strain

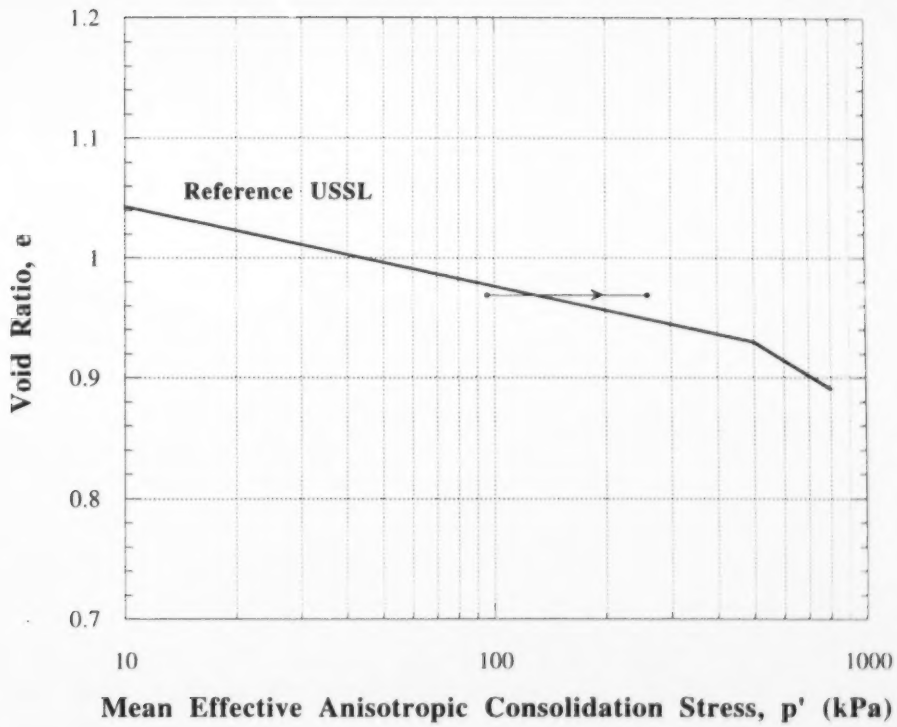

FIGURE 4.19 In-situ and Ultimate Steady State for AC Test on Undisturbed Sample of Fraser River Sand

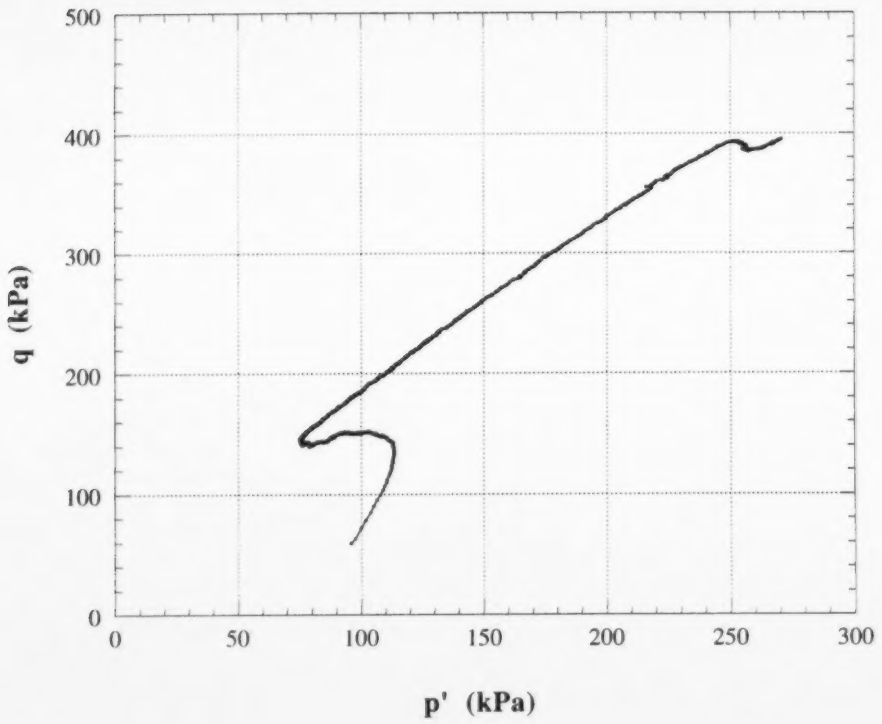

FIGURE 4.20 Stress Path for AC Test on Undisturbed Sample of Fraser River Sand (FSF)

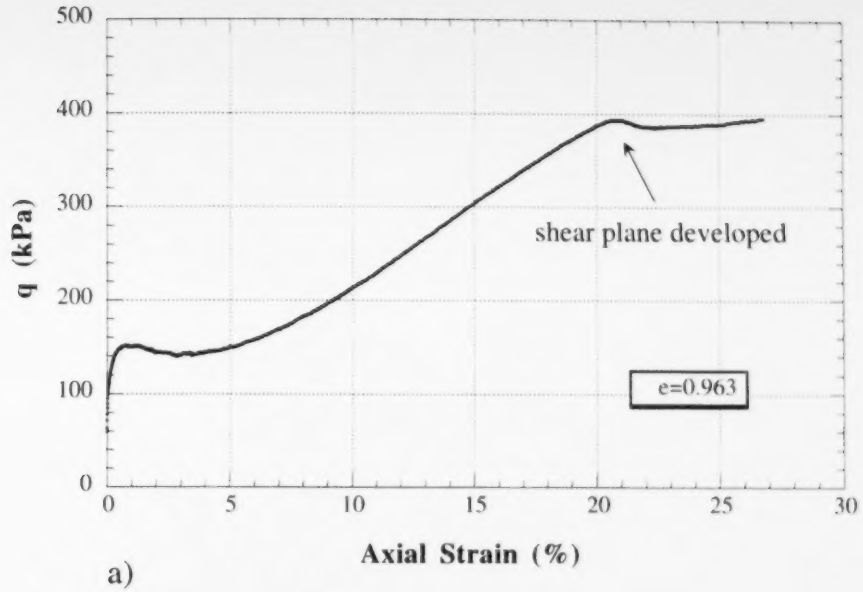

a)

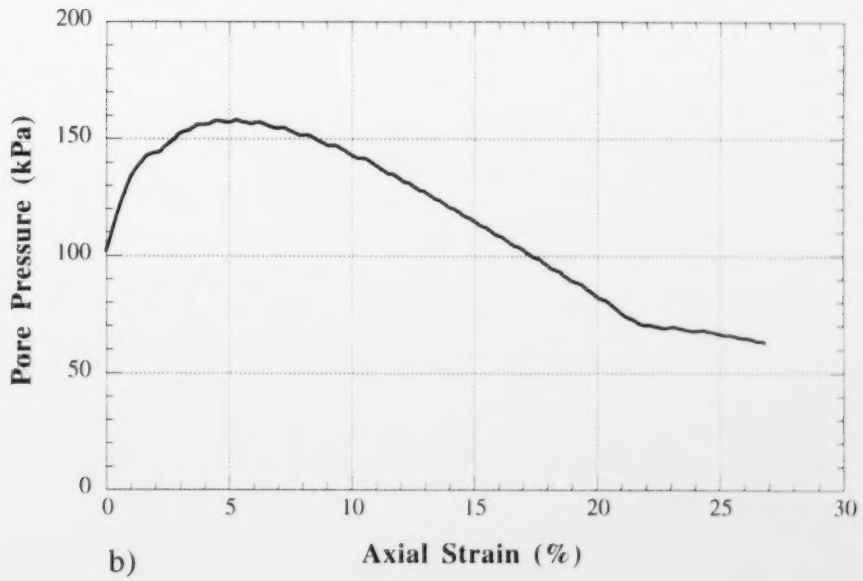

b)

FIGURE 4.21 Fraser River Sand AC Test Results
(Undisturbed Sample)
a) Deviator Stress (q) vs Axial Strain
b) Pore Pressure vs Axial Strain

CHAPTER 5

DISCUSSION AND ANALYSIS

5.1 Isotropically Consolidated (IC) Tests

The relationships obtained for Montana tailings sand, and the final results presented in this section have been developed based on triaxial tests on reconstituted samples of this sand. Hence, the resulting relationships will only represent young, uncemented cohesionless soil. The in-situ material could be slightly aged or cemented and therefore show a slightly different behavior. Both aging and cementation will tend to increase the measured shear wave velocity. Aging generally decreases the void ratio of a cohesionless soil and can result in more dilative response. Cementation can increase the small strain stiffness of a soil, however when strains are sufficient to break the cementation bounds, the large strain behavior can be contractant or dilatant depending on the void ratio.

5.1.1 Evaluation of In-situ States

The state parameter (Ψ) for Montana tailings sand can be evaluated based on shear wave velocity using the V_S parameters (A and B), and the USS parameters (Γ and λ_{1n}) from Table 4.3 and equation 2.27. The final equation

(equation 2.29) that describes the contractive/dilative boundary is repeated here as follows:

$$(V_S)_{\Psi=0}=\{A-B\times[\Gamma-\lambda_{in}\times \ln(\sigma'_v\times(1+2\times K_o)/3)]\}\times(\sigma'_v/100)^{0.25}\times(K_o)^{0.125} \quad [5.1]$$

Since the relationship have been developed based on the mean effective stress (p′), K_o has an influence. K_o is an in-situ property and can be estimated by some field testing (self-boring pressuremeter test), however the typical range of K_o for sand deposits is between 0.4 to 1.0. Thus σ'_v is the only variable in equation 5.1 and plots of V_S versus vertical effective stress can be developed.

Figure 5.1 shows the V_S-σ'_v relationship for various values of state parameter (Ψ) for the case of K_o=0.5 for the Montana tailings sand. It can be seen that for σ'_v=200, when state parameter changes from 0.1 to -0.2, V_S increases from 176 to 214 m/s (38 m/s increase). This variation in shear wave velocity with respect to vertical effective stress slightly increases with increasing in depth. This illustrates the need for accurate measurements of field V_S to evaluate the in-situ state of sandy soils.

5.1.1.1 Effect of K_o

Figure 5.2 shows the average contractive/dilative boundary (Ψ=0) for the Montana tailings sand in terms of V_S against σ'_v for various values of K_o. This figure shows that an increase in K_o, increases the value for V_S.

At σ'_v=200 kPa when K_o increases from 0.2 to 1, V_S increases from 166 to 208 m/s (42 m/s increase). This difference between velocities for various K_o values increases with increasing in depth.

5.1.1.2 Evaluation of Flow Liquefaction

The first step in the evaluation of flow liquefaction is to determine if the behavior of the material at large strains is contractive or dilative. If the behavior is found to be contractive the possibility of flow liquefaction exists. If the response of the material is dilative the potential for flow liquefaction does not exist but cyclic liquefaction may take place (Robertson *et al.*, 1994).

This evaluation requires the study of soil profile in terms of V_S against vertical effective stress (σ'_v). Shear wave velocity profile versus depth can be obtained from SCPT (Seismic Cone Penetration Test) or SASW (Spectral Analysis of Surface Waves) in-situ testing. The depth can be converted into σ'_v with the knowledge of bulk density of the soil, and the depth of the ground water table.

Finally the profile of in-situ V_S against σ'_v of the sand deposit can be compared with the contractive/dilative boundary obtained from e-p'-V_S correlation and USS parameters (Figure 5.2). If the field V_S values are below this boundary then the sand is in the contractive zone and the potential for flow liquefaction exists if the material is triggered to strain softening.

If the field velocity measurements plot above the boundary then a dilative behavior is expected and flow liquefaction will not happen, however the possibility of cyclic liquefaction should be taken into account.

If the in-situ V_S data plots near or on the boundary, because of the uncertainties that exist, engineering judgment should be employed to decide if the behavior of the material will be contractive or dilative. These uncertainties are due to experimental limitations in laboratory or in-situ measurements, lack of accuracy in estimating field parameters such as K_o, ground water level, etc.

Figure 5.3 shows contractive/dilative boundary for five different sands when K_o=0.5. Despite the scatter in V_{S1}-e plot due to the difficulties in measuring both V_S and e in the laboratories, the obtained boundaries appear to fall within a relatively narrow band. Alaska sand and Ottawa sand are the two limits of this band. The difference between shear wave velocities at the limits is about 33 m/s for most depths. This range of velocity with respect to our capabilities in measuring V_S in the field, is reasonably small. With the knowledge of the intrinsic grain characteristics of a soil (grain size distribution, grain shape, angularity, surface roughness, and mineralogical composition), and matching them with those for one of these five sands, the location of contractive/dilative boundary can be estimated for a new material.

Shear wave velocity is predominantly a function of the void ratio and effective stress condition in the soil. Grain characteristics, which can have a large effect on SPT and CPT penetration resistance, has little effect on shear wave velocity. Fabric, aging and cementation of the soil can also have an effect on shear wave velocity. Recently placed sand fills, such as tailings structures, are generally young and uncemented. Thus, aging and cementation are unlikely to be of major concern. Fabric can also influence V_S, however, there is evidence to suggest that fabric has little effect in shear wave velocity measurements for very loose sands (Sasitharan, 1994).

5.2 Anisotropically Consolidated (AC) Tests

In this section the results obtained from AC tests are discussed. Also test results from other laboratories will be included to give a wider picture of sand behavior.

Each test is given an identification code such as SS-MT-TCA. The first part is about the type of sand tested, i.e. Syncrude Sand (SS) or Fraser River Sand (FS). Second part shows the method of sample preparation, MT= Moist Tamped, WP= Water Pluviated and UT= Undisturbed. The third portion of identification string is about the type of the test; TCA= Triaxial Compression Anisotropic and TEA= Triaxial Extension Anisotropic, and TCI= Triaxial Compression Isotropic. All the tests were undrained.

The main factors influencing the undrained monotonic response of each sand are static shear (q_o), direction of loading, initial state (RSR), and soil structure. The effect of these parameters will be studied on Syncrude sand and Fraser River sand in the following sections:

5.2.1 Effect of "Static Shear (q_o)"

Figure 5.4 shows the effect of static shear on the response of Syncrude sand. Two compression tests, one anisotropically and the other isotropically consolidated, are shown for samples at the same states. The calculated brittleness indexes for the TCA and TCI are 5.34 and 0.89, respectively. It can be seen that the AC sample is 6 times more brittle than the IC sample. The two samples have almost the same void ratios and confining pressures (p'_o) at the start of shearing and both were prepared by moist tamping method. The stress-strain curves show that the IC test reached its peak at about 1% axial strain, however the AC test reached the peak resistance at almost 0.06% strain. Both tests reached identical ultimate stress condition at about 10% axial strain.

Figure 5.5 shows the influence of anisotropic consolidation on the response of Fraser River sand. Both samples were prepared by moist tamping technique and were consolidated to similar void ratios and confining stresses

prior to undrained loading. The response of the samples were similar to those of Syncrude sand samples. The AC sample with I_B= 4.12 was 5 times more brittle than the IC test with a brittleness index of 0.79. The AC test reached the peak deviator stress at 0.07% axial strain, but the IC test experienced the peak resistance at almost 1% strain. Both tests reached their ultimate condition at about 15% strain. The ultimate shear strength of AC test on Fraser River sand was slightly higher than that of IC test.

Both the TCA and TEA tests on Syncrude sand and Fraser River sand have the same ratio of M= q_{uss}/p'_{uss} and thus, identical mobilized friction angle at ultimate steady state.

Vaid *et al.* (1995) also showed that the application of static shear at constant confining pressure promotes more contractive behavior. Their results were obtained from triaxial tests on dense or medium loose water pluviated Syncrude sand specimens.

5.2.2 Effect of "Direction of Loading"

In this section the results of the compression and extension tests will be compared. The specimens were prepared by moist tamping method and consolidated to similar densities and confining stresses with almost equal static shear. Thus, the only difference between these tests would be the direction of loading, i.e. compression or extension.

Figure 5.6 shows the effect of "direction of loading" on the response of Syncrude sand samples. The I_B for compression test is 5.34 and for the extension test is 0.20. Therefore; the sample tested in compression is 27 times more brittle than the one sheared in extension.

The same experiment was carried out for the specimens of Fraser River sand. Figure 5.7 shows that I_B for TCA and TEA are 4.12 and 0.06, respectively. Thus, the sample under compression loading exhibited 69 times more brittle response than the specimen loaded in extension..

The amount of additional loading required to induce strain softening response is much less in compression than in extension due to the initial anisotropic stress state (K_o= 0.5). Compression tests on very loose sands showed significantly more brittle responses than extension test and samples failed immediately after being loaded in undrained compression shear. Vaid *et al.* (1995) showed that for water pluviated Syncrude sand samples at comparable void ratios and confining stresses, extension tests showed more softening behaviours than compression tests. However their specimens were generally dense or medium loose, and some of the tests were stopped before reaching USS.

The brittleness indexes were calculated based on the equations given in chapter 2, section 2.1.4.

5.2.3 Effect of "Initial State"

Figure 5.8 shows the normalized stress paths for anisotropically consolidated (K_o=0.5) Syncrude sand samples in undrained triaxial compression and extension. The reconstituted samples were prepared by moist tamping (present study) and water pluviation (Vaid *et al.*, 1995) method. The stress path from the compression test on an undisturbed sample is also shown.

The undisturbed sample (RSR= 0.66) which had the densest state showed a dilative response from the start of shearing until it reached ultimate steady state (Figure 5.8b).

Water pluviated specimens had slightly looser states relative to the undisturbed sample. Both tests showed an initial contractive response with dilative behavior at the end of the tests (limited strain softening). The compression test had RSR= 1.20 and the extension test had RSR= 1.14 (Figure 5.8b).

The moist tamped samples were much looser than the water pluviated ones. Both tests had clear contractive behavior (strain softening). The compression test with RSR= 23.22 showed much more brittle response relative to the extension test with RSR= 43.59, even though it had a lower RSR value (Figure 5.8a). The brittleness index for compression test is 5.34 and for extension test is 0.20. It seems that for a very loose sand, the compression loading promotes much more contractive response than extension loading, but dense sands under extension loading may be as brittle as those loaded in undrained compression shear.

Figure 5.9 shows the normalized stress paths from compression and extension tests on Fraser River sand. The undisturbed samples with relatively close RSR values (for compression RSR= 0.60 and for extension RSR= 0.89) showed similar limited softening responses. The brittleness index for compression test is 0.14 and for extension test is 0.11. A much lower minimum shear strength in triaxial extension was noticed than that in triaxial compression for undisturbed specimens (Figure 5.9b).

The water pluviated samples also showed limited strain softening behaviours. They both had RSR= 0.91 but the compression test was more brittle than the extension one. Brittleness index (I_B) for compression test is 0.34 and for extension test is 0.08. These two tests and the extension test on the undisturbed sample were not carried out to sufficiently large strains to evaluate if the ultimate steady state was the same for all the tests (Figure 5.9b). However the stress paths for all tests are moving toward a common ultimate state. Been

and Jefferies (1985) showed results to suggest that the strain levels required to attain ultimate state can sometimes exceed the capabilities of the triaxial equipment.

The moist tamped tests on Fraser River sand showed completely strain softening behavior and the compression test was much more brittle than the extension test. The RSR for compression and extension tests were 13.82 and 15.07, respectively but the compression test was almost 69 times more brittle than the extension one (Figure 5.9a).

Pestana and Whittle (1995) have shown that there appear to be a limiting consolidation line for a given sand beyond which the sand can not exist, at least in reconstituted state. This intrinsic Normal Consolidation Line (NCL) is similar to the loosest state consolidation line suggested by Ishihara (1993). The knowledge of the location of the loosest consolidation state relative to the USSL provides a measure of how loose the sand can possibly exist in reconstituted state (Ishihara, 1993). The consolidation lines for the loosest moist tamped samples in Figures 4.10 and 4.13 (chapter 4) can be the NCLs for these sands.

These results confirm that for very loose sands compression tests can promote more contractive response than extension tests, however for dense or medium loose sands the material behavior in extension tests may be as brittle as in compression tests.

5.2.4 Comparison of Laboratory and In-situ V_S

To compare the laboratory shear wave measurements with in-situ velocities, V_S were measured at the end of consolidation for undisturbed samples of Syncrude sand and Fraser River sand. Table 5.1 shows the obtained V_S values in laboratory and also the range of in-situ velocity measurements at

the corresponding depths where the undisturbed specimens were obtained from. Since the samples were consolidated approximately to their in-situ stresses and void ratios and they have the same fabric as the field material, the comparison between laboratory and field V_S is of considerable interest.

The results show that shear wave velocity measurements in the laboratory are in good agreement with the in-situ values. However the relatively wide ranges of field measurements indicate the need to more accurate in-situ values to verify this consistency.

5.2.5 Evaluation of Ultimate Steady State Lines

Figures 5.10 and 5.11 show the ultimate states for the triaxial tests from this study, and also other available test results for Syncrude and Fraser River sand. These data have been shown in e-log p′ plots relative to their Reference USSLs.

These plots show that samples of the same sand with different fabrics (method of preparation) and directions of loading (compression and extension) can have the same USSL. Some of the test results show that the experiments could not be carried out to sufficiently large strains to reach their ultimate steady states. These points are shown with arrows indicating the direction towards where their final state could move at large strains.

The two moist tamped Syncrude sand samples reached their ultimate states at significantly low stress levels (less than 10 kPa) due to their very loose initial states (Figure 5.10). The location of these two ultimate states relative to the Reference USSL indicate that the slope of the USSL for very low stresses is lower than that for higher confining pressures. Generally, it is difficult to find the location of USSL at extremely low stresses because of equipment

limitations. Tatsuoka *et al.* (1986) have reported that the USSL would be flatter at these low stresses.

5.2.6 Response Charts

Been and Jefferies (1985) suggested the use of state parameter (ψ) to define sand state. If the USSL can be assumed to be straight in e-lnp′ space over a given range of void ratio, the state parameter (Ψ) and Reference Stress Ratio (RSR) are related as follows:

$$\frac{p'_o}{p'_{uss}} = \exp\left(\frac{\Psi}{\hat{\lambda}_{\ln}}\right) = \text{Reference Stress Ratio (RSR)} \qquad [5.1]$$

where p'_o is the initial mean effective normal stress and p'_{uss} is the value of p′ at the same void ratio at ultimate steady state.

The slope of the USSL is a function of grain characteristics and stress level. At high stresses, the line becomes much steeper due to grain crushing indicating a more compressible material. Thus, the RSR is a more generic measure of sand state for a wide range of soils. When Ψ=0, RSR=1.0 and the state falls on the USSL in e-lnp′ space.

Based on the stress-strain curves from this study, other available test results, and with the knowledge of RSR values for these tests with respect to the Reference USSLs, **Response Charts** have been developed. These charts provide a quantitative evaluation of sands behaviour in terms of **Response Parameters** with RSR. Response Parameters are mainly "Brittleness Index", (I_B), "minimum undrained shear strength", (S_{min}), and "axial strain at minimum shear strength", (ε_{amin}). Figure 5.12 shows these parameters for both triaxil

compression and extension tests. The shear strength at quasi steady state will be referred to as the minimum undrained shear strength (S_{min}). For very loose sands this can be equal to the undrained shear strength at USS.

The data were obtained from undrained triaxial tests on AC samples of Syncrude sand and Fraser River sand, with different fabrics (method of preparation) and directions of loading (compression or extension).

Figure 5.13 shows brittleness index versus RSR for Fraser River sand. It can be noted that for dense sands (RSR<1), the compression tests can be as brittle as, or even less brittle than, the extension tests. As the sand becomes looser, compression loading promotes more brittle behaviour. For very loose sands (for example RSR>10), like the moist tamped specimens prepared in this research, the samples loaded in compression can be 30 (or even more) times more brittle than those loaded in extension.

The following relationships were obtained from the best fitted line through the points for Fraser River sand:

$$I_B = -0.137 + 0.308 \times (RSR) \quad \text{Fraser River sand, compression} \quad [5.2]$$

$$I_B = 0.051 + 9.1\times10^{-4} \times (RSR) \quad \text{Fraser River sand, extension} \quad [5.3]$$

The samples used in this plot were moist tamped, water pluviated and undisturbed specimens.

Figure 5.14 is a plot of S_{min}/p'_o with RSR. The USS lines have been plotted using the obtained M values form isotropic compression tests. The following relationships link S_{min}/p'_o to RSR:

$$S_{min}/p'_o = M_C/2\times(RSR) \quad \text{for Triaxial Compression (USS)} \quad [5.4]$$

$$S_{min}/p'_o = M_E/2\times(RSR) \quad \text{for Triaxial Extension (USS)} \qquad [5.5]$$

where;

M_C and M_E are values for compression and extension tests, respectively.

The TE-QSS line was used to evaluate the response of the dense or medium loose specimens, since they generally exhibit QSS before reaching their ultimate state. For plotting TE-QSS line, RSR in equations [5.5] was obtained with respect to the Quasi-Steady State Line (QSSL), rather than the USSL. A reasonable agreement between the data and the theoretical lines can be noticed. This plot shows that for medium loose (1<RSR<10), and dense sands (RSR<1.0) the extension direction of loading produces a lower minimum shear strength comparing to the compression loading. However, if the sand is very loose (RSR>10) both compression and extension loading can produce extremely low minimum strength at ultimate steady state.

Figure 5.15 shows the axial strain at minimum strength (ε_{amin}) versus RSR for Fraser River sand. Based on the resulting lines, it is shown that dense samples (RSR<1.0) in extension experienced more axial strain at S_{min} than those in compression loading. As RSR increases, the ε_{amin} in compression increases rapidly and it becomes more than ε_{amin} for extension tests. The following relationships were obtained from linear regression for Fraser River sand:

$$\varepsilon_{amin} = -0.187 + 1.176 \times (RSR) \quad \text{Fraser River sand, compression} \qquad [5.6]$$

$$\varepsilon_{amin} = 3.015 + 0.189 \times (RSR) \quad \text{Fraser River sand, extension} \qquad [5.7]$$

Figure 5.16 shows I_B versus RSR for Syncrude sand. Like the results for Fraser River sand, compression tests can be as brittle as extension tests for dense Syncrude sand specimens, but loose samples of Syncrude sand are

significantly more brittle in compression than in extension. The following relationships can be defined for Syncrude sand to relate I_B to RSR:

$$I_B = 0.154 + 0.224 \times (RSR) \quad \text{Syncrude sand, compression} \quad [5.8]$$

$$I_B = 0.104 + 2.2\times10^{-3} \times (RSR) \quad \text{Syncrude sand, extension} \quad [5.9]$$

Figure 5.17 shows S_{min}/p'_o with RSR for Syncrude sand. The obtained results explain that very loose samples can have extremely low shear strength at QSS or USS in both compression and extension. Dense and medium loose samples exhibit greater minimum shear strength in compression than in extension. Thus, for a sand with low RSR (RSR<1.0), extension tests with low minimum shear strength can govern the design, but for very loose sands this may not be true.

Figure 5.18 illustrates the relationship between ε_{amin} and RSR for Syncrude sand. The resulting lines for compression and extension indicate a similar trend for Syncrude sand. Very loose Syncrude sand samples exhibited larger strains at minimum shear strength in compression than in extension, whereas dense specimens had higher ε_{amin} when loaded in extension.

The obtained relationships for ε_{amin} versus RSR can be expressed as follow:

$$\varepsilon_{amin} = 0.148 + 1.007 \times (RSR) \quad \text{Syncrude sand, compression} \quad [5.10]$$

$$\varepsilon_{amin} = 2.729 + 0.253 \times (RSR) \quad \text{Syncrude sand, extension} \quad [5.11]$$

Figures 5.19, 5.20 and 5.21 present all the data for both Syncrude sand and Fraser River sand together. Since the data are plotted against RSR, the type of

sand does not influence the results greatly. The following relationships can be used to estimate response parameters of sands in compression and extension direction of loading when in-situ RSR values are known:

$$I_B = 0.055 + 0.245 \times (RSR) \quad \text{Compression} \quad [5.12]$$

$$I_B = 0.073 + 2.5\times10^{-3} \times (RSR) \quad \text{Extension} \quad [5.13]$$

$$\varepsilon_{amin} = 0.082 + 1.047 \times (RSR) \quad \text{Compression} \quad [5.14]$$

$$\varepsilon_{amin} = 2.806 + 0.246 \times (RSR) \quad \text{Extension} \quad [5.15]$$

Some of the tests were terminated before the ultimate conditions were achieved and this can be a reason for some scatter in the plots. It is obvious that more test results are required to provide more accurate equations, but these plots clearly illustrate the general trend for the Response Charts and provide a link between the in-situ state of sands and their response characteristics.

All the data required for these plots are summarized in Table 5.2.

Type of sand	Range of in-situ V_S (m/s)	Laboratory V_S (m/s)
Syncrude	221-313	263
Fraser River	170-184	184

Table 5.1 Laboratory and in-situ shear wave velocities

Test No.	e_c^*	$p'_o{}^{**}$ (kPa)	ψ	RSR	I_B	S_{min}/ p'_o	ε_{amin} (%)
FS-UT-TCA[1]	0.990	72.0	0.004	1.15	0.00	1.99	0.0
FS-UT-TCA[1]	0.983	74.7	-0.002	0.94	0.00	2.07	0.0
FS-UT-TCA[1]	0.942	73.3	-0.043	0.22	0.00	2.79	0.0
FS-UT-TCA[3]	0.963	96.0	-0.015	0.60	0.14	0.73	2.3
FS-UT-TEA[1]	0.982	73.3	-0.003	0.89	0.11	0.05	5.7
FS-UT-TEA[1]	0.914	82.7	-0.068	0.10	0.00	0.18	1.6
FS-UT-TEA[1]	0.910	65.3	-0.079	0.07	0.02	0.14	1.5
FS-MT-TCA[3]	1.010	433.8	0.076	13.80	4.12	0.11	16.1
FS-MT-TEA[3]	1.013	428.0	0.079	15.09	0.06	0.13	5.7
FS-WP-TCA[2]	0.925	536.3	-0.003	0.91	0.34	0.41	1.2
FS-WP-TEA[2]	0.925	536.3	-0.003	0.90	0.08	0.08	3.8
SS-WP-TCA[1]	0.810	533.3	0.033	1.20	0.78	0.39	2.0
SS-WP-TCA[1]	0.788	266.7	-0.115	0.53	0.63	0.41	1.5
SS-WP-TCA[1]	0.777	133.3	-0.253	0.25	0.00	1.13	0.0
SS-WP-TCA[1]	0.815	66.7	-0.341	0.15	0.00	3.28	0.0
SS-WP-TEA[1]	0.801	533.3	0.024	1.14	0.12	0.05	3.1
SS-WP-TEA[1]	0.765	266.7	-0.138	0.47	0.05	0.09	3.0
SS-WP-TEA[1]	0.781	133.3	-0.249	0.26	0.15	0.02	2.7
SS-WP-TEA[1]	0.803	66.7	-0.353	0.14	0.10	0.05	2.7
SS-MT-TCA[3]	0.879	334.2	0.047	23.22	5.34	0.02	23.5
SS-MT-TEA[3]	0.889	322.1	0.057	43.59	0.20	0.00	13.8
SS-UT-TCA[3]	0.778	347.8	-0.077	0.66	0.00	1.65	0.0

1) Vaid *et al.* (1995)

2) Thomas (1992)

3) present study

* void ratio at the end of consolidation

** mean effective normal stress at the end of consolidation

Table 5.2 Response Parameters for all the AC tests on Fraser River sand and Syncrude sand

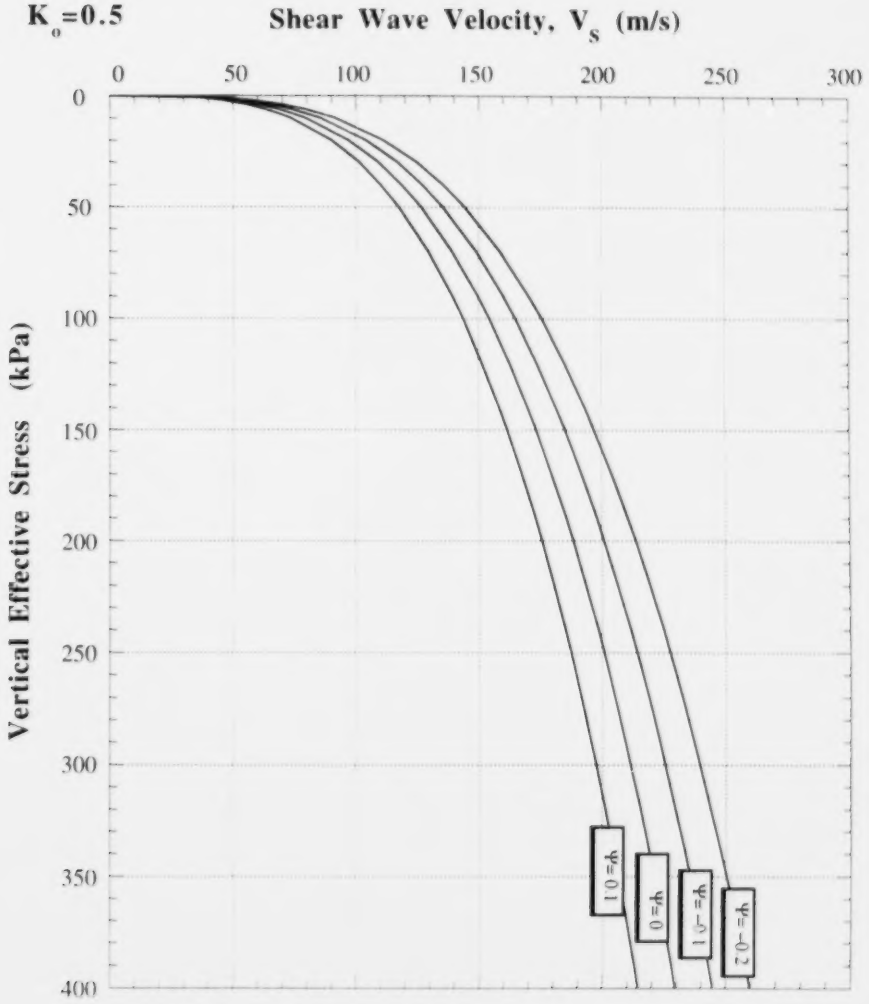

FIGURE 5.1 Profiles of State Parameter (Ψ) in terms of Shear Wave Velocity and Vertical Effective Stress for K_o=0.5 for Montana Sand

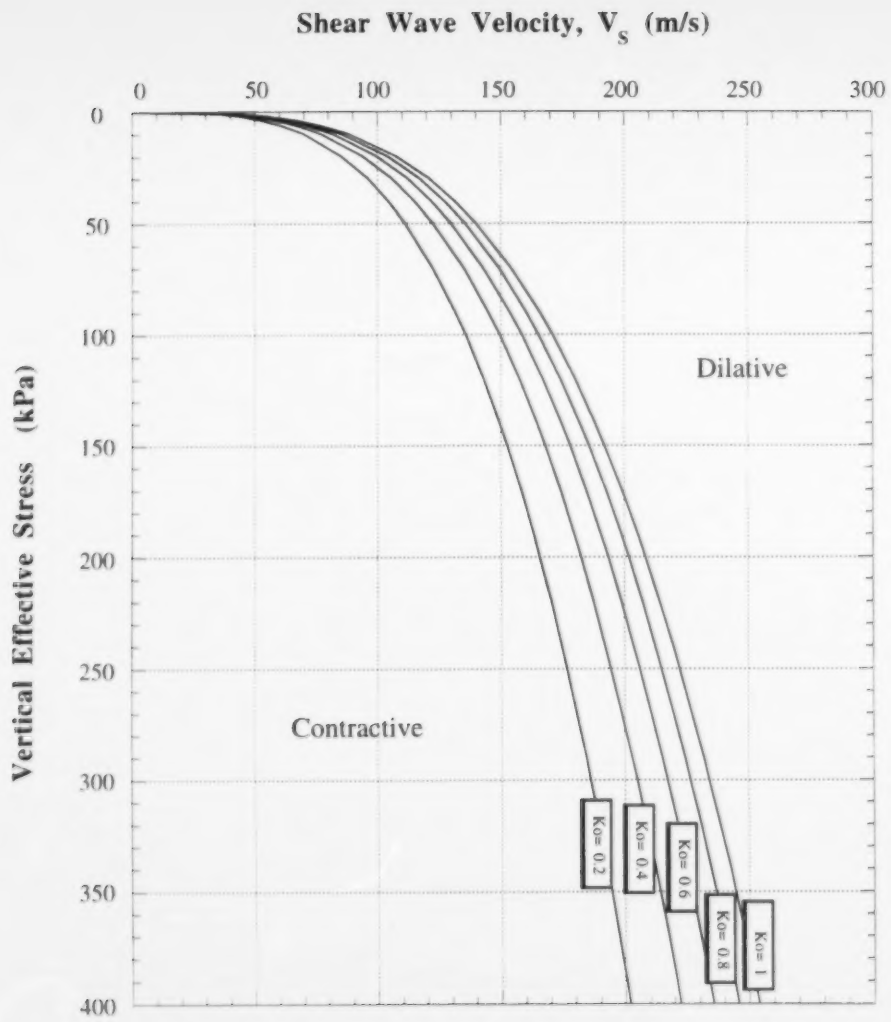

FIGURE 5.2 Shear Wave Velocity at Ultimate Steady State (Ψ=0) vs Vertical Effective Stress for Varying K_o Values for Montana Sand

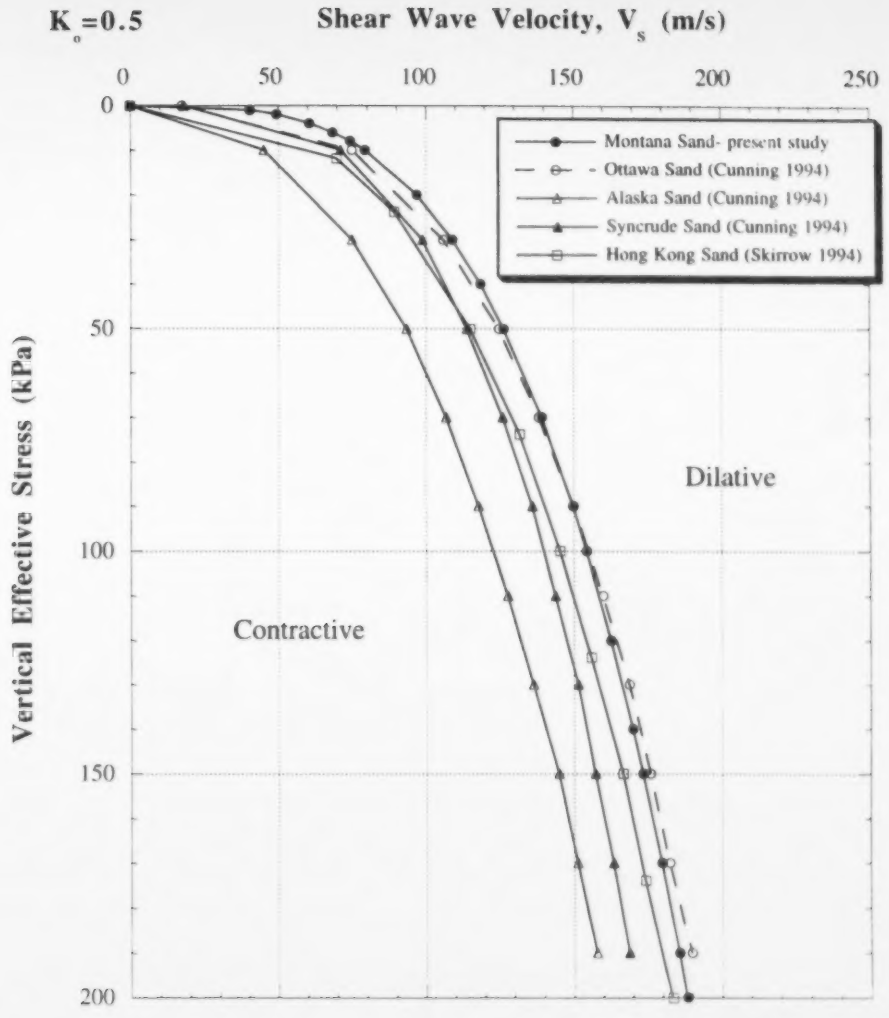

FIGURE 5.3 Contractive/dilative Boundaries for Several Sands (K_o=0.5)

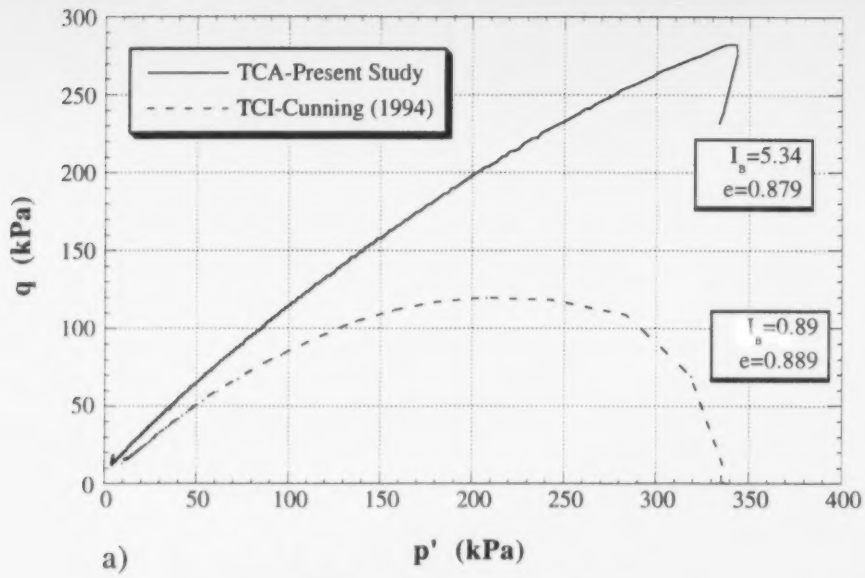

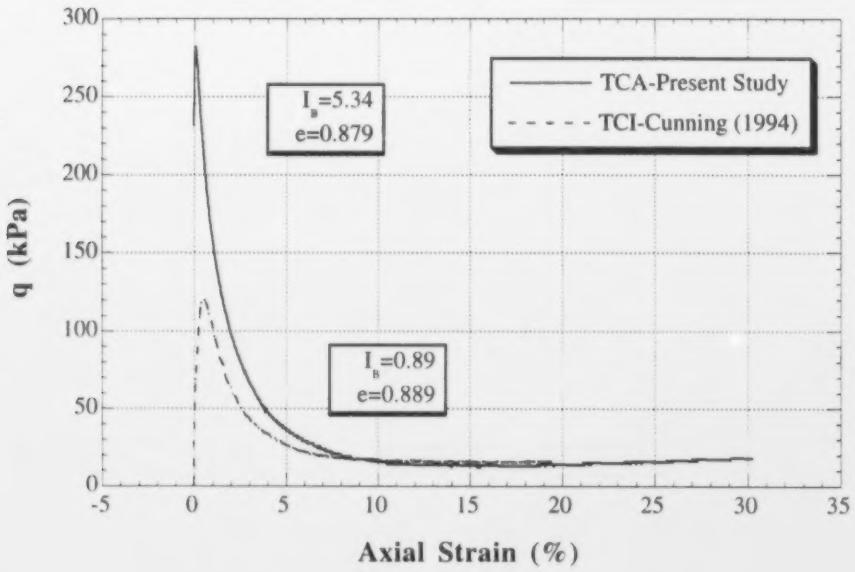

FIGURE 5.4 Effect of "Static Shear (q_o)" on Syncrude Sand
a) Stress Paths
b) Stress vs Strain

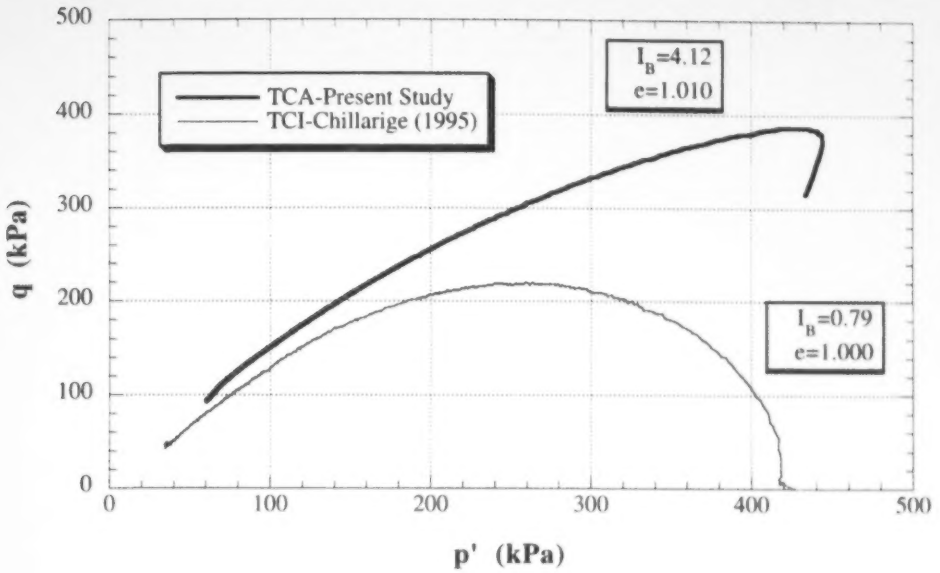

a)

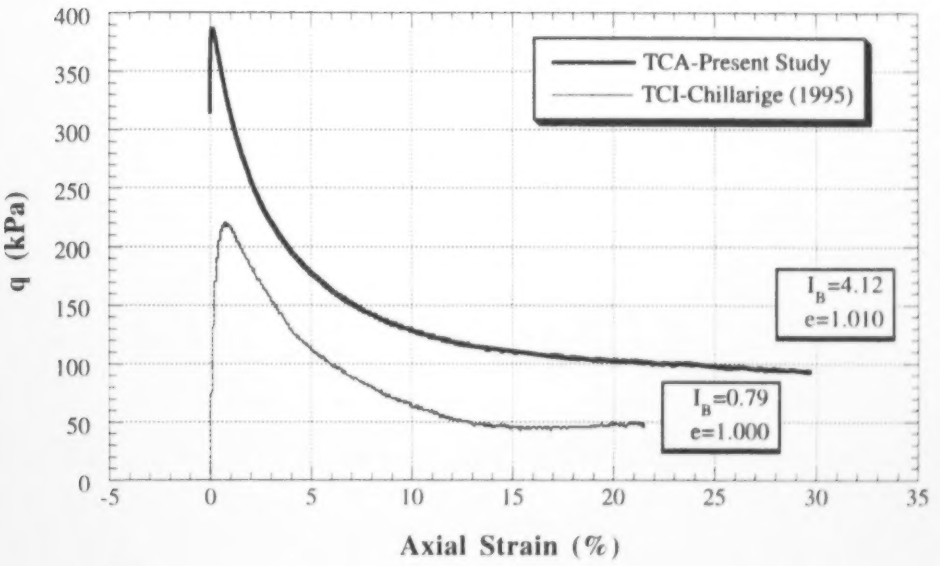

b)

FIGURE 5.5 Effect of "Static Shear (q_o)" on Fraser River Sand

a) Stress Paths
b) Stress vs Strain

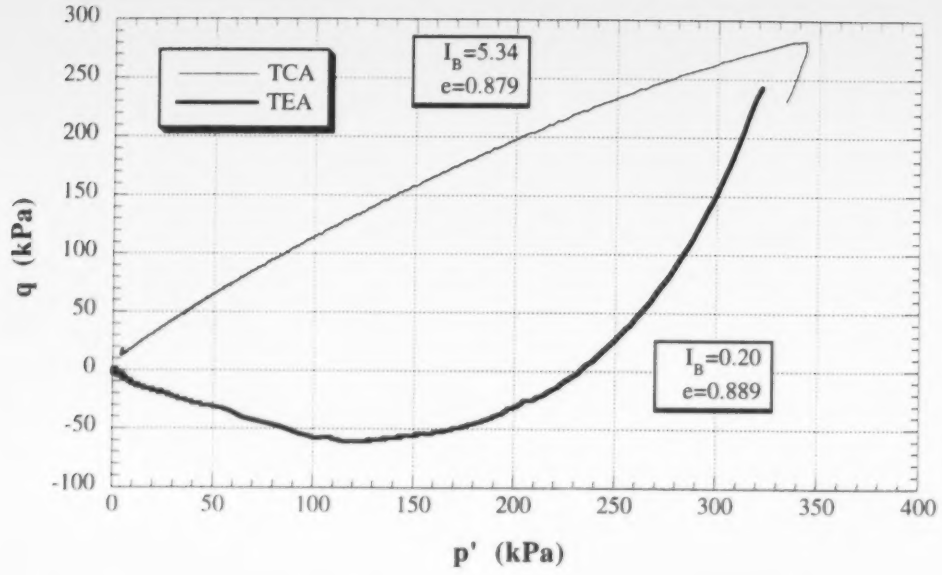

a)

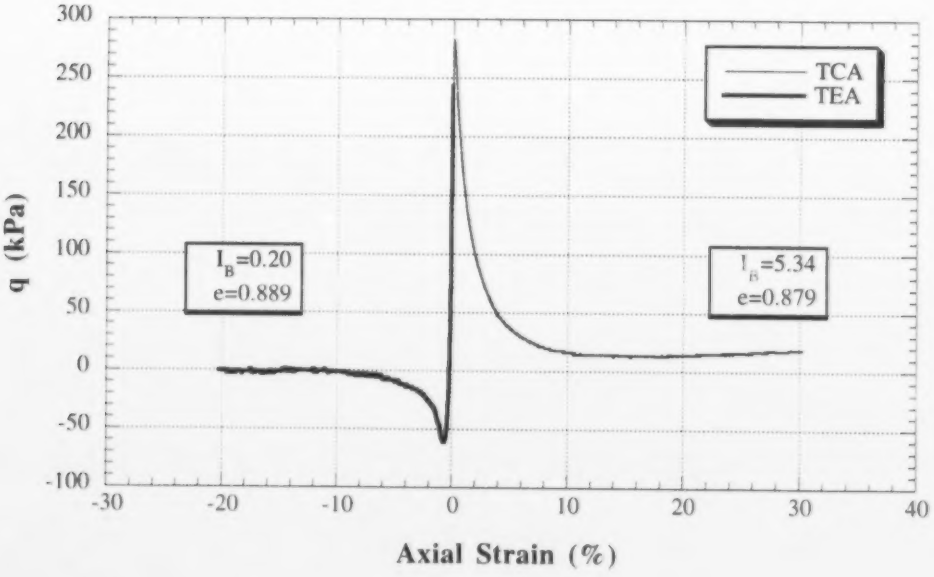

b)

FIGURE 5.6 Effect of "Direction of Loading" on Syncrude Sand
a) Stress Paths
b) Stress vs Strain

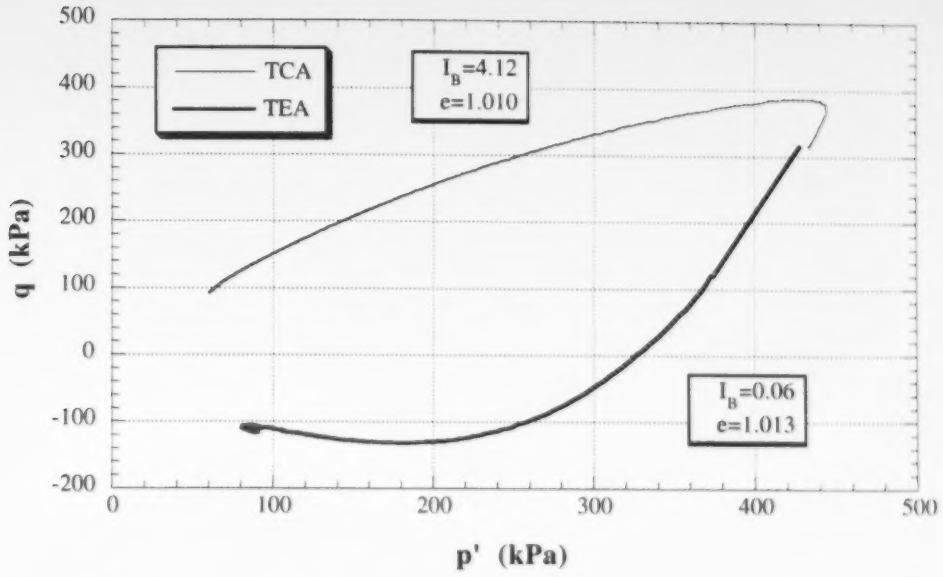

a)

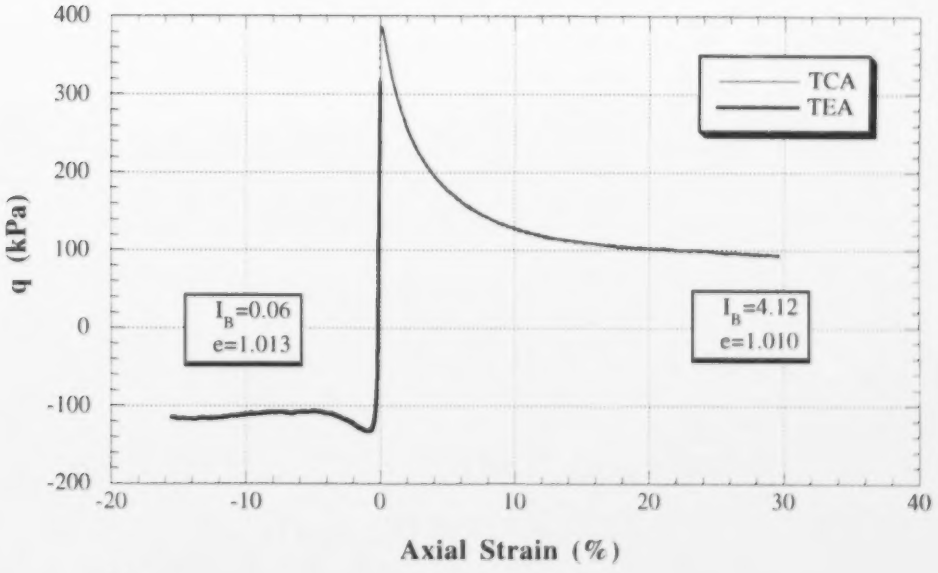

b)

FIGURE 5.7 Effect of "Direction of Loading" on Fraser River Sand
a) Stress Paths
b) Stress vs Strain

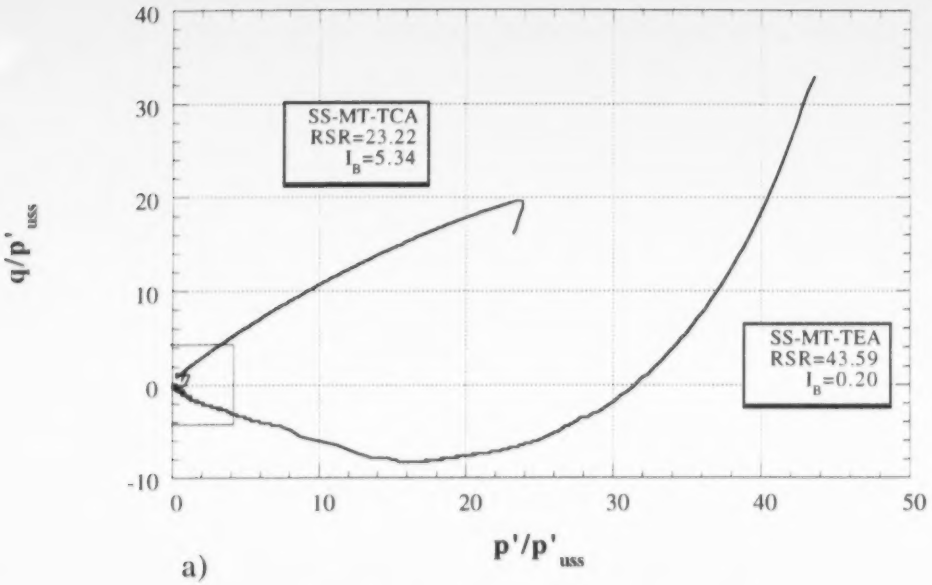

a)

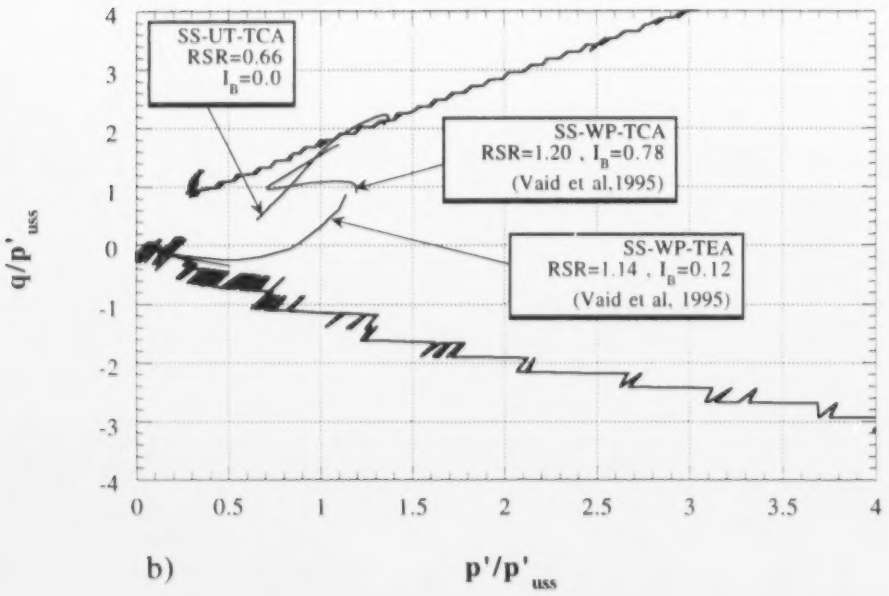

b)

FIGURE 5.8 Effect of "Initial State" on Syncrude Sand
a) Stress Paths
b) Stress Paths for Dense Samples

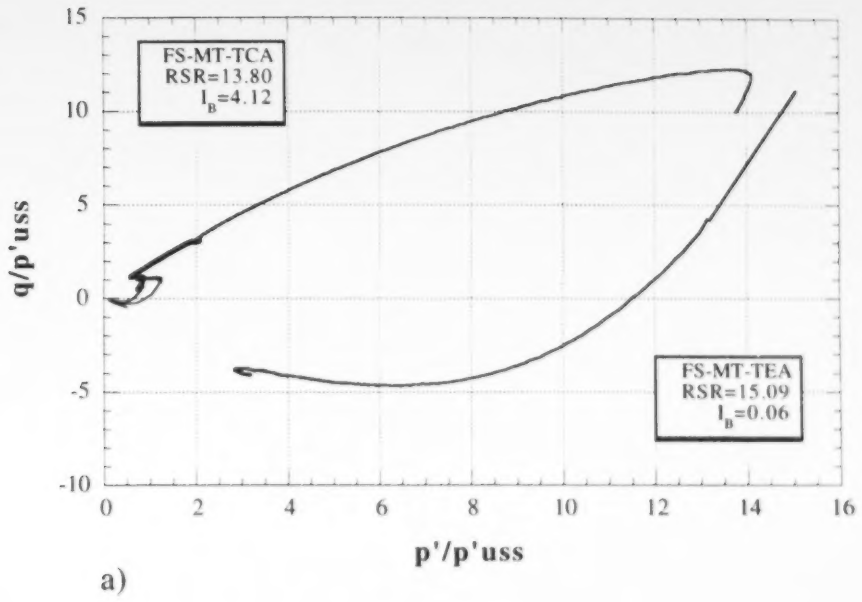

a)

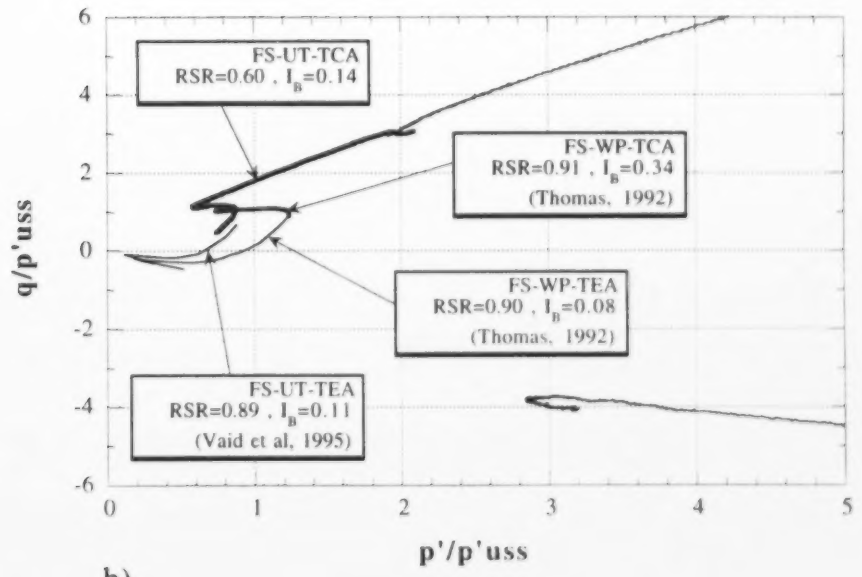

b)

FIGURE 5.9 Effect of "Initial State" on Fraser River Sand
a) Stress Paths
b) Stress Paths for Dense Samples

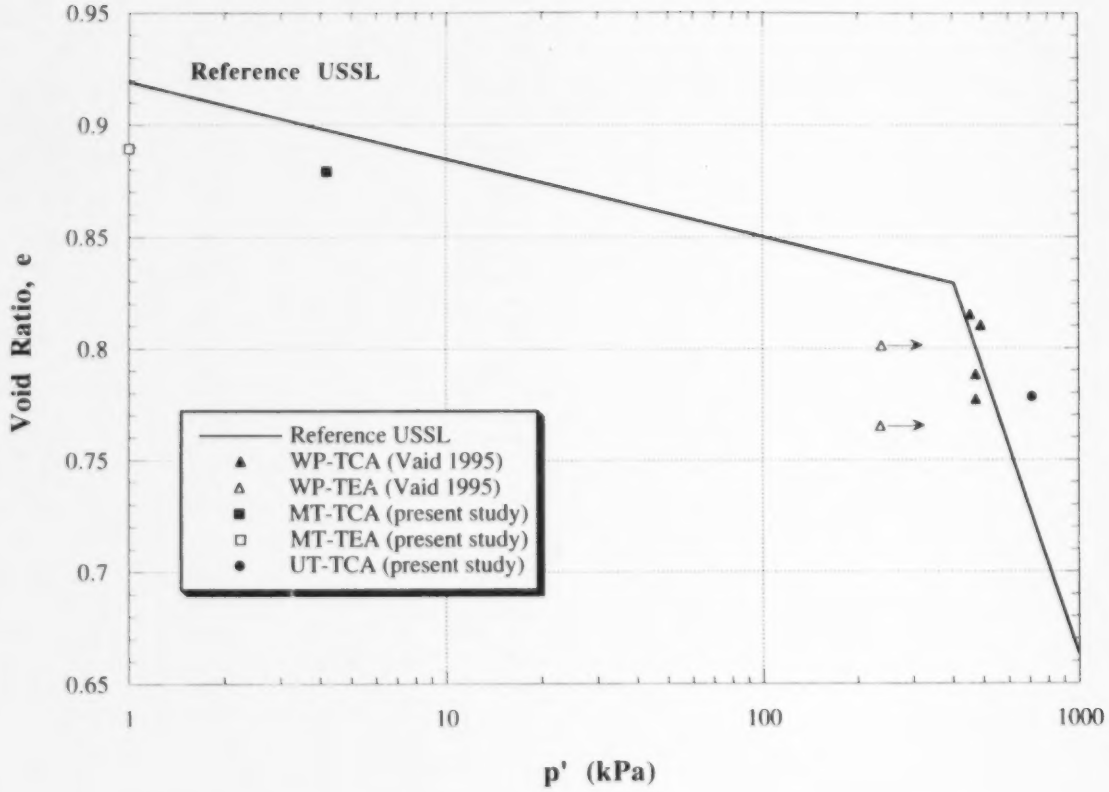

FIGURE 5.10 Ultimate States of All AC Tests on Syncrude Sand and Their Locations Relative to the Reference USSL

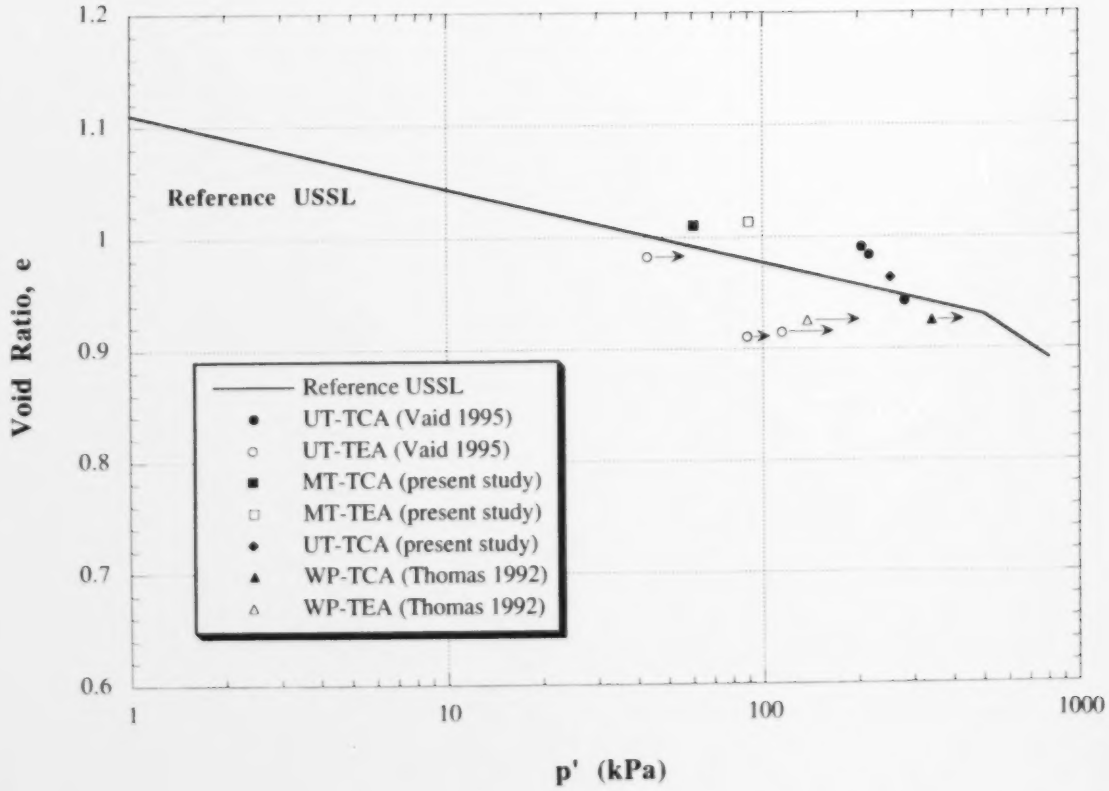

FIGURE 5.11 Ultimate States of All AC Tests on Fraser River Sand and their Locations Relative to the Reference USSL

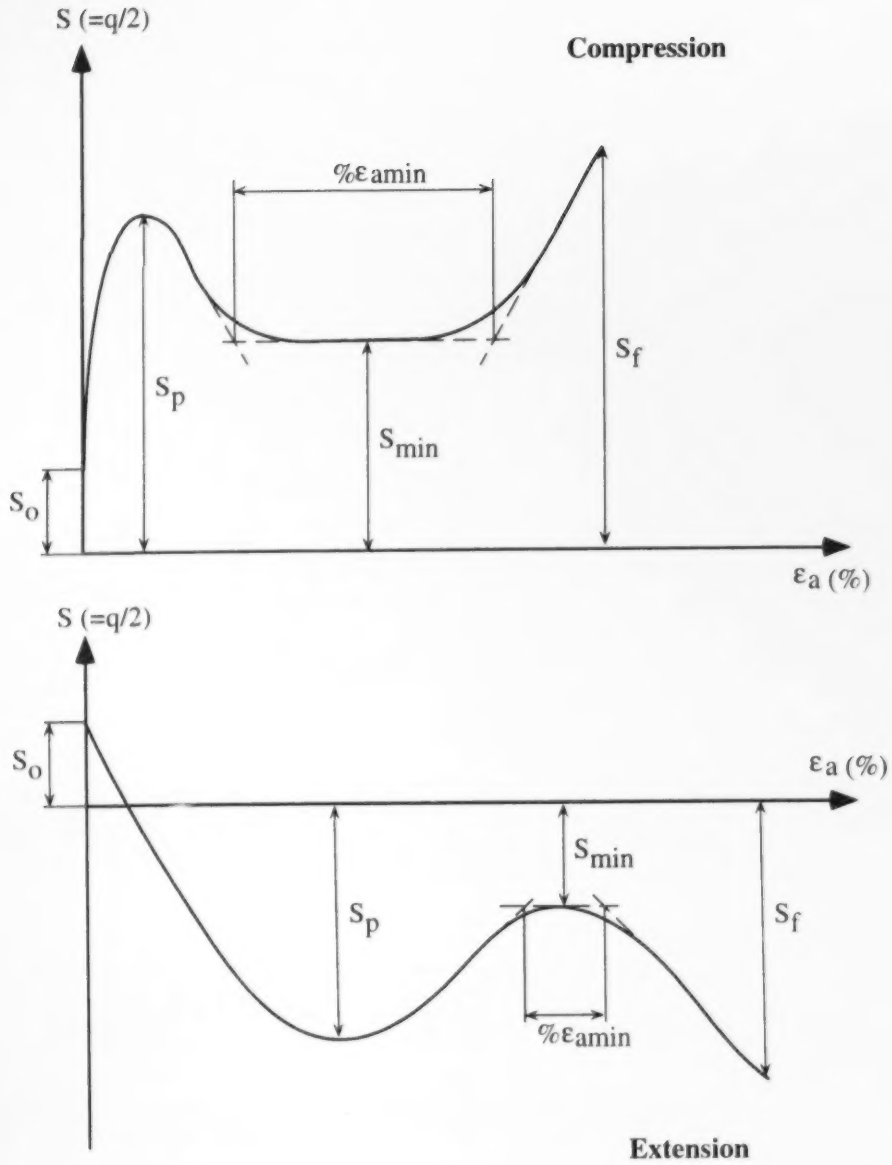

FIGURE 5.12 Response Parameters fot Triaxial Compression and Extension Tests (after Fear *et al.*, 1995)

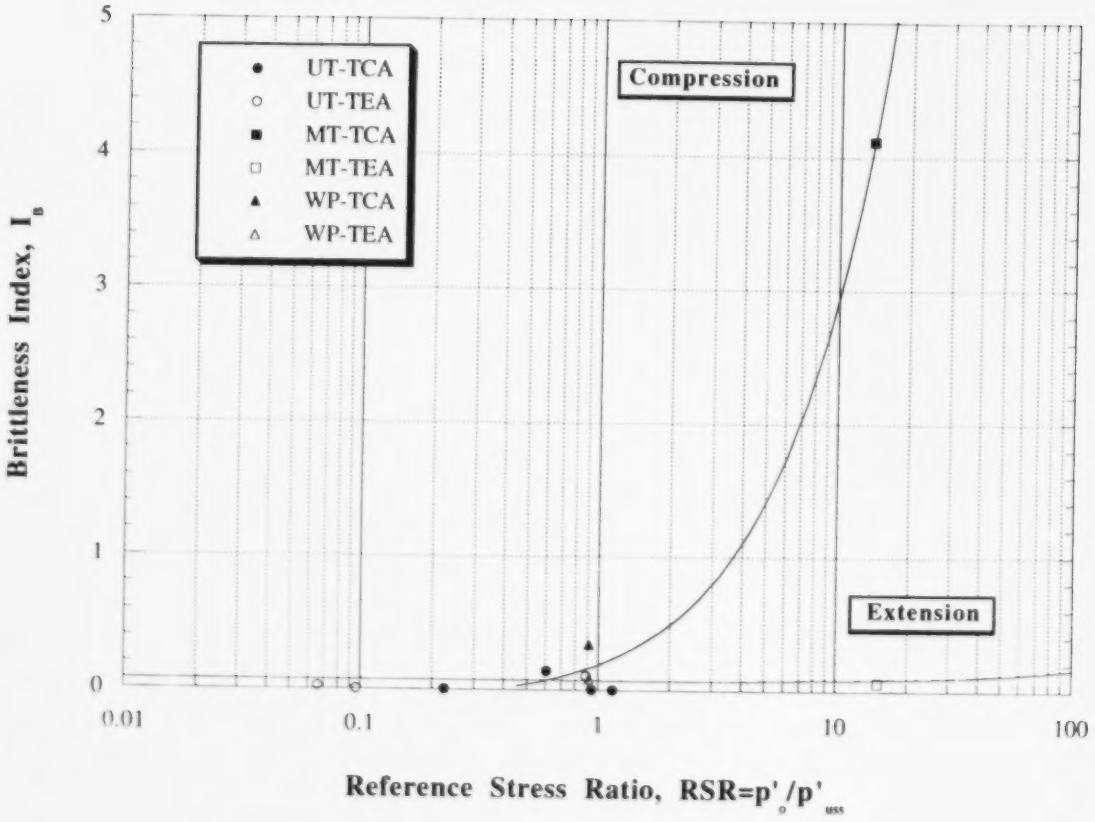

FIGURE 5.13 Brittleness Index vs RSR for All AC Tests on Fraser River Sand

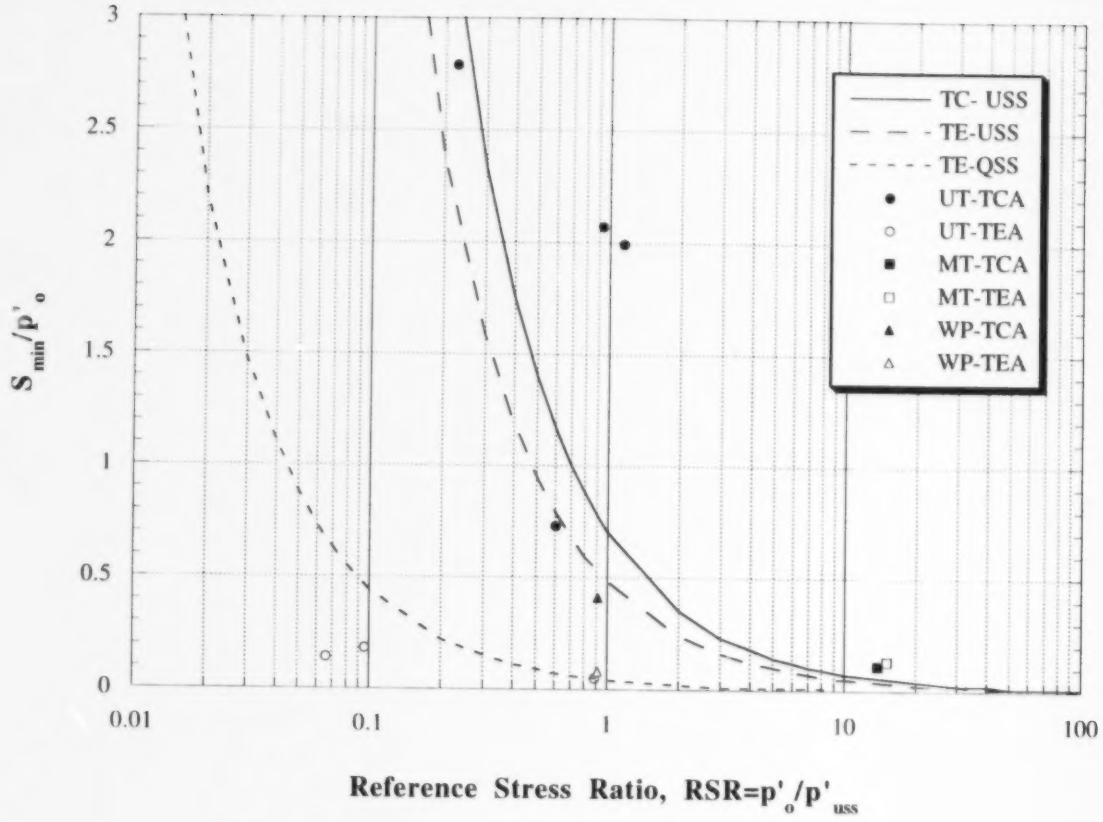

FIGURE 5.14 S_{min}/p'_o vs RSR for All AC Tests on Fraser River Sand

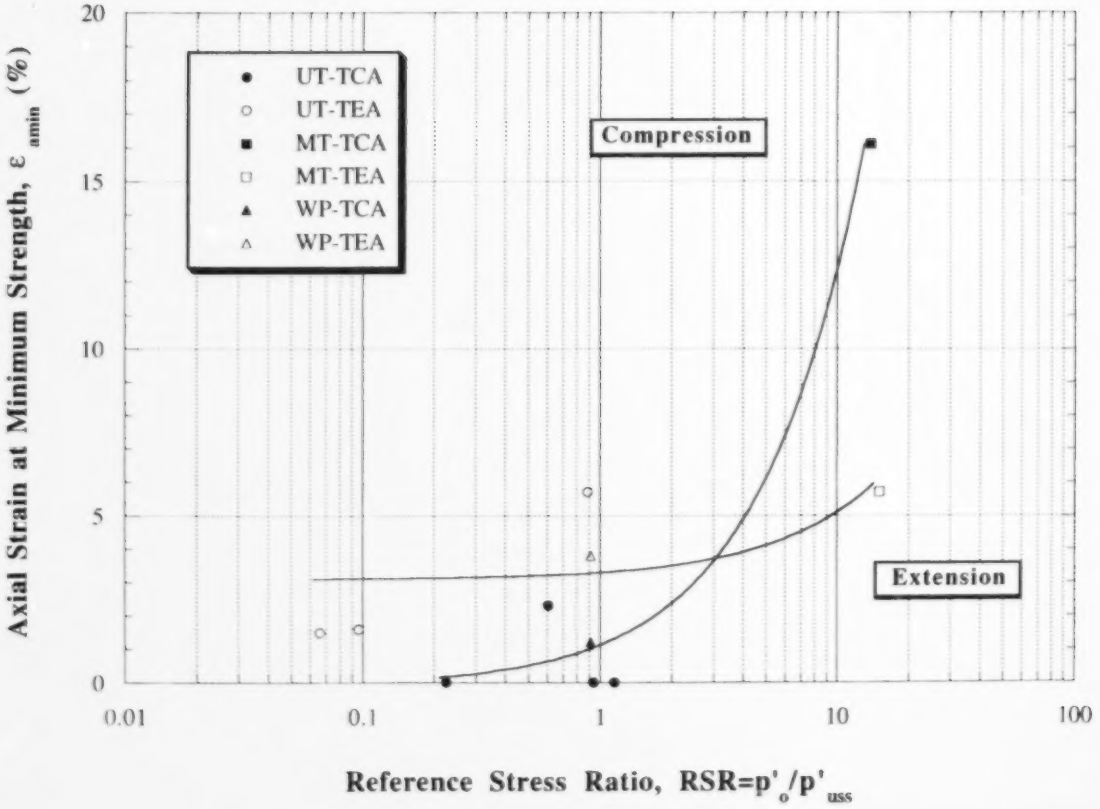

FIGURE 5.15 ε_{amin} vs RSR for All AC Tests on Fraser River Sand

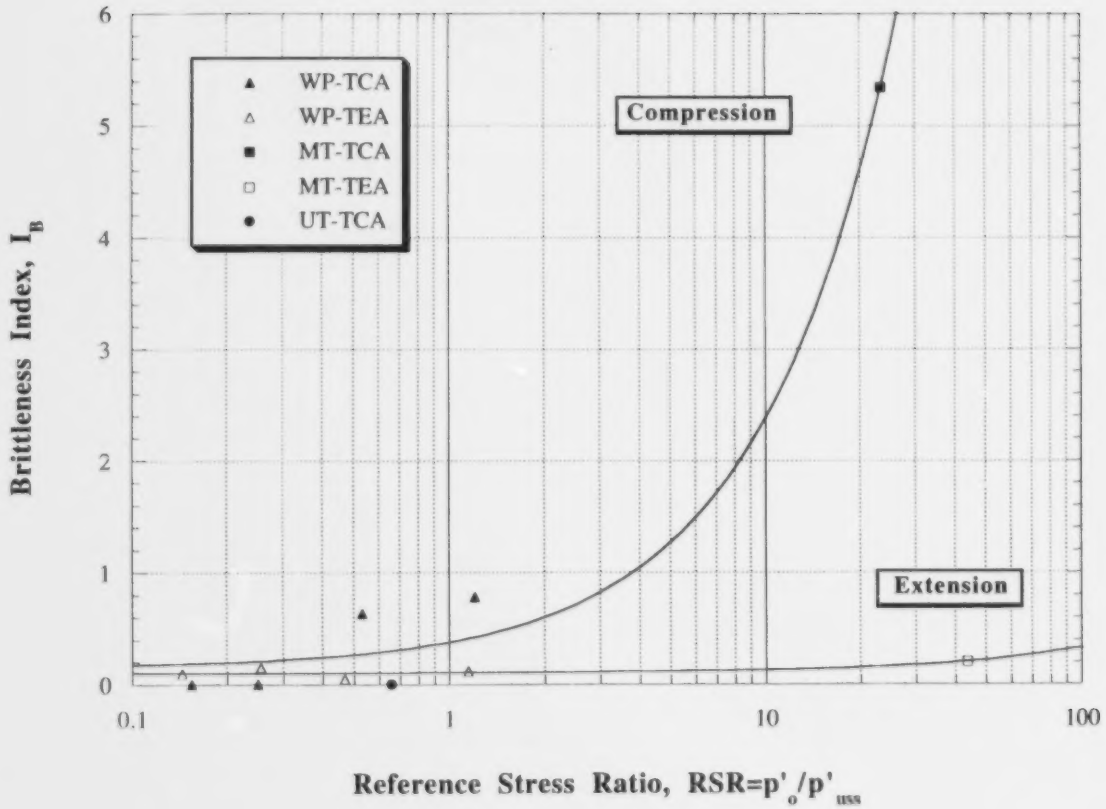

FIGURE 5.16 Brittleness Index vs RSR for All AC Tests on Syncrude Sand

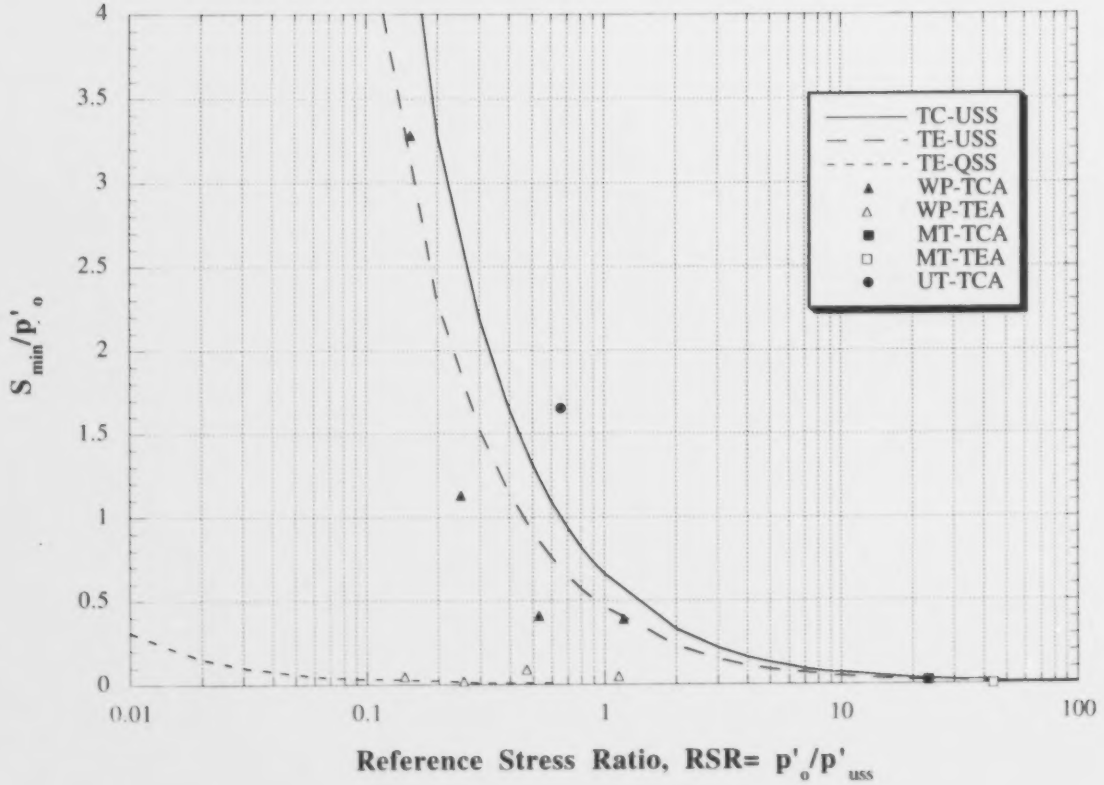

FIGURE 5.17 S_{min}/p'_o vs RSR for All AC Tests on Syncrude Sand

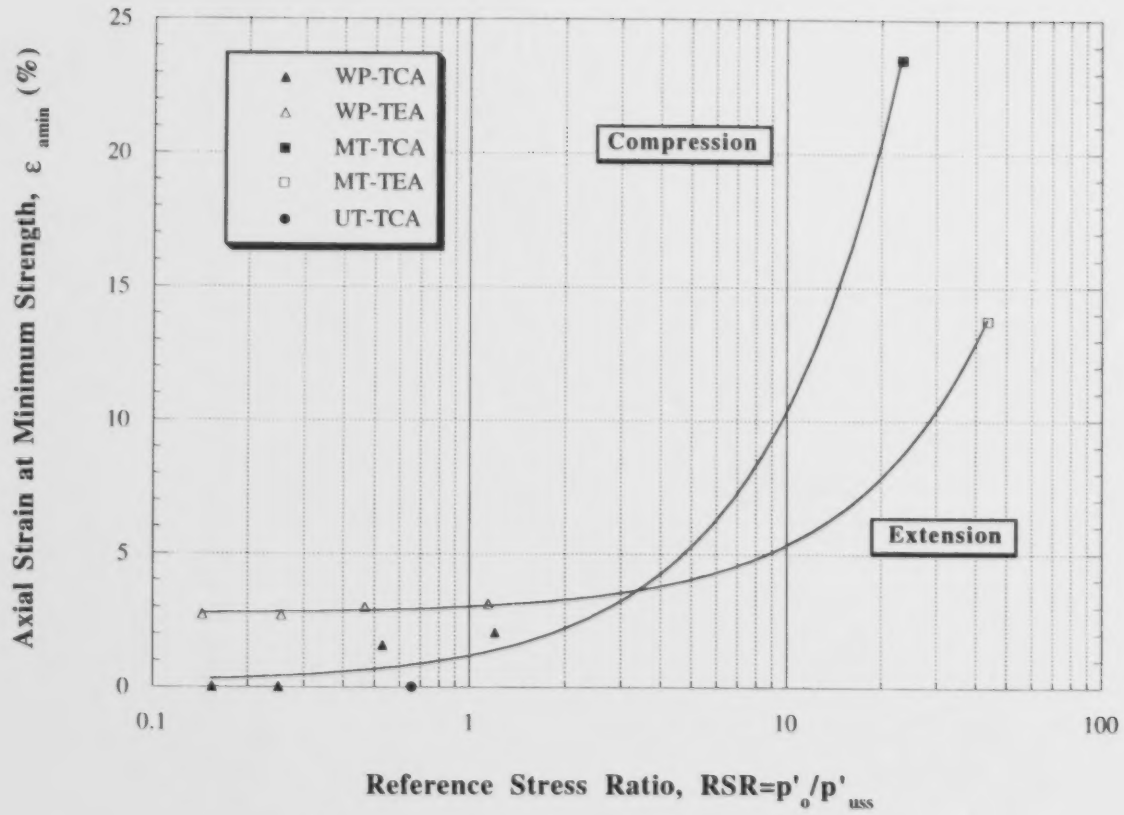

FIGURE 5.18 ε_{amin} vs RSR for All AC Tests on Syncrude Sand

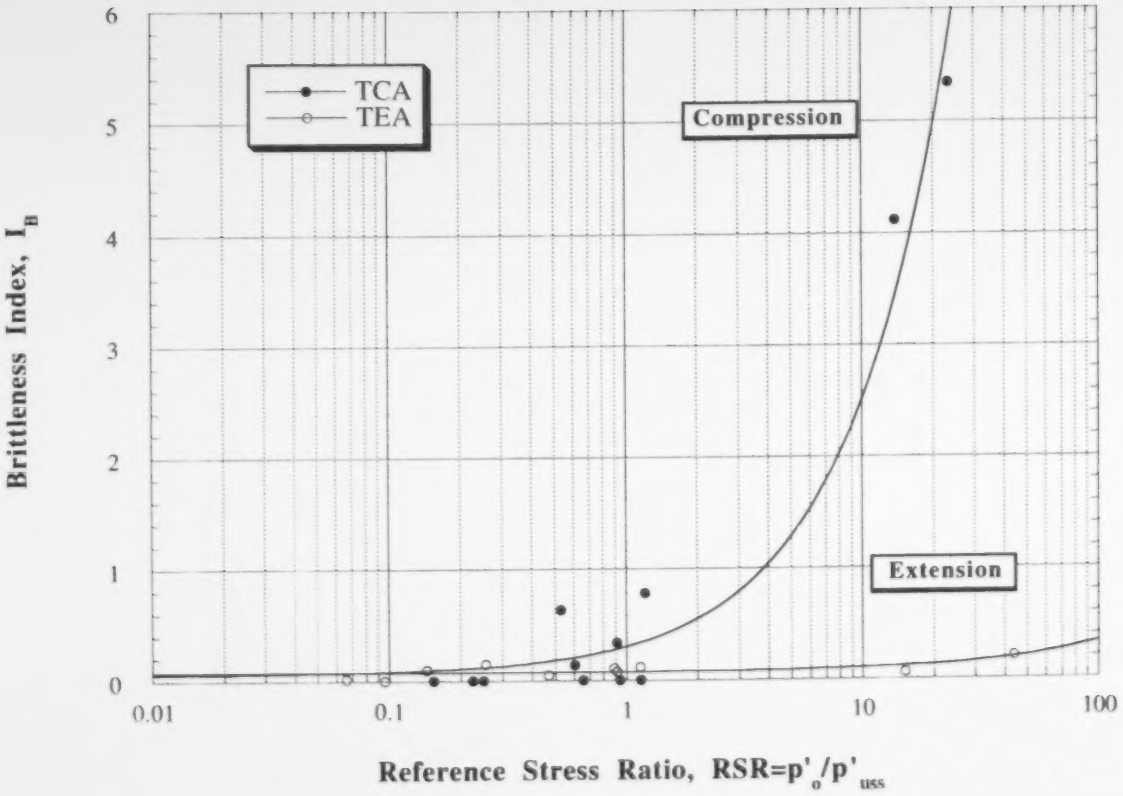

FIGURE 5.19 Brittleness Index vs RSR for All AC Tests on Fraser River Sand and Syncrude Sand

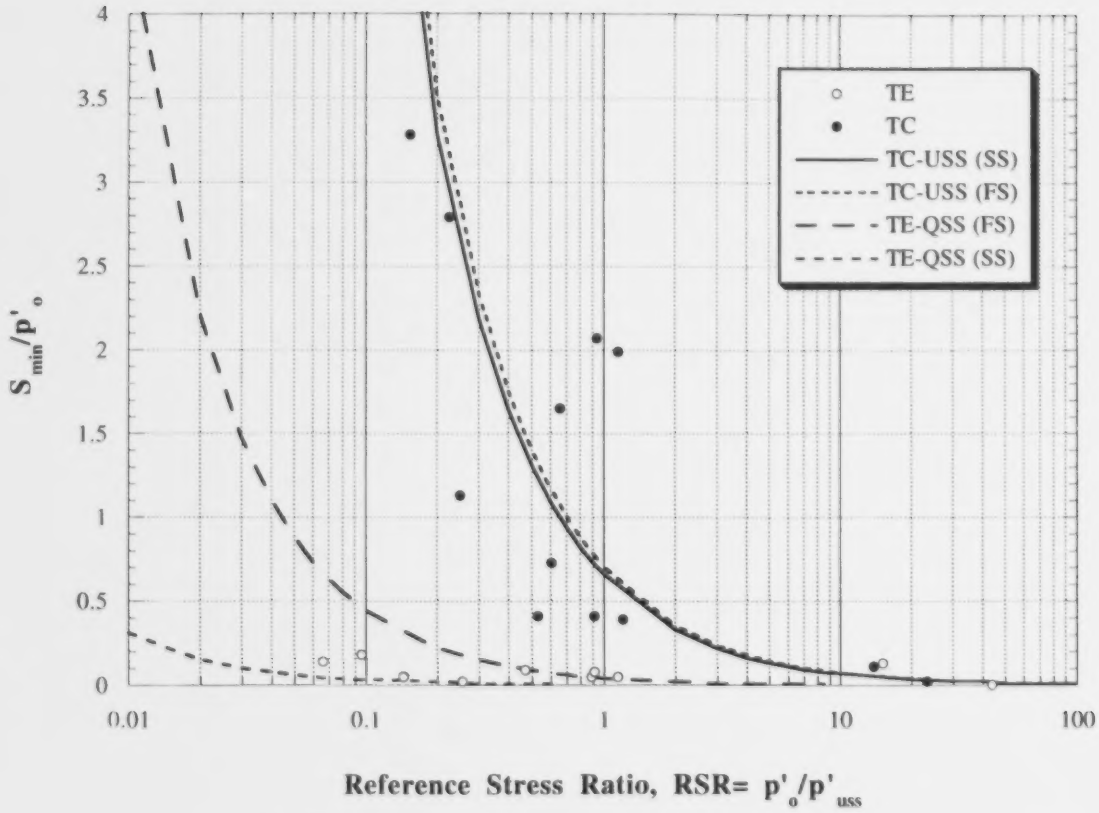

FIGURE 5.20 S_{min}/p'_o vs RSR for All AC Tests on Fraser River Sand and Syncrude Sand

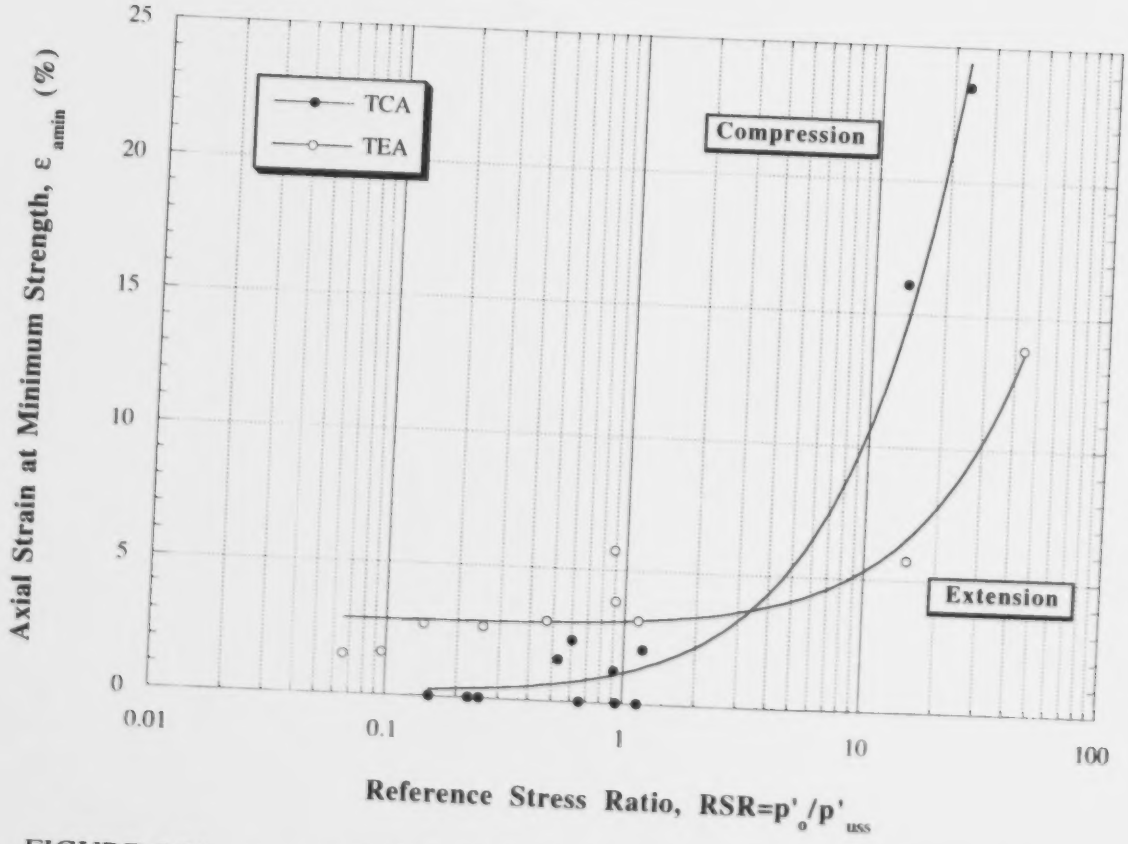

FIGURE 5.21 ε_{amin} vs RSR for All AC Tests on Fraser River Sand and Syncrude Sand

CHAPTER 6

SUMMARY AND CONCLUSIONS

The objectives of this research were:

1) To evaluate a procedure to estimate the in-situ state of sands using shear wave velocity.

2) To investigate the response of anisotropically consolidated sands in both compression and extension direction of loading.

3) To link the in-situ state of sands to their Response Parameters for a wide range of densities, to better evaluate the behaviour of cohesionless soils at large strains.

Evaluation of liquefaction potential is difficult, due to the complex phenomena involved and the variations in grain characteristics and in-situ soil state. If the saturated sand is very loose, the soil could be strain softening in undrained shear, and flow liquefaction is possible

The primary step in any liquefaction evaluation is to estimate the in-situ state of sands. Since the cost of in-situ ground freezing is high, the need to obtain high quality undisturbed samples to find the state of the soil will depend on project requirements.

Shear wave velocity was measured during consolidation, and used to develop a relationship between void ratio (e), mean effective normal stress (p′), and V_S. A modified triaxial apparatus was used and bender elements were incorporated in the base pedestal and loading head of the set up. Flush mounted bender elements were modified as a part of this research to be used for testing frozen, undisturbed specimens. The material tested was Montana tailings sand; a uniform, moderately compressible sand with 20% fines. Isotropically consolidated moist-tamped samples of Montana sand were tested in both drained and undrained compression loading. Based on shear wave velocity measurements, V_S parameters (A and B) were determined. Shear loadings were carried out to obtain the USS parameters (Γ, λ_{ln} and M), and also the location of USSL in e-ln p′ plot.

The seismic CPT provides the opportunity to measure shear wave velocity in the field and hence, develop a site specific correlation between V_S and cone resistance (q_c). The resulting e-p′-V_S relationship combined with the knowledge of in-situ stresses (i.e. the depth of ground water table, K_o value, and bulk density of the soil) and field V_S measurements, provide an estimation of in-situ void ratios. When field void ratios are plotted in e-ln p′ space, relative to the USSL, the state of the soil in terms of state parameter (ψ) or RSR can be estimated. The state of the sand provides valuable information to define the response of the material at large strains.

As a result, a flow liquefaction evaluation procedure was developed. USS parameters (Γ and λ_{ln}), and V_S parameters (A and B), forming the four soil constants, were used to define a contractive/dilative boundary in V_S-σ'_v plot. When in-situ V_S data are plotted with respect to this boundary, the response of the sand at large strains can be estimated in terms of contraction or dilation.

The contractive/dilative boundary for Montana sand, and four other sands were plotted together. It was shown that these boundaries fall within a relatively narrow band, and it is expected that most other sands would also have

a boundary in this area. Thus, the position of the contractive/dilative boundary for a given sand can be estimated with the knowledge of its grain characteristics.

In addition to void ratio and initial mean effective normal stress, several other factors will also influence the response of sands, including initial deviator stress (q_o), direction of loading (compression or extension), and soil structure (fabric, aging, cementation).

Two different types of sand (Syncrude tailings sand with 12% fines, and Fraser River sand with 5% fines) were studied to investigate the effect of some of these factors on their undrained monotonic behaviour. Since all of the existing knowledge concerning anisotropic behaviour of sands comes from laboratory tests on dense or medium loose samples, the reconstituted specimens in this part of the research were tested under "Very Loose" states (RSR>10).

The sands were found to be inherently anisotropic with different responses in different directions of loading. The behaviour of anisotropically consolidated sands were shown to be vastly different from that of isotropically consolidated material. Since an element of soil in the ground is generally under anisotropic consolidation, these differences can be very important for flow liquefaction studies. The anisotropically consolidated (AC) samples of Syncrude sand, and Fraser River sand were much more brittle in undrained triaxial compression loading than isotropically consolidated (IC) specimens of the same sand at the same void ratios and confining stresses. Both AC and IC samples were shown to have similar shear strengths at USS, whereas their brittleness indexes were significantly different.

An experimental study was conducted to evaluate the response of AC samples under compression and extension loading. Very loose specimens of the same sand with identical void ratios, under almost equal effective stresses, were prepared by moist tamping method. These samples were then loaded in undrained shear from a state of K_o consolidation line in compression and extension. Different behaviour was observed in compression and extension.

The AC samples under compression failed almost immediately after being loaded, whereas more additional loading was required to bring those sheared in extension to failure due to their initial anisotropic (K_o) condition. Both compression and extension tests showed clear strain softening responses, but the samples loaded in compression were much more brittle than those loaded in extension.

To study the effect of initial in-situ state, and also soil structure on the response of sandy soils, some high quality undisturbed frozen samples of Syncrude sand and Fraser River sand were also tested. It was critical to thaw and test those undisturbed samples under their in-situ void ratios and stresses. A successful method for thawing frozen samples was developed, and employed to maintain their in-situ conditions during thawing and consolidation. As a result, the frozen samples were thawed under their in-situ stresses. The undisturbed specimens were found to be denser than the loosest reconstituted, moist-tamped samples. Thus, they showed mainly dilative behaviours at large strains. The normalized stress path plots of the undisturbed, and reconstituted samples provided a powerful method to compare their responses. It was shown that the undisturbed samples possessed much lower RSR values than the loosest moist-tamped specimens, and that their behaviour can be explained within the framework of critical state soil mechanics.

Shear wave velocity measurements were also carried out at the end of consolidation of these undisturbed specimens, and the results were compared with the in-situ velocity measurements. Even though there appeared to be a reasonable agreement between the two sets of measurements, it was noticed that further developments are required to obtain more accurate in-situ shear wave velocity measurements.

Results from this research and previously published data were compiled to evaluate sand behaviour for a wider range of densities and soil structure. Results from undrained triaxial tests (compression and extension) on

anisotropically consolidated undisturbed, moist-tamped and water pluviated samples were compared. The ultimate states from these tests showed that there appears to be a unique USSL for each sand. Although some of the tests could not be carried out to sufficiently large strains to reach USS, the stress paths for all the tests indicate that their final states are moving towards a single USSL. As well, the USSL for Syncrude sand was shown to be flatter at very low stress levels.

Based on the available data, Response Charts were developed to link the in-situ state of sands (which can be estimated using V_S) to their Response Parameters. These parameters are mainly "Brittleness Index", (I_B), "minimum undrained shear strength", (S_{min}), and "axial strain at minimum shear strength", (ε_{amin}). Since the charts are plotted against RSR, the effect of material type should not be significant, thus results for several sands can be compared. The Response Charts can link the in-situ state of sands, and subsequently their in-situ shear wave velocity measurements (when e-p'-V_S correlation is developed in the laboratory) to their Response Parameters. As a result, the Response Parameters can be plotted versus depth or vertical effective stress (σ'_v). Finally, continuous profiles of liquefaction potential in a repeatable and cost effective manner can be produced.

The present study clearly shows that to evaluate flow liquefaction potential, sands should be tested under their in-situ states, and appropriate direction of loading. Conventional triaxial compression tests on isotropically consolidated sand samples can provide misleading information for liquefaction analyses. The obtained Response Charts indicate very loose sands will exhibit significantly different behaviour under undrained monotonic compression and extension loading relative to dense or medium loose sands at large strains. From the flow liquefaction evaluation point of view, loading in extension may control the design of dense or medium loose sand deposits, whereas compression loading can govern the analysis for "very loose" structures.

What follows is the summary of the obtained results in this research:

1) A procedure was introduced to estimate the in-situ state of Montana sand using shear wave velocity.

2) A method was suggested to determine contractive/dilative boundary for a given sand.

3) Anisotropically consolidated loose sands were more brittle than isotropically consolidated samples at the same state.

4) Very loose anisotropically consolidated samples with similar states were significantly more brittle in compression than in extension loading.

5) Undisturbed samples of Syncrude sand and Fraser River sand were shown to be denser than the loosest moist tamped specimens.

6) Response Charts were developed to link the in-situ state of sands to their Response Parameters.

7) Ultimate steady state line was shown to be unique for a given sand. The line appeared to be flatter at very low confining pressures.

8) Laboratory shear wave velocities were shown to be in agreement with in-situ velocity measurements.

9) A method was introduced for thawing the frozen undisturbed samples for triaxial testing.

6.1 Recommendation for Future Research

The present study investigated the behaviour of anisotropically consolidated samples, under compression and extension direction of loading. It also provides a procedure to estimate the in-situ state of sandy soils using shear wave velocity measurements. Future work is needed to extend the results of this study. In this view it would be desirable to carry on the present work in the following areas:

1) More advanced methods of determining shear wave velocities in the laboratory, using the first pulse arrival method are required.

2) Results from this study showed that more accurate in-situ shear wave velocity measurements are necessary to evaluate the in-situ state of sandy deposits.

3) Most of the anisotropic tests on reconstituted samples in this research were carried out on very loose specimens. More tests are required to study the response of cohesionless soils for a wider range of densities.

4) The influence of direction of loading relative to the bedding planes (α_σ) using hollow cylinder torsion tests (HCT) should be investigated. Compression and extension tests only give information for two directions of loading, i.e. α_σ=0 and α_σ=90°, respectively. The HCT tests on specimens with various void ratios can provide valuable information to expand the results of this study.

5) The database presented in this study need to be extended to provide more accurate Response Charts.

6) Results from this study, and other data showed that the contractive/dilative boundary in terms of shear wave velocity for most sands fall within a relatively narrow band. Further work can be carried out to study more sands and verify this finding.

7) Triaxial tests carried out to evaluate flow liquefaction should be continued to large strains until the ultimate steady state is reached. At these large strains specimens undergo non-uniform deformations, and the available corrections for the area of samples may not be realistic. Thus, further research should be carried out to measure the lateral deformation of saturated samples at large strains.

8) In-situ soils can be aged or cemented. Investigations need to be under taken to study the influence of aging and cementation on shear wave velocity measurements, and also the response of sands under monotonic loading.

9) The influence of fabric on sand behaviour has not been addressed satisfactorily. This study suggests that ultimate steady state at large strains is independent of fabric for the range of test conditions and sands examined. There is evidence indicating that stress-strain response is fabric-dependent. Therefore, a method to study the effect of initial fabric is required. In this regard, it is important to produce the field fabric to understand the response of a soil.

REFERENCES

Alarcon-Guzman, A., and Leonards, G. A., (1988). "Discussion: Liquefaction evaluation procedure," *Journal of Geotechnical Engineering, ASCE,* 114, No. 2, pp. 232-236.

Atkinson, J. H., and Bransby, P. L., (1978). "The Mechanics of soils, an introduction to Critical State Soil Mechanics," McGraw-Hill, London, England.

Ayoubian E., A., and Hofmann, B. A., (1995). "Preliminary report on thawing of undisturbed frozen specimens for triaxial testing," CANLEX internal report.

Been, K., and Jefferies, M. G., (1985). "A state parameter for sands," *Geotechnique*, 35, pp. 99-112.

Been, K., Jefferies, M. G., and Hachey, J (1991). "The critical state of sands," *Geotechnique*, 41(3), pp. 365-381.

Bishop, A. W., (1971). "Shear strength parameters for undisturbed and remolded soil specimens," *Roscoe Memorial Symposium*, Cambridge University, pp. 3-58.

Bishop, A. W., (1973). "The stability of tips and spoil heaps," *Quarterly Journal of Engineering Geology*, 6, pp. 335-376.

Brignoli, E. G. M., Marino, G., Stokoe, K. H. II, (1995). "Measurement of shear waves in laboratory specimens by means of piezoelectric transducers," *ASTM.*

Casagrande, A., (1965). "The role of the calculated risk in earthwork and foundation engineering," The Terzaghi lecture, *Journal of soil mechanics and foundation Division*, ASCE, 91(4), pp. 1-40.

Casagrande, A., (1975). "Liquefaction and cyclic deformation of sands, a critical review," *Harvard Soil Mechanics Series*, No. 88, Harvard University, Cambridge, MA.

Castro, G., (1969). "Liquefaction of sands," *Harvard Soil Mechanics Series,* No. 81, Harvard University, Cambridge.

Castro, G., Enos, J. L., France, J. W., and Poulos, S. J., (1982). "Liquefaction induced by cyclic loading," *Report to National Science Foundation,* Washington, D.C., No. NSF/CEE-82018.

Chaney, R. C., and Fang, H. Y., (1991). "Liquefaction in the coastal environment: an analysis of case histories," *Marine Geotechnology,* 10, pp. 343-370.

Chillarige, A. R. V., (1995). "Liquefaction and seabed instability in the Fraser River Delta," Ph.D. thesis, Department of Civil Engineering, University of Alberta, Edmonton, Canada.

Cunning, J. C., (1994). "Shear wave velocity measurement of cohesionless soils for evaluation of in-situ state," M.Sc. thesis, Department of Civil Engineering, University of Alberta, Edmonton, Canada.

De Alba, P., Baldwin, K., Janboo, V, Roe, G., and Celikkol, B., (1984). "Elastic wave velocities and liquefaction potential," *Geotechnical Testing Journal,* 7(2), pp. 77-88.

Dyvik, R., and Madshus, C., (1985). "Laboratory measurements of G_{max} using bender elements," *Proceeding, Advances in the Art of testing Soils under Cyclic Conditions, ASCE Annual Convention,* Detroit, Michigan, October 1985, pp. 186-196.

Dyvik, R., and Olsen, T. S., (1991). "G_{max} measured in oedometer and DSS test using bender elements," *Norges Geotekniske Institute Publication No. 181.*

Fear, C. E., and Robertson P. K., (1995). "Estimating the undrained strength of sand: a theoretical framework," *Canadian Geotechnical Journal,* 32(4).

Fear, C. E., Robertson, P. K., Hofmann, B. A., Sego, D. C., Campanella, R. G., Byrne, P. M., Davies, M. P., Konrad, J.-M., Küpper, A., List, B., and Youd, L., (1995). "Summary of CANLEX Phase I site characterization," *Proceeding of the 48th Canadian Geotechnical Conference,* Vancouver, B.C., 1, pp. 331-340.

Georgiannaou, V. N., (1988). "Behaviour of clayey sands under monotonic and cyclic loading," Ph.D. thesis, Department of Civil Engineering, Imperial College of Science, Technology and Medicine, London, England.

Hardin, B. O., and Richart, F. E. Jr., (1963). "Elastic wave velocities in granular soils," *Journal of Soil Mechanics and Foundation Division, ASCE,* 89(1), 33-65.

Hardin, B. O., and Black, W. L., (1968). "Vibration modulus of normally consolidated clays," *ASCE Journal of the Soil Mechanics and Foundation Division,* 94(SM2), pp. 253-369.

Hofmann, B. A., Sego, D. C., and Robertson, P. K., (1994). "Undisturbed sampling of a deep loose sand deposit using ground freezing" *Proceedings of the 47th Canadian Geotechnical Conference,* Vancouver, B.C., 1, pp. 77-80.

Hughes, J. M. O., Roy, D., Campanella, R. G., Byrne, P. M., and Robertson, P. K., (1995). Phase I, pressuremeter testing for CANLEX at Syncrude Test Site. *Proceeding of the 48th Canadian Geotechnical Conference,* Vancouver, B.C., 1, pp. 77-80.

Hungr, O., and Morgenstern, N. R., (1984). "Experiments on the flow behaviour of granular materials at high velocity in an open channel," *Geotechnique,* 34(3), pp. 405-413.

Isenhower, W. M., Stokoe, K. H., II, and Allen, J. C., (1987). "Instrumentation for torsional shear/resonant column measurements under anisotropic stresses," *Geotechnical Testing Journal, ASTM.*

Ishihara, K., Verdugo, R., and Acacio, A. A., (1991). "Characterization of cyclic behaviour of sand and post-seismic stability analysis," *9th Asian Regional Conference on Soil Mechanics and Foundation Engineering.* Bangkok, Thailand, 2, pp. 17-40.

Ishihara, K., (1993). "Liquefaction and flow failure during earthquakes," *The 33rd Rankine Lecture, Geotechnique,* 43(3), pp. 351-415.

Kuerbis, R. H., Negussey, D., and Vaid, Y. P., (1988). "Effect of gradiation and fines content on the undrained response of sand," *ASCE Specialty Conference Hydraulic Fill Structures,* Fort Collins, CO., pp. 330-345.

Kuerbis, R. H., (1989). "The effect of gradiation and fines content on the undrained loading response of sand," M.A.Sc thesis, Department of Civil Engineering, University of British Columbia, Vancouver, Canada.

Kuerbis, R. H., and Vaid, Y. P., (1990). "Corrections for membrane strength in the triaxial test," *Geotechnical Testing Journal, GTJODJ,* 13, No. 4, pp. 361-369.

Koppejan, A. W., Van Wamelen, B. M., and Weinberg, L. J. H., (1948). "Costal landslides in the Dutch province of Zealand," *Proceedings of the 2nd International Conference on soil Mechanics and foundation Engineering,* Rotterdam, Holland, pp. 89-96.

Lawrence, F. V., (1963). "Propagation of ultrasonic waver through sand," Research Report R63-8, Massachusetts Institute of Technology, Cambridge, MA.

Lawrence, F. V., (1965). "Ultrasonic shear wave velocity in sand and clay," Research Report, R65-05, Soil Publication No. 175, Massachusetts Institute of Technology, Cambridge, MA.

Lee, K. L., and Seed. H. B., (1967). "Drained strength characteristics of sands," *Journal of Soil Mechanics and Foundation Division, ASCE*, 93, No. SM6, pp. 117-141.

McRoberts, E. C., and Morgenstern, N. R., (1974). "A note on pore water expulsion during freezing," Department of Civil Engineering, University of Alberta, Edmonton, Canada.

Morgenstern, N. R., (1967). "Submarine slumping and the initiation of turbidity currents," *Marine Geotechnique*, Edited by A. F. Richards, Urbana, Illinois, University of Illinois Press, pp. 189-210.

Mulilis, J. P., Seed, H. B., Chan, C. K., Mitchell, J. K., and Arulanandan, K., (1977). "Effects of sample preparation on sand liquefaction," *ASCE Journal of the Geotechnical Engineering Division*, 103, No. GT2, pp. 91-108.

Nicholson, P. G., Seed, R. B., and Anwar, H. A., (1993). "Elimination of membrane compliance in undrained triaxial testing. I. Measurement and evaluation," *Canadian Geotechnical Journal*, 30, pp. 727-738.

Pestana, J. M., and Whittle, A. J., (1995). "Compression model for cohesionless soils," accepted for publication in *Geotechnique*.

Pitman, T. D., (1993). "Effect of fines and gradation on collapse surface of loose saturated sands," M.Sc. thesis, Department of Civil Engineering, University of Alberta, Edmonton, Canada.

Poulos, S. J., (1981). "The steady state of deformation," *ASCE Journal of Geotechnical Engineering Division*, 107(GT5), pp. 553-561.

Poulos, S. J., Castro, G., and France, J. W., (1988). "Closure to discussion: Liquefaction evaluation procedure," *Journal of Geotechnical Engineering, ASCE*, 114, No. 2, pp. 251-259.

Robertson, P. K., and Campanella, R. G., (1983). "Interpretation of cone penetration tests, Part I: Sands," *Canadian Geotechnical Journal*, 20, pp. 718-733.

Robertson, P. K., Campanella, R. G., Gillespie, D. and Rice, A., (1986). "Seismic CPT to measure in-situ shear wave velocity," *ASCE Journal of Geotechnical Engineering*, 112(8), pp. 791-803.

Robertson, P. K., Woeller, D. J. and Finn, W. D. L., (1992a). "Seismic cone penetration test for evaluating liquefaction potential under cyclic loading," *Canadian Geotechnical Journal*, 29, pp. 686-695.

Robertson, P. K., Sasitharan, S., Cunning, J. C. and Sego, D. C., (1995). "Shear-wave velocity to evaluate in-situ state of Ottawa sand," *ASCE Journal of Geotechnical Engineering*, 121, pp. 262-273.

Robertson, P. K., (1994). "Suggested terminology for liquefaction," *Proceeding of the 47th Canadian Geotechnical Conference*, Halifax, Nova Scotia, pp. 277-286.

Robertson, P. K., and Fear, C. E., (1995). "Liquefaction of sands and its evaluation," *IS Tokyo 95, First international conference on earthquake geotechnical engineering, Keynote Lecture, November 1995.*

Roscoe, K. H., and Poorooshasb, (1963). "A fundamental principal of similarity in model tests for earth pressure problems," *Proceedings of the 2nd Asian Conference on Soil Mechanics,* 1, pp. 134-140.

Roscoe, K. H., Schofield, A. N., and Wroth, C. P. (1958). "On the yielding of soils," *Geotechnique,* 8, pp. 22-53.

Roseler, S. K., (1979). "Anisotropic shear wave modulus due to stress anisotropy," *Journal of Geotechnical Engineering, ASCE,* 105(7), 871-880.

Sanchez-Salinero, I., Roesset, J. M., and Stokoe, K. H., II, (1986). "Analytical studies of body wave propagation and attenuation," *Geotechnical Engineering GR86-15,* University of Texas at Austin.

Sasitharan, S., (1994). "Collapse behaviour of very loose sand," Ph.D. thesis, Department of Civil Engineering, University of Alberta, Edmonton, Canada.

Sasitharan, S., Robertson, P. K., and Sego, D. C., (1994a). "Sample disturbance from shear wave velocity measurements," *Canadian Geotechnical Journal,* Ottawa, Canada, 31, 119-124.

Sasitharan, S., Robertson, P. K., Sego, D. C., and Morgenstern, N. R., (1994b). "Collapse behaviour of sand," *Canadian Geotechnical Journal,* 30, pp. 569-577.

Schwarz, H. U., (1982). "Subaqueous slope failures-experiments and modern occurrences," *Contributions to Sedimentology,* Edited by Fuchtbauer, F., Lisitzyn, A. P., Milliman, J. D., and Seibold, E., Stuttgart.

Schimming, B. B., Haas, H. J., and Saxe, H. C., (1966). "Study of dynamic and static friction failure envelopes," *ASCE Journal of the Soil Mechanics and Foundation Engineering Division,* 92(SM2), pp. 105-124.

Seed, H. B. (1968). "Landslides during earthquakes due to soil liquefaction," *Journal of the Soil Mechanics and Foundation Division, ASCE*, 94, SM 5, pp. 1053-1122.

Seed, H. B. (1979). "Soil liquefaction and cyclic mobility evaluation for level ground during earthquakes," *Journal of Geotechnical Engineering, ASCE*, 105, No. 2, pp.201-255.

Seed, H. B., Idriss, I. M., and Arango, I., (1983). "Evaluation of liquefaction potential using field performance data," *ASCE,* 109, GT3, pp. 458-482.

Sego, D. C., Robertson, P. K., Sasitharan, S., Kilpatrick, B. I, and Pillai, V. S., (1994). "Ground freezing and sampling of foundation soils at Duncan dam," *Canadian Geotechnical Journal,* 31(6), pp. 939-950.

Shirley, D. J., and Anderson, A. L., (1975). "Acoustical and Engineering properties of Sediments," Applied Research Laboratories, University of Texas at Austin, Report No. ARL-TR-75-58.

Skirrow, R. K., (1996). "The effects of fines content on the monotonic triaxial testing of cohesionless soils for evaluation of in-situ state," M.Sc. thesis, Department of Civil Engineering, University of Alberta, Edmonton, Canada.

Sladen, J. A., D'Hollander, R. D. and Krahn, J. (1985a). "Back analysis of the Nerlerk berm liquefaction slides," Canadian Geotechnical Journal, 22, pp. 579-588.

Sladen, J. A., D'Hollander, R. D. and Krahn, J. (1985b). "The liquefaction of sands, a collapse surface approach," Canadian Geotechnical Journal, 22, pp. 564-578.

Sladen, J. A., and Oswell, J. M. (1989). "The behaviour of very loose sand in the triaxial compression test," Canadian Geotechnical Journal, 26, 103-113.

Sladen, J. A., and Handford, G., (1987). "A potential systematic error in laboratory testing of very loose sands," *Canadian Geotechnical Journal,* 24, pp. 462-466.

Stokoe, K. H. II, Lee, H. H. S., and Knox, D. P., (1985). "Shear moduli measurements under true triaxial stresses," *Proc., Adv. in the art of testing soils under cyclic condition, ASCE,* New york, NY, pp. 166-185.

Tatsuoka, F., Sakamoto, M., Kawamura, T., and Fukushima, S., (1986). "Strength and deformation characteristics of sand in plane strain compression at extremely low pressures," *Soils Foundations*, 26, No.1, pp. 65-84.

Terzaghi, K., and Peck, R. B., (1948). "Soil mechanics in engineering practice," John Wiely and Sons, Inc., 2nd edition.

Terzaghi, K., (1956). "Varieties of submarine slope failures." *Proceedings of 8th Texas Conference on Soils and Foundations Engineering.* University of Texas, Austin, pp. 1-41.

Tokimatsu, K., and Hosaka, Y., (1986). "Effects of sample disturbance on dynamic properties of sand," *Soils and Foundations,* 26(1), pp. 53-46.

Thomas, J., (1992). "Static, cyclic and post liquefaction undrained behaviour of Fraser River sand," M.A.Sc. thesis, University of British Columbia, Vancouver, Canada.

Vaid, Y. P., and Chern, J. C., (1983). "Mechanism of deformation during undrained loading of saturated sands," *International Journal of Soil Dynamics and Earthquake Engineering.* 2, No. 3, pp. 171-177.

Vaid, Y. P., and Negussey, D., (1984). "A critical assessment of membrane penetration in the triaxial test," *Geotechnical Testing Journal* , 7(2), pp. 70-76.

Vaid, Y. P., Chung, E. K. F., and, Kuerbis, R. H., (1990a). "Stress path and steady state," *Canadian Geotechnical Journal,* 27, pp. 1-7.

Vaid, Y. P., (1994). "Void ratio computations of frozen samples," CANLEX report.

Vaid, Y. P., (1994). "Computations of void ratio of laboratory sand specimens," CANLEX report.

Vaid, Y. P., and Thomas, J., (1995). "Liquefaction and postliquefaction behaviour of sand," *Journal of Geotechnical Engineering, ASCE,* 121, No. 2, pp. 163-173.

Vaid, Y. P., Sivathayalan, S., Uthayakumar, M., and Eliadorani A., (1995a). "Liquefaction potential of reconstituted Syncrude sand," *Proceeding of the 48th Canadian Geotechnical Conference,* Vancouver, B.C., 1, pp. 319-330.

Vaid, Y. P., Uthayakumar, M., Sivathayalan, S., Robertson, P. K., and Hofmann, B. A., (1995b). "Laboratory testing of Syncrude sand," *Proceedings of the 48th Canadian Geotechnical Conference,* Vancouver, B.C., 1, pp. 223-232.

Wu, W., and Kolymbas, D., (1991). "On some issues in triaxial extension tests," *Geotechnical testing Journal,* GTJODG, 14, No. 3, pp. 276-287.

Yoshimi, Y., Tokimatsu, K., and Hosaka, Y., (1989). "Evaluation of liquefaction resistance of clean sands based on high-quality undisturbed samples," *Soils and Foundations,* 29, pp. 93-104.

Yu, P., and Richart, F. E. Jr. (1984). "Stress ratio effect on modulus of dry sand," *Journal of Geotechnical Engineering, ASCE,* 110(3), pp. 331-341.

Appendix A

Triaxial Testing Procedure

Reconstituted Sample Preparation

The moist tamping technique was employed for the preparation of reconstituted samples in this study. The requirements for the sample preparation method were first to obtain homogeneous specimens with uniform void ratio and consistent fines content with that of the input material, and secondly to produce the loosest possible structure.

A known mass of dry sand is mixed with water to achieve a moisture content of about 5%. This small moisture content gives the cohesionless soil an apparent cohesion that allows the preparation of very loose samples.

A membrane is stretched on the inside face of a split mold which is mounted to the base pedestal of the triaxial setup. A vacuum of about 25 kPa is applied to the split mold to stretch the membrane to the inside face of the mold so that uniform samples can be formed in the cavity. Then the well mixed moist sand is placed in four layers into the membrane. Each layer of sand is compacted with a drop hammer weighting 148 grams falling between 10 to 15 mm. The number of blows is increased for each additional layer to obtain a uniform density in the sample. Variation in the void ratio of the sample can be achieved by varying the hammer fall height, and number of blows per layer.

The use of the moist tamping method was proven by Sasitharan (1994) to produce samples of uniform consistency. From the results of freezing of

samples after preparation, the void ratio profile with height was shown to be consistent.

After placing, and leveling the top layer, the loading head with bender element system is placed on the sample surface. Then the membrane is pulled and sealed to the top cap. After the sample is enclosed by the membrane, the vacuum is switched for application to the drainage port to support the sample. Then the vacuum connection to the mold is removed, and the mold is dismantled. The sample diameters are measured, and the cell is assembled. The sample height is determined with a dial gauge, and is referenced to a known dummy sample height. The first reading on LVDT is made at this point so that all the changes in the height of the specimen during cell assembly, saturation and consolidation can be monitored. The cell is then mounted in the frame, and filled with water. A cell pressure of about 30 kPa is applied and vacuum is removed.

Sample Saturation

Carbon dioxide is percolated through the sample from both of the bottom drainage ports for about 20 minutes from each port. The CO_2 displaces the air that fills the voids after sample preparation. De-aired, distilled water was then flushed through the specimen from the drainage ports to displace the CO_2 that was in the voids.

Back pressure saturation is used to saturate the sample. The degree of saturation is measured by calculating Skempton B parameter. Cell and back pressure are increased in increments of 50 kPa when a difference of 25 kPa is maintained between these two pressures. The build up of pore pressure in undrained condition should be equal to the increase in cell pressure if the sample

is fully saturated. When B value reaches 0.96 or greater, the sample is considered to be fully saturated.

Consolidation

At consolidation stage the drainage valve is open, and appropriate cell pressure and vertical force are applied in each increment to consolidate the specimen under isotropic or anisotropic condition. Consolidation is continued to the desired consolidation stresses and void ratio.

Shear wave velocity measurements are taken in each increment of consolidation and the corresponding stresses and void ratios are registered. The current height of the sample is to be measured when calculating the V_S measurements.

The consolidation of the sample is monitored by the change in the reading of the volume change device.

Shear loading

After consolidation, the drainage valve is closed for undrained shearing and left open for drained loading. A constant rate of 0.15 mm/min is selected for the strain controlled tests. The shearing of the sample should be continued to large strains to ensure that the ultimate steady state is reached.

During shearing all data are stored at appropriate time intervals on an IBM computer.